The synthesis and evaluation of 8-benzyloxycaffeine analogues as inhibitors of monoamine oxidase B

Belinda Strydom
B.Pharm

Dissertation submitted in partial fulfilment of the requirements for the degree *Magister Scientiae* in Pharmaceutical Chemistry at the North-West University, Potchefstroom Campus.

Supervisor:	Prof. J.P. Petzer
Co-supervisor:	Prof. J.J. Bergh
Assistant supervisor:	Prof. S.F. Malan

2009
Potchefstroom

ABSTRACT

Monoamine oxidase, especially monoamine oxidase B (MAO-B), plays a major role in the therapy of Parkinson's disease (PD). MAO-B is the main enzyme responsible for the catabolism of dopamine in the substantia nigra of the brain. Inhibition of MAO-B may thus conserve dopamine in the brain and provide symptomatic relief to PD patients.

MAO inhibitors are currently being studied as a treatment strategy for neurodegenerative diseases such as PD. In addition to symptomatic relief, MAO inhibitors are also thought to have neuroprotective properties and may slow the neurodegenerative process and thus the progress of the disease. The most common MAO-B inhibitor used for the treatment of PD is selegiline [(R)-deprenyl], an irreversible inhibitor. Unfortunately, selegiline has psycotoxic and cardiovascular adverse effects due to amphetamine metabolites formed during its oxidation. This justifies the need for the development of novel, safe and reversible MAO-B inhibitors for the treatment of PD.

Among recently discovered reversible inhibitors of MAO-B are safinamide and (E)-8-(3-chlorostyryl)caffeine (CSC). CSC consists of a caffeine ring with a styryl side chain at C-8 of the caffeine ring. Both of these moieties are critical to CSC's MAO-B inhibition activity since CSC exhibits a dual binding mode with the caffeine ring located in the substrate cavity of the enzyme while the styryl side chain extends into the entrance cavity. Safinamide also exhibits this dual binding mode, but in this case it is the benzyloxy side chain which extends into the entrance cavity of the enzyme. In this study we examined the effect of benzyloxy substitution at C-8 of caffeine on MAO-B inhibition activity by synthesizing a series of 8-benzyloxycaffeine analogues and by evaluating them as inhibitors of MAO.

The target compounds were synthesized by condensing 8-chlorocaffeine with the appropriate benzylalcohol at high temperatures in the presence of metallic sodium. The inhibitory activity of the compounds toward baboon liver MAO-B and recombinant human MAO-A and -B were measured and expressed as IC_{50} values.

The IC_{50} values obtained for human MAO-B compared very well to that of mitochondrial baboon liver MAO-B, which indicates that the active sites and inhibitor specificities of these two enzymes are very similar. Baboon liver MAO-B was most potently inhibited by 8-(3-trifluoromethylbenzyloxy)caffeine with an IC_{50} value of 0.112 ± 0.016 μM. Human MAO-B on the other hand was most potently inhibited by 8-(3-bromobenzyloxy)caffeine with an IC_{50} value of 0.068 ± 0.003 μM. These inhibitors are more potent than CSC, the lead compound for this study, which has an IC_{50} value of 0.146 ± 0.001 μM for MAO-B. From these results it can be concluded that substitution of caffeine at C-8 with a benzyloxy side chain is at least as effective as substitution with a styryl side chain for enhancing MAO-B inhibitory activity.

8-Benzyloxycaffeine and its analogues proved to be inhibitors of human MAO-A as well, although less potent compared to MAO-B. The most potent inhibitor was 8-(3-methylbenzyloxy)caffeine with an IC_{50} value of 0.397 ± 0.013 μM.

It was determined that the target compounds bind reversibly to all three enzymes and that the mode of inhibition is competitive. A Hansch-type structure-activity relationship (SAR) study showed that MAO-B inhibition activities correlated negatively with the Hansch lipophilicity constant (π) and the Hammett constant (σ) of the substituent at C-3 of the benzyloxy ring. This means that more hydrophobic and electron withdrawing substituents will result in better inhibitors of human as well as baboon liver MAO-B. Docking studies further revealed that the 8-benzyloxycaffeine analogues traverse both cavities of MAO-B with the caffeine ring oriented towards the FAD-cofactor while the benzyloxy side chain protrudes into the entrance cavity. The 8-benzyloxycaffeine analogues oriented itself similarly within the MAO-A cavity with the bezyloxy side chain rotated to avoid steric interaction with the Phe 208 residue .

The observation that 8-benzyloxycaffeine and its analogues inhibit both MAO-B and MAO-A make these compounds ideal drug candidates since both enzymes are targets for the treatment of PD.

UITTREKSEL

Die ensiem, monoamienoksidase B (MAO-B), speel 'n belangrike rol in die behandeling van Parkinsonisme. MAO-B is hoofsaaklik verantwoordelik vir die afbraak van dopamien in die brein en is dus 'n belangrike geneesmiddelteiken. Deur die inhibisie van MAO-B kan dopamienuitputting voorkom word en simptomatiese verligting van Parkinsonisme teweeggebring word.

MAO-B inhibisie het die verdere voordeel dat dit nie net simptomatiese verligting verskaf nie, maar waarskynlik ook die meganisme van neurodegenerasie kan vertraag. Daar is tans 'n aantal MAO-B inhibeerders wat gebruik word teen Parkinsonisme waarvan selegilien, 'n onomkeerbare inhibeerder, die algemeenste is. Selegilien het egter psigotoksiese en kardiovaskulêre newe-effekte as gevolg van amfetamienmetaboliete wat tydens selegilien se metabolisme gevorm word. Hierdie tekortkominge noodsaak die ontwikkeling van nuwe, veilige en omkeerbare inhibeerders van MAO-B vir die behandeling van Parkinsonisme.

Daar is onlangs ontdek dat safinamied en (E)-8-(3-chlorostiriel)kafeïen (CSC) omkeerbare inhibeerders van MAO-B is. CSC is saamgestel uit 'n kafeïenring met 'n stirielsyketting op C-8. Albei hierdie entiteite is essensieel vir die inhibisie van MAO-B aangesien CSC beide die ingangs- en substraatholte van MAO-B beset. Die verbinding is só georiënteer sodat die kaffeïenring in die substraatholte bind terwyl die stirielsyketting tot in die ingangsholte strek. Safinamied bind soortgelyk aan CSC in MAO-B se aktiewe setel maar in dié geval is dit die bensieloksiesyketting wat tot in die ingangsholte strek. In hierdie studie word die MAO-B inhiberende effek van bensieloksiesubstitusie op C-8 van kafeïen ondersoek deur 'n reeks 8-bensieloksiekafeïen-analoë te sintetiseer en te evalueer as MAO-B inhibeerders.

Die teikenverbindings is gesintetiseer deur die kondensasie van 8-chlorokafeïen met 'n bensielalkohol in die teenwoordigheid van natrium by hoë temperature. Inhibisie-aktiwiteite van die verbindings teenoor bobbejaanlewer MAO-B en rekombinante mens MAO-A en –B is bepaal en uitgedruk as IC_{50}-waardes.

Soortgelyke IC_{50}-waardes vir bobbejaanlewer MAO-B en mens MAO-B is verkry wat 'n aanduiding is dat dié twee ensieme soortgelyke bindingsetels en inhibeerdervoorkeure het. Die mees potente inhibeerder vir bobbejaanlewer MAO-B was 8-(3-trifluorometielbensieloksie)kafeïen met 'n IC_{50}-waarde van 0.112 ± 0.016 µM. Rekombinante mens MAO-B is die sterkste geïnhibeer deur 8-(3-bromobensieloksie)kafeïen met 'n IC_{50}-waarde van 0.068 ± 0.003 µM. Dit blyk dat hierdie inhibeerders meer potent is as CSC wat bobbejaanlewer MAO-B inhibeer met 'n IC_{50}-waarde van 0.146 ± 0.001 µM. Die gevolgtrekking kan gemaak word dat die substitusie van 'n bensieloksiesyketting op C-8 van kaffeïen ten minste so effektief is soos substitusie met 'n stirielsyketting om die inhibisie van MAO-B te verbeter.

MAO-A inhibisie is ook waargeneem vir die 8-bensieloksiekafeïenanaloë. Die mees potente inhibeerder was 8-(3-metielbensieloksie)kafeïen met 'n IC_{50}-waarde van 0.397 ± 0.013 µM.

Die studie het ook aangetoon dat 8-bensieloksiekafeïenanaloë bobbejaanlewer MAO-B en mens MAO-A en –B omkeerbaar en kompeterend inhibeer. 'n Hansch-tipe struktuur-aktiwiteitsverwantskap-studie het onthul dat MAO-B inhibisie-aktiwiteit negatief korreleer met die Hansch-lipofilisiteitskonstante (π) en die Hammett-konstante (σ) van die substituente op C-3 van die bensieloksiering. Dit impliseer dat substituente wat meer hidrofobies en elektron-ontrekkend is, beter inhibisie van MAO-B tot gevolg sal hê. Rekenaarmodeleringstudies het gewys dat 8-bensieloksiekafeïenanaloë albei holtes in die MAO-B aktiewe setel beset met die kafeïenring na die FAD-kofaktor in die substraatholte gerig terwyl die bensieloksiesyketting tot in die ingangsholte strek. Die 8-bensieloksiekafeïenanaloë het op soortgelyke wyse in MAO-A se aktiewesetel gebind met die bensieloksiesyketting sodanig geroteer dat steriese hindernis met die Phe-208 residu voorkom word.

8-Bensieloksiekafeïenanaloë is dus ideale geneesmiddelkandidate aangesien hierdie verbindings MAO-A en –B inhibeer en beide van hierdie ensieme teikens is vir die behandeling van Parkinsonisme.

TABLE OF CONTENTS

Chapter 1

Introduction

1.1 Overview and background

Parkinson's disease is an age related disease with typical psycho motoric symptoms and degeneration of the dopaminergic neurons in the substantia nigra pars compacta (SNpc) of the brain (Przedborski, 2005). Popular treatment for this disease involves replenishing dopamine levels with the dopamine precursor, L-dopa and to use dopamine agonists. These treatments do not prevent the progress of the disease, it only treats the symptoms (Lees, 2005). For a drug to prevent or slow the progress of this disease, it would have to be able to slow the neurodegenerative process.

MAO-B inhibitors seem to posess the ability to slow the process of neurodegeneration. The mechanism by which MAO-B inhibitors are neuroprotective is based on the prevention of the formation of toxic products produced by MAO-B oxidation activity (aldehydes and H_2O_2) (Fig. 1.1). This reduces oxidative stress and slows neuronal cell death (Youdim *et al.*, 2006).

$$\text{Amine (primary)} \xrightarrow{\text{MAO-B}} H_2O_2 + NH_3 + \text{Aldehyde}$$

Figure.1.1 General reaction, illustrating the formation of toxic products during MAO-B oxidation.

Monotherapy with one such inhibitor, selegiline, caused a small delay in the initiation of L-dopa therapy. However, selegiline is usually administered as combination therapy with L-dopa to reduce the dosage of L-dopa needed (Riederer *et al.*, 2004). A disadvantage of selegiline is that it possesses psychotoxic and cardiovascular adverse effects. These adverse effects are caused by amphetamine derivatives formed during the metabolism of selegiline (Lees, 2005). Furthermore, selegiline is an irreversible or suicide inhibitor, and does not allow competition with other substrates. These shortcomings of selegiline fuels the need for the development of new, reversible MAO-B inhibitors with better safety profiles.

A MAO-B inhibitor that is currently being investigated for use in PD treatment, is rasagiline. In contrast to selegiline, rasagiline is not metabolized to amphetamine derivatives and is thus a safer treatment option, though still an irreversible inhibitor (Lees, 2005). Other recently studied inhibitors include (E)-8-(3-chlorostyryl)caffeine (CSC) which is a potent, reversible inhibitor of MAO-B as well as an adenosine A_{2A} receptor antagonist (Vlok *et al.*, 2006). A_{2A} antagonists are presently being considered as a treatment option for the motoric symptoms in PD. There is also reason to believe that A_{2A} antagonists have the ability to protect dopaminergic neurons against neurodegeneration (Chen *et al.*, 2001). Developing drugs that has a dual action by inhibiting MAO-B and antagonizing A_{2A} receptors offers a novel approach to PD treatment (Petzer *et al.*, 2003).

1.2 Rationale

There exists a need for the development of new, selective and competitive inhibitors of MAO-B for the treatment of PD. Current available therapies are not adequate and mostly treat the symptoms. Development of novel MAO-B inhibitors presents the opportunity to produce a drug that not only treats the symptoms, but also exerts neuroprotective properties.

The aim of this project is to synthesize the 8-benzyloxycaffeine analogues (**1a–g**) illustrated in Table 1.1 and to evaluate them as potential MAO inhibitors. In this study, MAO activity measurements will be based on the extent to which kynuramine or 1-methyl-4-(1-methylpyrrol-2-yl)-1,2,3,6-tetrahydropyridine (MMTP) is oxidized *in vitro* by MAO (Vlok *et al.*, 2006).

Table 1.1 The series of 8-benzyloxycaffeine analogues selected for this study.

-R	
-H	**1a** 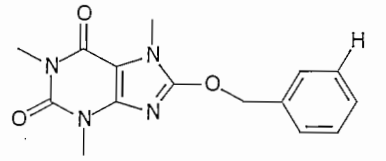
-Cl	**1b** 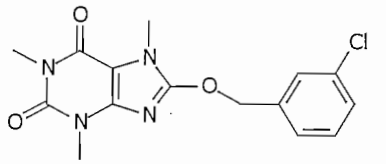
-Br	**1c** 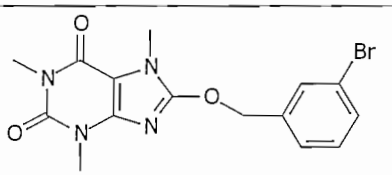
-F	**1d** 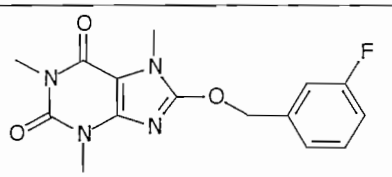
$-CF_3$	**1e** 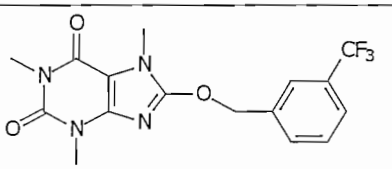
$-CH_3$	**1f** 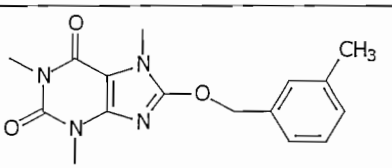
$-OCH_3$	**1g** 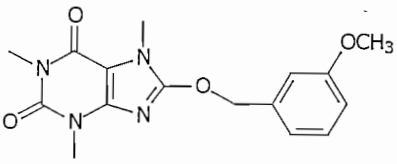

Theoretically, 8-benzyloxycaffeine and its analogues should act as good inhibitors of MAO-B since they are caffeine derivatives with substituents at C-8. Caffeine was found to be a weak inhibitor of MAO-B, but addition of a side chain at C-8 of the caffeine ring increased inhibitor potency remarkably as shown by the potent inhibitor CSC (Fig. 1.2) (Vlok *et al.*, 2006). The benzyloxy side chain is present in a variety of known potent MAO-B inhibitors. For example, coumarin derivatives (Fig. 1.2) and safinamide (Fig. 1.2) contain the benzyloxy side chain in their structures and are potent MAO-B inhibitors (Binda *et al.*, 2007). The structure of 8-benzyloxycaffeine combines the caffeine ring system with the benzyloxy side chain, both elements found in known potent MAO-B inhibitors.

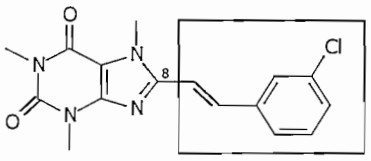

CSC

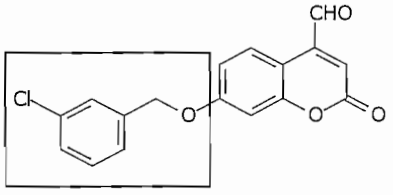

7-(3-Chlorobenzyloxy)-4-carboxaldehyde-coumarin

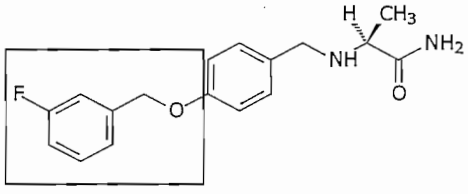

Safinamide

Figure 1.2 Inhibitors of MAO-B. Note the presence of the side chain at C-8 of the caffeine ring of CSC. The coumarin derivative as well as safinamide contains a benzyloxy functional group.

Chapter 2

Literature study

2.1 Parkinson's disease

2.1.1 Symptoms and characteristics

Parkinson's disease (PD) is an overwhelming disease that markedly alters the sufferer's quality of life without necessarily shortening it. It is an age related disease characterized by the specific degeneration of dopaminergic neurons in the substantia nigra pars compacta (SNpc) and the depletion of the neurotransmitter, dopamine in the striatum. PD is progressive, implying that dopamine depletion and neurodegeneration increase over time. Normally dopamine is responsible for effective motoric function in the body, therefore the depletion of dopamine causes movement disorders such as bradykinesia, freezing, tremors and postural instability. Replenishing the low dopamine levels brings symptomatic relief.

Another characteristic is the formation of Lewy Bodies in affected brain areas. Lewy Bodies consist of aggregated proteins which could be a contributing factor to the occurrence of PD. Strictly, PD is not a genetic disease, however, there exists forms of PD caused by genetic mutations. These mutations can cause the production of faulty proteins that contribute to the accumulation of unwanted proteins (Lees, 2005; Przedborski, 2005).

Increased levels of MAO-B were observed in the brains of PD patients as well as decreased levels of aldehyde dehydrogenase and glutathione (GSH). This also plays a role in the progress of the disease as will be discussed next (Youdim *et al.*, 2006).

2.1.2 Mechanism

The precise mechanism by which idiopathic PD is caused is still unclear, but a few of the factors thought to contribute will be discussed. It should be made clear that it is not likely that PD is caused by only one of these mechanisms, but rather by a combination of these factors in a susceptible person that triggers a series of events that lead to the occurrence of PD (Dauer *et al.*, 2003).

Dopamine depletion associated with PD is caused by the neuronal death of dopaminergic pathways. Interestingly, it was found that neurons containing neuromelanin are more susceptible to this destructive path.

MAO-B is implicated in three mechanisms of neurodegeneration in the SNpc. Firstly, by the formation of reactive oxygen species (ROS) during the oxidation of amines in the body (Fig. 2.1). ROS by itself can cause neuronal damage but there is also a possibility that it can react with other reactive molecules such as peroxy nitrate to inflict even greater damage (Przedborski 2005). The H_2O_2 formed by MAO-B is not adequately metabolized in PD patients as a result of lower GSH levels in these patients (Riederer *et al.*., 1989). Glutathione is the substrate of glutathione peroxidase that metabolizes H_2O_2. Accumulated H_2O_2 is then able to readily react with Fe^{2+} to form $OH^{\cdot}$ radicals (Fenton reaction) (Fig. 2.1). $OH^{\cdot}$ radicals are destructive molecules that cause damage to neuronal cells and ultimately lead to apoptosis. Since PD is an age related disease and Fe^{2+} levels in the brain increases with age (Mandel *et al.*, 2005), the ideal circumstances are created for the Fenton reaction to occur.

Secondly, accumulation of neurotoxic aldehydes is a further result of the MAO-B catalytic cycle and may contribute to neurodegeneration. Low levels of the enzyme aldehyde dehydrogenase (ADH) in the SNpc of PD patients is responsible for the accumulation of aldehydes (Fig. 2.1) (Youdim *et al.*, 2006). Thirdly, models of the pre-neurotoxin 1-methyl-4-phenyl-1,2,3,6-tetrahydropyridine (MPTP) suggest that an environmental toxin may be responsible for parkinsonism. MAO-B is the enzyme which activates MPTP to the active neurotoxin. The active form of MPTP, 1-methyl-4-phenylpyridinium (MPP^+), is taken up in

the mitochondria where it interferes with the H^+ transduction system and eventually leads to lower ATP production, oxidative stress and neuronal cell damage (Smeyne *et al.*, 2004).

In al three the above mentioned mechanisms, MAO-B is the enzyme that catalyzes the reaction to form the toxic or harmful products.

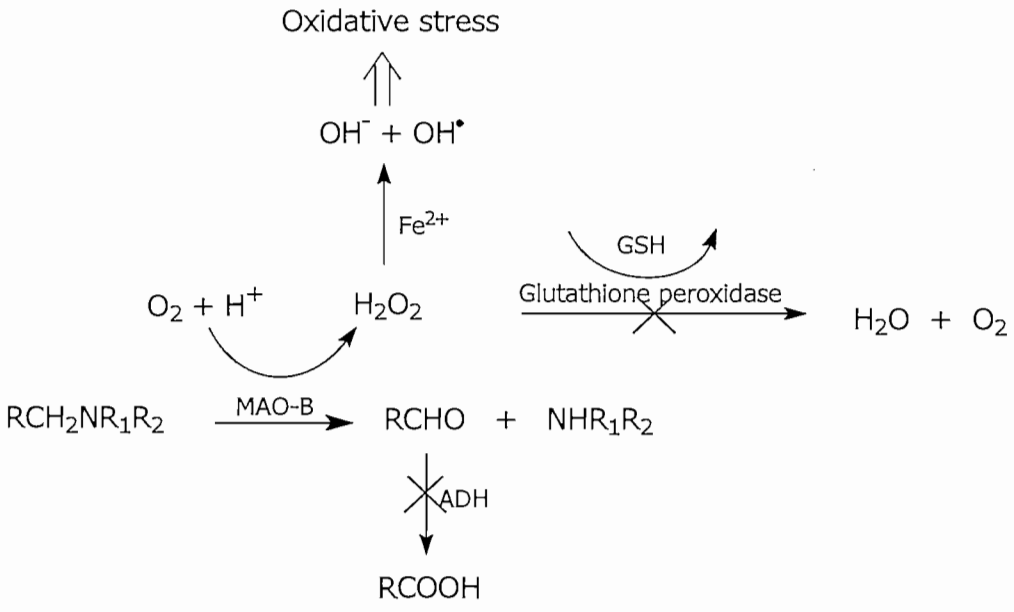

Figure 2.1 Mechanisms of neurotoxicity in PD thought to be mediated via the oxidation process of MAO-B.

Uncertainty still remains about the function or role of Lewy Bodies in PD. There are two contradicting theories about Lewy bodies. The one supports the notion that they protect the body from misfolded and unwanted proteins by confining it to small compartments while the other imply that they contribute to the toxicity associated with PD. The toxicity theory of Lewy Bodies are supported by the fact that the accumulation of misfolded proteins may eventually lead to toxicity, as the system responsible for the degeneration of these proteins is severely hampered in PD. The formation of ROS also promotes the misfolding of proteins and places greater pressure on the system responsible for removing these proteins (Dauer *et al.*, 2003).

Genetics also play a role in the occurrence of PD, although it is responsible for a small minority of the cases. Mutations in proteins, such as α-sinuclein and ubiquitin for example, was observed in certain persons and gave better insight of PD on a genetic level (Polymeropoulos *et al.*, 1997; Leroy *et al.*, 1998).

Although the precise mechanism of PD remains unknown, drugs and treatment strategies to maintain and relieve the symptoms of this destructive disease can still be developed.

2.1.3 Treatment

There are various treatments for PD, but the most common treatment option includes L-dopa for mono or combination therapy. L-dopa directly stimulates dopamine release in the brain. Dopamine agonists such as pergolide also increase dopamine mediated neurotransmission through the stimulation of dopamine receptors. Replenishing dopamine levels unfortunately only treats the symptoms and not the cause of the disease. Furthermore, chronic use of L-dopa has its disadvantages in the form of the on-off effect (fluctuations in motoric response). Dopamine agonists on the other hand has adverse effects such as dizziness, nausea, vomiting and somnolence (Lees, 2005).

Anticholinergic drugs are used for its ability to correct the balance between dopamine and acetylcholine in the striatum. However, a major drawback is the occurrence of anticholinergic side effects. Other treatment options include drugs with neuroprotective properties such as amantadine and the MAO-inhibitors. Amantadine has anticholinergic properties while it enhances dopamine secretion and inhibits its reuptake, but also has significant adverse effects (Lees, 2005).

MAO-inhibitors (specifically the B isoform) exerts neuroprotective effects and can be used in combination with other drugs. MAO-B inhibitors currently in use include selegiline. Unfortunately selegiline causes sympathomimetic side effects due to its amphetamine metabolites. Another MAO-B inhibitor that is presently being investigated is rasagiline, a safer option than selegiline as it is not metabolized to amphetamine derivatives. MAO-B

inhibitors is of particular interest since it presents a way to treat the symptoms as well as protecting dopaminergic neurons (Guttman *et al.*, 2003; Rascol *et al.*, 2002).

A_{2A} antagonists have neuroprotective properties and are currently being examined as a strategy of treating the motoric symptoms in PD patients. The possibility of designing a dual action drug that inhibits A_{2A} as well as MAO-B is an attractive new possibility for PD treatment (Petzer *et al.*, 2003).

Antioxidants is also worth mentioning as a treatment option for PD as the destruction caused by ROS can be reduced through the binding of antioxidants to ROS. Thus, antioxidants may also exert a neuroprotective effect (LeWitt *et al.*, 2008).

There is a need for the development of new drugs for the treatment of PD that do not present with such hazardous side effects as observed with most of the current treatments. It is also desired that drugs for the treatment of PD should possess protective activity against neurodegeneration.

2.2 MPTP

The neurotoxin, 1-methyl-4-phenyl-1,2,3,6-tetrahydropyridine (MPTP) (Fig. 2.2), was first discovered to produce parkinsonian symptoms in drug abusers who illegally attempted to synthesize 1-methyl-4-phenyl-4-propionpiperidine (MPPP) (Fig. 2.2), an analogue of meperidine (Bové *et al.*, 2005). MPTP was formed as a by-product and caused dopamine depletion as well as SN degeneration and other motoric symptoms typical of PD. However, the formation of Lewy Bodies were miniscule (Blum *et al.*, 2001). This discovery presented the opportunity to create animal models of PD to aid research on this topic (Singer *et al.*, 1988).

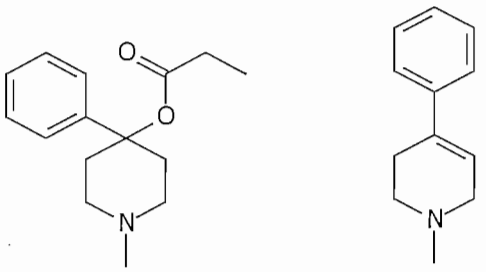

MPPP MPTP

Figure 2.2 Structures of MPPP and MPTP

2.2.1 The mechanism of MPTP toxicity

MPTP is a substrate of MAO-B and is oxidized to the active metabolite, MPP^+, in the astrocytes [Fig. 2.3 (i)]. Because of the polarity of MPP^+, it is necessary for the molecule to cross the neuronal membrane by means of a transporter. This is accomplished by competing with the dopamine transport system (DAT) of these neurons. Once inside, MPP^+ enters the mitochondria where it binds to complex I. Consequent inhibition of electron flow in the mitochondria and a reduction in ATP formation leads to oxidative stress and ROS formation [Fig. 2.3 (ii)] (Smeyne *et al.*, 2004). Alternatively, the intracellular MPP^+ can be taken up in vesicles or bound to neuromelanin. If this happens, MPP^+ is rendered inactive. It is thought that this could be a protective mechanism of the body against the toxic substance [Fig. 2.3 (iii)] (Blum *et al.*, 2001).

MPTP is thought to exert its neurodestructive path in various ways. Aside from contributing to oxidative stress, MPTP increases iron levels, creating ideal circumstances for the Fenton reaction to take place [Fig. 2.3 (iv)]. The mechanism by which MPTP increases iron is still unclear but it is believed that the destruction of the terminals of nigrostriatal neurons by MPTP increases transferrin mediated neuronal iron uptake. It is believed that the enhanced uptake of tranferrin and iron assists post-traumatic neuronal recovery and repair (Mochizuki *et al.*, 1994). The intermediate compound of MPTP oxidation, $MPDP^+$, also has the potential to form a superoxide radical during its auto oxidation that can potentiate destruction and cell death.

Formation of peroxynitrate, an immensely destructive, oxidizing molecule, is possible through the reaction of superoxide radicals and nitric oxide that is produced by glial cells [Fig. 2.3 (v)] (Smeyne *et al.*, 2004).

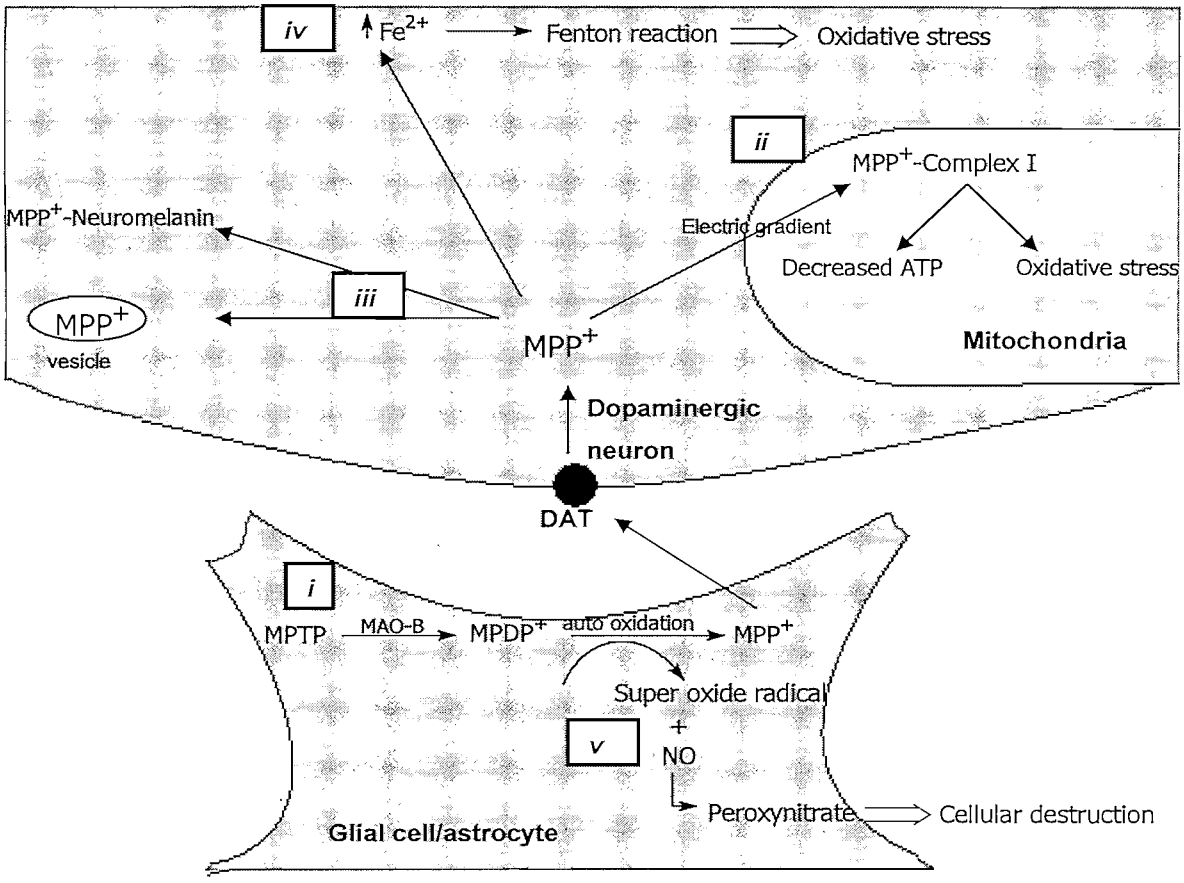

Figure 2.3 Illustration of the mechanism of MPTP toxicity.

The discovery that MPTP, an exogenous substance, can induce parkinsonian symptoms in humans, led to the hypothesis that environmental factors such as pesticides might be a contributing factor in the ethiology of PD (Elbaz *et al.*, 2007). Indeed, other toxin induced models of PD include rotenone, a pesticide and paraquat, a herbicide (Bové *et al.*, 2005).

2.3 Monoamine oxidase

2.3.1 General background

Monoamine oxidase (MAO) is the enzyme responsible for the oxidation of amines and plays a role in the maintenance of normal brain function as well as certain personality traits and addictive behaviour. It serves as a metabolic barrier by oxidizing amines that can be potentially harmful and terminates the action of certain neurotransmittors. Ultimately MAO exerts a protective action (Youdim *et al.*, 2006).

MAO consists of two isoforms, MAO-A and MAO-B, that share 70% sequence identity, but are encoded by different genes (Edmondson *et al.*, 2004). Both enzymes are bound to the outer membrane of the mitochondria and contains a flavin adenine dinucleotide (FAD) co-factor (Binda *et al.*, 2002).

The two isoforms differ from each other in substrate specificity as well as their inhibitors. MAO-A preferably oxidizes serotonin (5-HT) and is inhibited by low concentrations of clorgyline. MAO-B oxidizes benzylamine and 2-phenylethylamine, while it is inhibited by low concentrations of selegiline. Both isoenzymes utilize dopamine as substrate, but since MAO-B is the isoform that is predominantly present in the basal ganglia, dopamine oxidation in the brain is largely due to MAO-B activity (Youdim *et al.*, 2006).

MAO-B is the enzyme that catalyzes the oxidation of certain amines to their corresponding aldehydes and hydrogen peroxide and in the case of monoamines also to ammonia. In high concentrations these products can be harmful and contribute to neurodegeneration as in the case of PD (Riederer *et al.*, 2004).

Studies regarding MAO-B have been very limited as a result of an inadequate expression system for this enzyme. It is very difficult to produce sufficient amounts of pure enzyme for study purposes. Bovine liver is a good source of MAO-B, but recently human MAO-B has been successfully expressed in yeast cells (*pichia pastoris).* The MAO-B expressed in yeast cells yielded satisfactory amounts of pure enzyme to enable the determination of the x-ray crystal structure (Newton-Vinson *et al.*, 2000).

Other sources of MAO are human placenta (contains mostly MAO-A), blood platelets (pure MAO-B source) (Salach *et al.*, 1987) and baboon liver (mainly a source of MAO-B) (Vlok *et al.*, 2006). The problem with mechanically extracting MAO-B from tissue lies in the fact that MAO-B is a membrane bound enzyme and some of its activity may be dependant on this. Thus, removing the enzyme from the membrane may alter its activity. Another factor that can hinder the physical extraction of the enzyme is the hydrophobic nature of MAO-B (Newton-Vinson *et al.*, 2000).

Opportunity presents itself in therapeutic treatment through MAO inhibition. MAO-A inhibitors are already used as anti-depressants. Selegiline, a MAO-B inhibitor, is used as an antiparkinsonian drug due to its neuroprotective properties (Youdim *et al.*, 2006).

2.3.2 Role in Parkinson's disease

MAO-B is the preferred enzyme for oxidation of dopamine in the brain due to the high MAO-B concentrations in the basal ganglia (Youdim *et al.*, 2006). As mentioned earlier, the oxidation of amines can produce harmful products such as aldehydes and H_2O_2. In the brain, dopamine is oxidized by MAO-B to form these products and since PD patients have a tendency toward elevated levels of MAO-B, this oxidation process will occur more frequently (Youdim *et al.*, 2006).

The accumulation of aldehydes and H_2O_2 presents a problem in PD patients. These patients exhibit low aldehyde dehydrogenase and glutathione peroxidase activities, the enzymes for metabolizing aldehydes and H_2O_2, respectively. High concentrations of aldehydes are neurotoxic while H_2O_2 contributes to ROS formation and reacts with iron to form $OH^{\cdot}$ radicals that has the ability to damage neuronal cells (Riederer *et al.*, 2004).

Furthermore, MPTP is oxidized to its harmful, active form, MPP^+, by MAO-B. This suggests a possible role of MAO-B in the conversion of other exogenous toxins to their active forms that can contribute to the occurrence of PD (Blum *et al.*, 2001).

It has become clear that MAO-B plays an important role in the mechanism of PD. Thus, inhibition of this enzyme can bring relief of PD. Such inhibitors can bring symptomatic relief by elevating dopamine levels and serve as a neuroprotector by preventing the formation of aldehydes and H_2O_2 (Fernandez *et al.*, 2007). In summary, MAO-B inhibitors (specifically selegiline) (1) reduce free radicals (2) prevent possible activation of pre-toxins and (3) protect against further neuronal degeneration (Riederer *et al.*, 2004).

2.3.3 Three dimensional structure

MAO-B:

It was only recently that the crystal structure of MAO-B was solved to a resolution of 3 Å (Fig. 2.4) (Binda *et al.*, 2002). This is significant in that it is now possible to verify the binding conformation of several inhibitors and substrates within the MAO-B enzyme by crystallizing the enzyme while the inhibitor is bound to it and then solving the structure. A variety of these inhibitor-enzyme complexes have been solved (Hubalek *et al.*, 2005). Understanding the way in which MAO-B interacts and binds the inhibitor, enables us to create more potent and effective inhibitors by developing compounds that better fit and interact within the MAO-B structure.

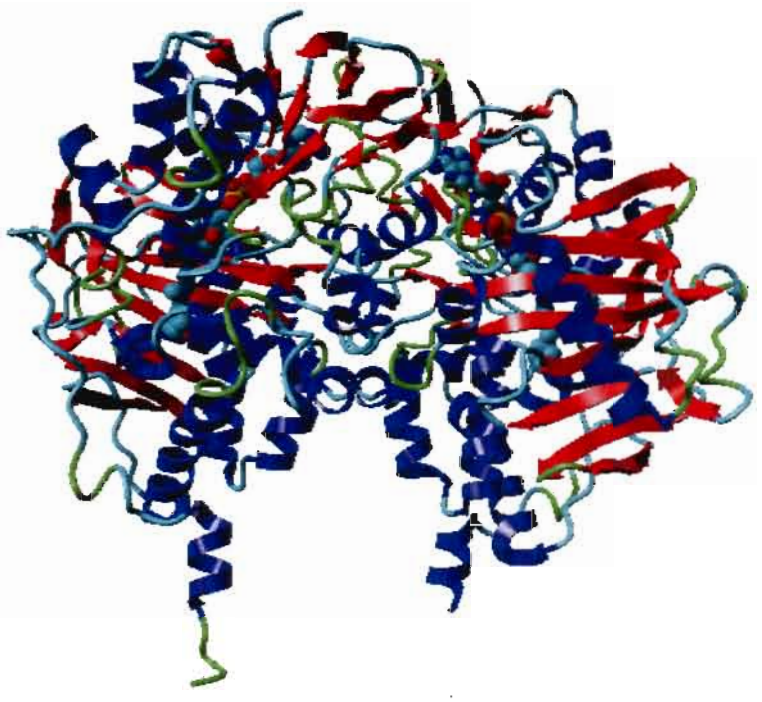

Figure 2.4 The three dimensional structure of the MAO-B dimer.

The MAO-B structure revealed several aspects that contribute to a better understanding of the binding mode of substrates and inhibitors of this enzyme. It is now known that MAO-B consists of 520 amino acids (Binda *et al.*, 2002) and that the active site consists of two cavities, an entrance and a substrate cavity (Binda *et al.*, 2003) that are separated by a 'gate' formed by the residue Ile-199 (Fig. 2.5). This gate can rotate into a closed conformation, separating the two cavities, or an open conformation, fusing the cavities. The conformation of the Ile-199 gate is dependant on the type of substrate or inhibitor bound to the enzyme (Hubalek *et al.*, 2005).

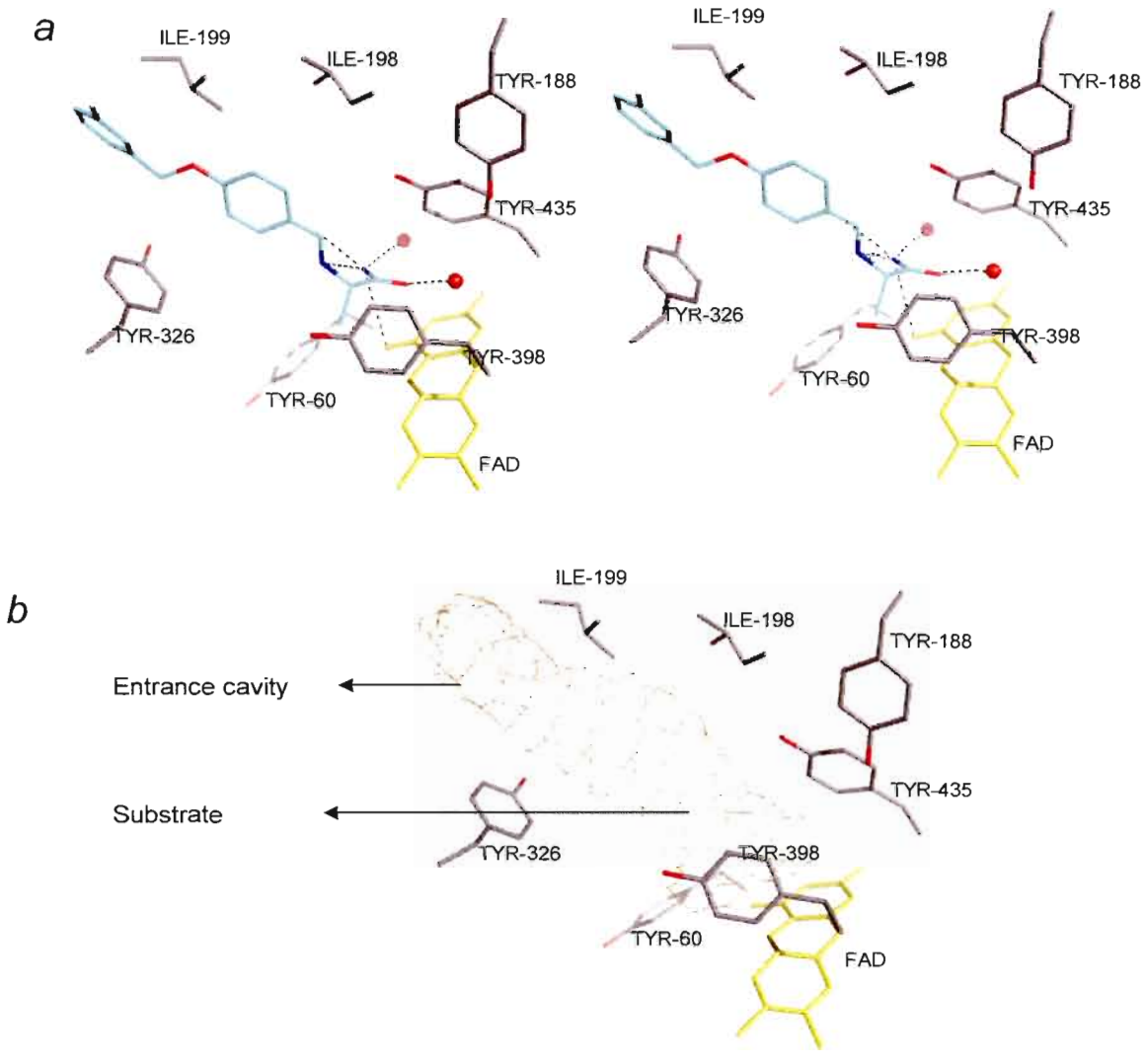

Figure 2.5 ***a***) Stereo view of safinamide (in cyan) docked within MAO-B. The Ile199 'gate' is in an open conformation. Selected residues that lines the cavity is also included here. Water molecules in the cavity are represented by red spheres while hydrogen bonds are indicated by dashed lines. ***b***) The entrance and substrate cavities within MAO-B.

Certain inhibitors such as 1,4-diphenyl-2-butene and CSC (Fig. 2.6) span both cavities which results in the open conformation of the gate (Binda *et al.*, 2003). Inhibitors that occupy both cavities were found to be selective for MAO-B and did not bind to MAO-A (Hubalek *et al.*, 2005). This is a consideration in the creation of novel selective MAO-B inhibitors.

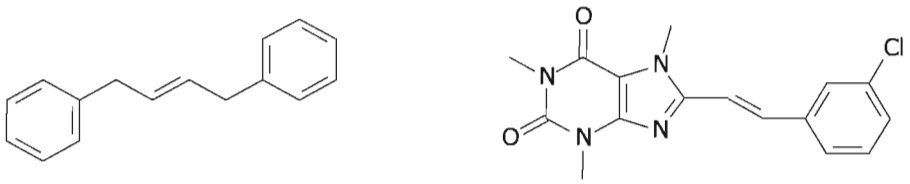

1,4-Diphenyl-2-butene

CSC

Figure 2.6 Chemical structures of MAO-B inhibitors that span both the entrance and the substrate cavities of the enzyme.

The entrance and substrate cavities are hydrophobic in nature and thus prefer the binding of non-polar groups. Near the FAD co-factor a hydrophilic area exists that is thought to aid the recognition and orientation of substrates. An aromatic cage for the recognition of amines is formed by FAD and two residues, Tyr-398 and Tyr-435 (Fig. 2.7) (Li *et al.*, 2006).

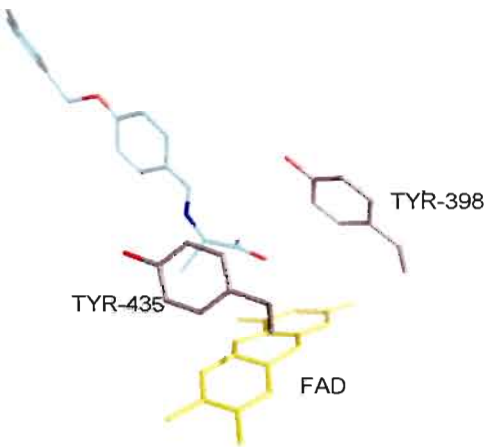

Figure 2.7 An illustration of the aromatic cage formed by FAD and the two amino acids, Tyr-398 and Tyr-435. The ligand (safinamide) is showed in cyan while the FAD is yellow and the amino acids are in grey.

Another interesting discovery is the non-planar conformation of the oxidized FAD that probably assists with substrate binding. A point worth mentioning is the *cis* conformation of the cysteinyl residue (Cys-397-Tyr-398) linking with the FAD co-factor (Fig. 2.8). This is a feature unique to MAO-B. Usually the *trans* conformation is energetically more favourable, but in this case the *cis* conformation is believed to assist in orientating Tyr-398 in a favourable position within the active site (Binda *et al.*, 2003).

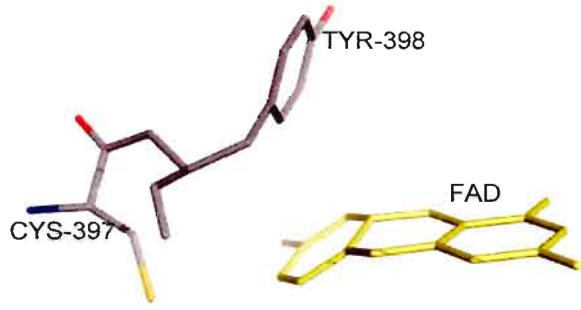

Figure 2.8 Illustration of the *cis* conformation of Tyr-398 and Cys-397.

Binding specificity of substrates to MAO-B is most likely regulated by the shape and size of the active site. Since the active site of MAO-B is believed to be relatively large, bulkier compounds would presumably be better substrates (Binda *et al.*, 2002). Oxidation of substrates occurs at the 5 or 4a positions of FAD (Fig. 2.9). Therefore it is necessary that the amine functional group is orientated towards the FAD co-factor within the substrate cavity.

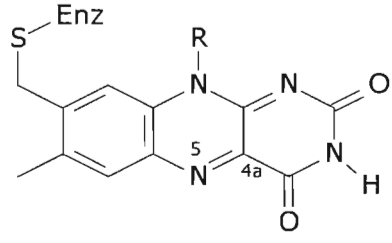

Figure 2.9 Structure of the FAD co-factor

Safinamide (Fig. 2.10), a MAO-B inhibitor, contains a 3-fluorobenzyloxy group that occupies the entrance cavity, while the amidine is located in the substrate cavity when bound within MAO-B. As mentioned earlier, this is an ideal binding mechanism for a selective MAO-B inhibitor (Binda *et al.*, 2007).

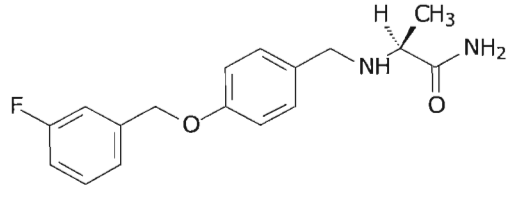

Figure 2.10 Chemical structure of safinamide

MAO-B is a membrane bound enzyme, found on the outer membrane of the mitochondria. The mechanism of membrane binding occurs through the C-terminus, via a hydrophobic α helix (Binda *et al.*, 2003). Whether the helix totally traverses the mitochondrial membrane is still uncertain, but there is evidence in the structural data that there might be additional sites that interact with the membrane to facilitate binding (Edmondson *et al.*, 2004). Furthermore, the crystal structure revealed that MAO-B forms dimers on the mitochondrial surface through monomer-monomer interactions (Binda *et al.*, 2002).

MAO-A:

The structure of MAO-A was solved at a resolution of 3 Å (Fig. 2.11). The results indicate that this enzyme, unlike MAO-B, naturally occurs as a monomer on the outer mitochondrial membrane (De Colibus *et al.*, 2005).

It was found that the structure of MAO-A does not differ that much from the structure of MAO-B. The active binding site of these enzymes (including the FAD co-factor) is essentially the same, indicating that they possibly have the same catalytic mechanism. One of the unique characteristics of MAO-A is the substitution of a Phe-208 in the analogous position of MAO-B's Ile-199. This mutation results in the elimination of an entrance cavity. MAO-A has only one binding cavity, the active site, which is shorter and wider in comparison to MAO-B's active site. Another characteristic is the presence of a cavity-shaping loop 210-216 (Fig. 2.12) (De Colibus *et al.*, 2005; Son *et al.*, 2008).

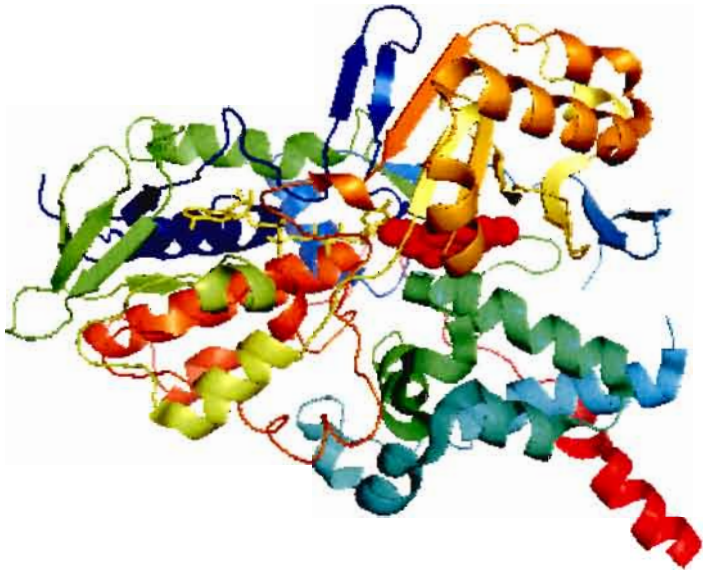

Figure 2.11 The overall structure of the human MAO-A monomer.

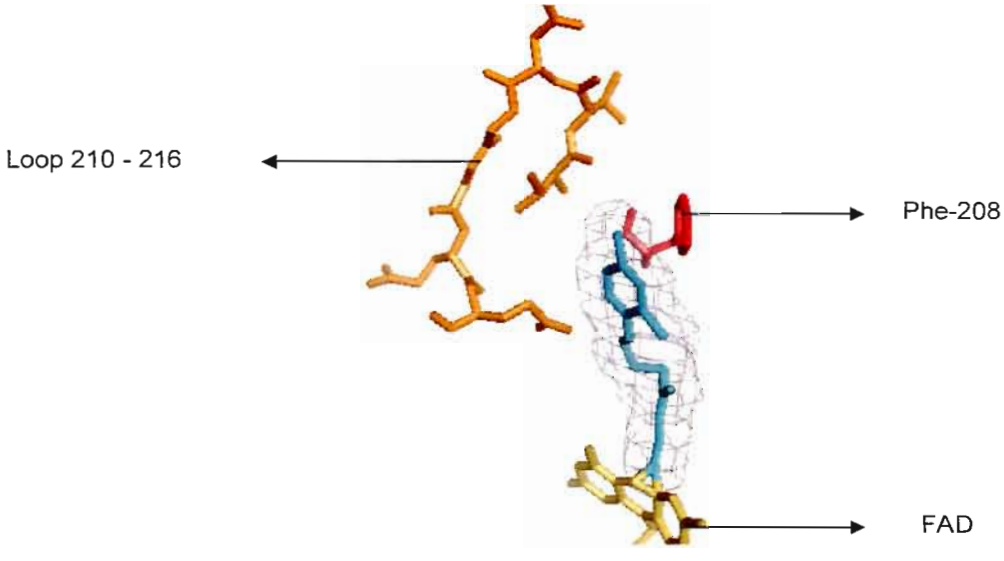

Figure 2.12 The active site cavity of human MAO-A. The substrate is illustrated in cyan while the FAD co-factor is yellow.

2.3.4 Catalytic cycle

MAO-B and MAO-A are flavin containing enzymes, implying that they both contain a FAD co-factor (Fig. 2.9). This FAD co-factor is absolutely necessary for catalysis. As mentioned in 2.3.3 it is believed that MAO-A and MAO-B have the same catalytic mechanism because their catalytic sites are very similar. MAO-B catalyses the oxidation of various amines. During this oxidation process the FAD co-factor is reduced and an imine is formed. The formed imine is hydrolyzed to form an aldehyde and ammonia in the case of primary amines (secondary and tertiary amines produces another amine). The reduced FAD reacts with oxygen to form H_2O_2 and is re-oxidized. Thus, oxygen is the final electron receiver to form the potentially harmful product, H_2O_2 (Edmondson *et al.*, 2004). A general oxidation reaction catalyzed by MAO-B is illustrated in figure 2.13 (Binda *et al.*, 2002).

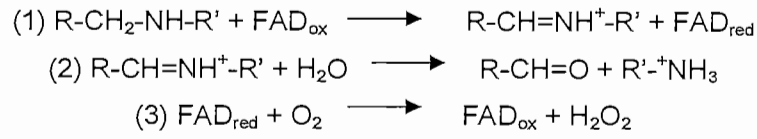

Figure 2.13 (1) CH bond cleavage with FAD reduction. (2) aldehyde formation by imine hydrolysis. (3) FAD oxidation with hydrogen peroxide formation.

Two possible mechanisms are proposed for MAO catalysis, namely a single electron transfer (SET) mechanism (Silverman, 1995) and a polar nucleophilic mechanism. The SET mechanism is depicted in figure 2.14. In the first step of the reaction there is a single electron oxidation of the ion pair on the amine nitrogen which leads to the formation of a aminium cation radical and a flavin radical. The presence of an aminium usually lowers the pKa of the α-C-H which is supposed to facilitate the withdrawal of ^{+}H by a base in the active site of the enzyme. Current knowledge of the crystal structure of MAO shows that there is no amino acid residues in the active site that can extract the ^{+}H. Studies done on the energetic potential needed for the SET mechanism implied that the potential needed for SET is much greater than the actual measured potential of flavin (Edmondson *et al.*, 2004).

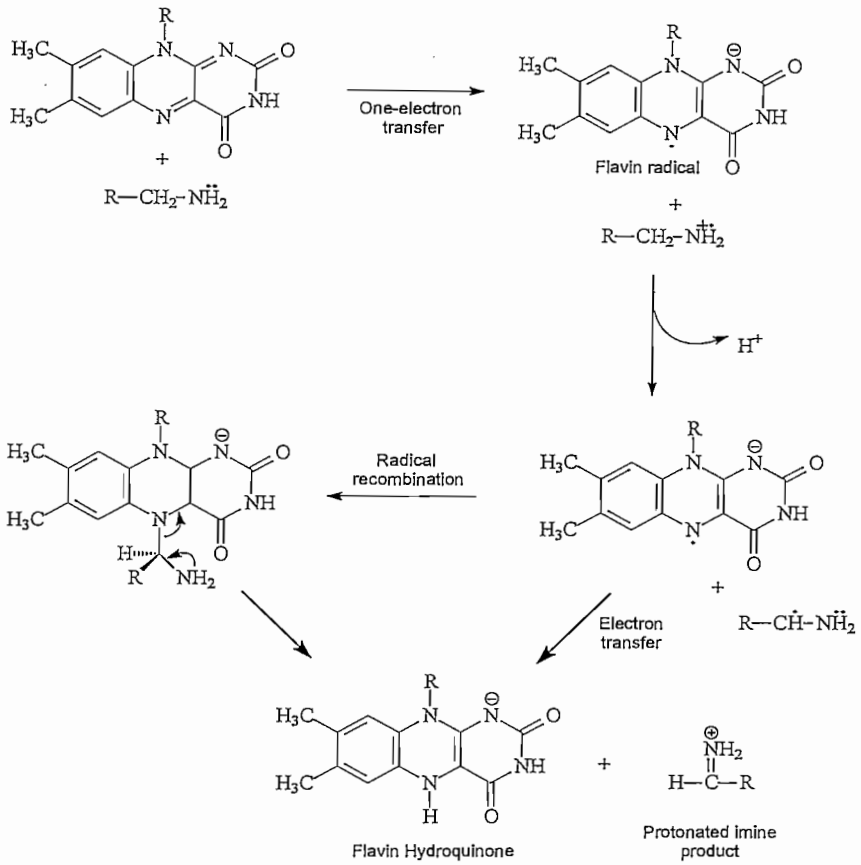

Figure 2.14 The single electron transfer mechanism.

With the polar nucleophilic mechanism (Fig. 2.15) the first step is believed to be an nucleophilic attack of the flavin at C-4 by a deprotonated amine. This nucleophilic attack causes the N-5 of the flavin to become a strong enough base to extract ^{+}H from the substrate. The polar nucleophilic theory is much more likely than the SET mechanism and is supported by current knowledge of the structure of MAO (Edmondson *et al.*, 2004).

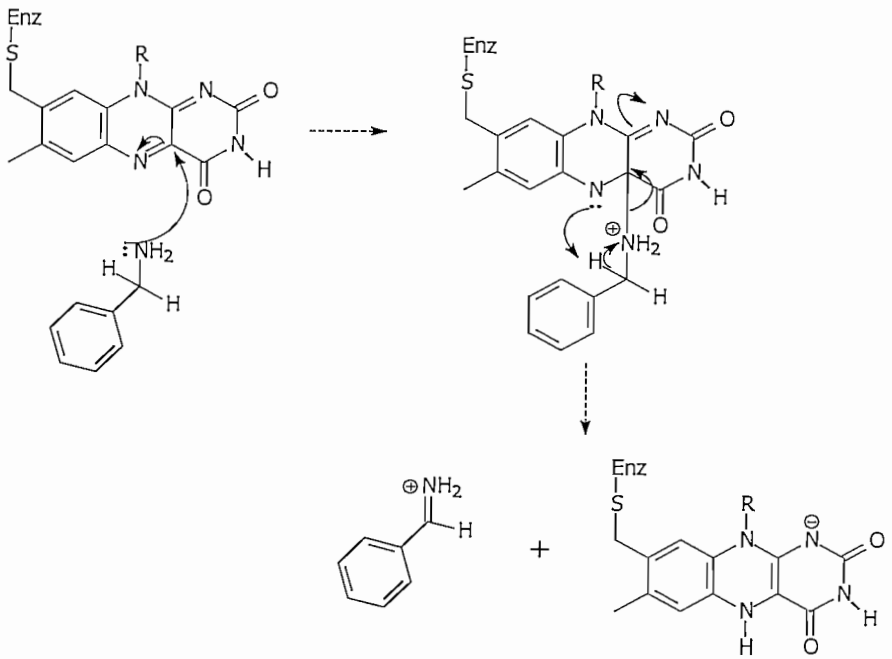

Figure 2.15 The polar nucleophilic mechanism

Substrates of MAO-B include the inhibitor selegiline and the neurotoxin MPTP. These and other substrates interact with the FAD co-factor at the 5 or 4a positions where the substrate is then oxidized while the FAD is reduced. Interaction of the substrates with FAD takes place by binding of the amine substrate's nitrogen to the specific position on the FAD co-factor, depending on the substrate properties. This interaction results in the cleavage of the α-CH bond of the substrate with the simultaneous reduction of the FAD co-factor (Li *et al.*, 2006). Rasagiline, a reversible inhibitor of MAO-B binds to position 5 of FAD as depicted in figure 2.16 (Binda *et al.*, 2004).

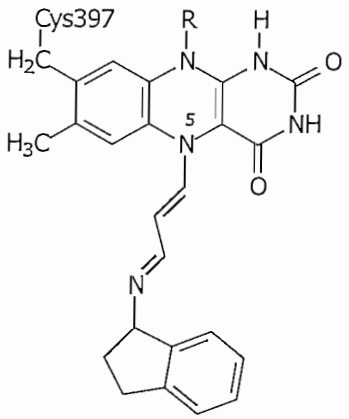

Figure 2.16 Binding mode of the inhibitor, rasagiline to the FAD co-factor

MPTP oxidation by MAO-B produces the toxic product, MPP^+, that leads to the occurance of parkinsonian symptoms. The mechanism by which MPTP is converted to the toxic MPP^+ is illustrated in figure 2.17.

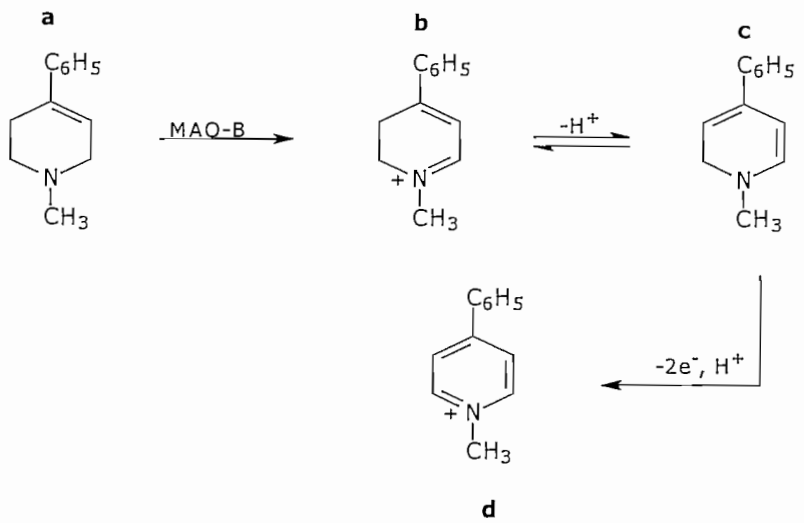

Figure 2.17 The oxidation of MPTP (**a**) results in the intermediate product $MPDP^+$ (**b**) $MPDP^+$ is further oxidized to the neurotoxin MPP^+ (**d**), possibly through the formation of the corresponding free base (**c**).

MAO-B catalyzes the 2 electron oxidation of MPTP to form an intermediate product, $MPDP^+$. This intermediate metabolite is further oxidized by another 2 electron oxidation, probably via the corresponding free base, to form the final neurotoxic product, MPP^+ (Nicklas *et al.*, 1985; Ramsay *et al.*, 1991).

2.3.5 Known inhibitors

Inhibitors of MAO-B can be divided into two classes, namely reversible and irreversible inhibitors, among which selective and non-selective inhibitors exist. Some of the older inhibitors like tranylcypromine are non-selective, irreversible inhibitors that inhibit both MAO-B and MAO-A (Riederer *et al.*, 2004). Irreversible inhibitors do not allow competition with other substrates, thus the normal metabolism of certain substrates are hampered. The need to develop selective MAO-B inhibitors arises from the fact that dopamine oxidation in the brain is mainly due to MAO-B activity (Lees, 2005).

The only selective MAO-B inhibitor currently in use for the treatment of PD is the irreversible inhibitor, selegiline (Fig. 2.18). Selegiline can be used as monotherapy or more often as combination therapy with L-dopa. Unfortunately this drug is subject to the first pass effect and is extensively metabolized by the liver before it can exert its therapeutic effect. Furthermore, metabolism of selegiline yields amphetamine derivatives that causes sympathomimetic side effects.

Another selective inhibitor of MAO-B that is currently being considered as treatment for PD is rasagiline (Fig. 2.18). Rasagiline is also an irreversible inhibitor without the side effects of selegiline since it is not metabolized to amphetamine derivatives (Riederer *et al.*, 2004).

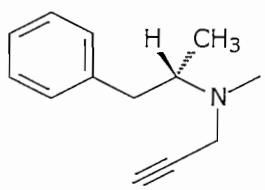

Selegiline

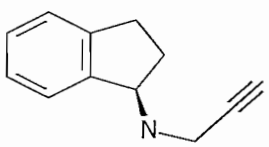

Rasagiline

Figure 2.18 The chemical structures of selegiline and rasagilline.

The current challenge is to develop selective, reversible MAO-B inhibitors for the treatment of PD. Among the inhibitors are CSC and several of its analogues. CSC is a potent MAO-B inhibitor with concurrent adenosine A_{2A} receptor antagonistic actvity. Since the inhibition of the adenosine A_{2A} receptor also has a therapeutic effect on PD, inhibiting both the A_{2A} receptor and MAO-B creates a novel means of treating PD. Certain structural features were found to enhance CSC's ability to inhibit MAO-B. It was found that the *trans* configuration of the styryl moiety of CSC as well as 1,3,7-trimethyl substitution on the xanthenyl ring are required for MAO-B inhibition. CSC is thought to occupy both cavities within the MAO-B enzyme with the caffeine group orientated towards the FAD co-factor. An analogue of CSC, KW-6002 (Fig. 2.19), is a potent A_{2A} receptor agonist and is presently undergoing clinical trials for use in PD. It is a moderately potent MAO-B inhibitor with definite neuroprotective effects. It has a K_i value of 28 μM for the inhibition of MAO-B. The K_i value of CSC is 70 nM (Vlok *et al.*, 2006; Petzer *et al.*, 2003; Van den Berg *et al.*, 2007).

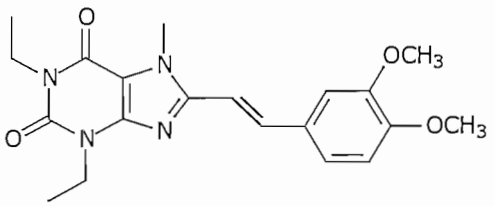

Figure 2.19 Chemical structure of KW-6002

Other potent MAO-B inhibitors worth mentioning are coumarin derivatives and safinamide. The benzyloxy side chain appears to be critical for activity for both the coumarin derivatives and safinamide (Binda *et al.*, 2007; Gnerre *et al.*, 2000). Another inhibitor is 3-methyl-8-(4,4,4-trifluoro-butoxy)indenol[1,2-c]pyridazine-5-one (Fig. 2.20), a very potent, selective and reversible inhibitor that was recently developed (Ooms et al., 2003).

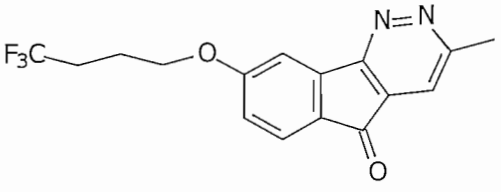

Figure 2.20 The chemical structure of 3-methyl-8-(4,4,4-trifluoro-butoxy)indenol[1,2-c]pyridazine-5-one.

2.3.6 Genetics

Genetics played an important role in better understanding how MAO-A and MAO-B functioned and the physiological effect that these enzymes exert. Through cDNA cloning the amino acid sequences of MAO-A and -B were elucidated. This revealed that MAO-A and MAO-B share a 70% amino acid sequence identity, consisting of 527 and 520 amino acids, respectively. The determination of MAO-B's structure was made possible by genetic engineering and was discussed in 2.3.3 (Nagatsu 2004; Shih *et al.*, 1999).

The difference in primary amino acid sequence and promoter organization in MAO-A and MAO-B is thought to be responsible for the differences in the catalytic activity and tissue specificity between these two isoforms (Nagatsu 2004; Shih *et al.*, 1999).

Genes encoding for MAO are situated on the X chromosome where both isoforms consist of 15 exons with identical exon-intron organization. Exon 12 codes for the FAD binding site and shares a 93,9% similarity between MAO-A and MAO-B. The fact that this exon is so highly conserved suggests that the two isoforms share a common ancestral gene. Norries disease is a disease where both the genes encoding for MAO-A and –B are deleted and results in symptoms like blindness, hearing loss and mental retardation (Nagatsu 2004; Shih *et al.*, 1999).

Interestingly, it was found that MAO-B activity in the brain increases with age, possibly due to glial cell proliferation. Another discovery was the effect that MAO, especially MAO-A, had on addictive behaviour. Smokers presented with diminished levels of MAO-A in the brain, although the mechanism remains unclear. Alcoholics showed signs of lowered MAO-B, but mutations on MAO-A was thought to be the culprit. For research purposes MAO knockout mice were created (where the MAO-A and –B genes were deleted) to investigate the effects of MAO deletion. In MAO-A knockout mice signs of aggression were observed. This aggressive behaviour was also observed in a Dutch family with a complete deficiency of MAO-A. A reason for this phenomenon can be the elevated serotonin levels in these persons due to its lack of oxidation by MAO-A (Nagatsu 2004; Shih *et al.*, 1999).

Understanding the genetics of MAO, and MAO-B specifically, enabled scientists to elucidate the structure of this enzyme and its role in the development of PD. This is an essential part in the development of new MAO-B inhibitors for the treatment of PD.

2.3.7 Other amine oxidases

Other than FAD-containing amine oxidases (AO), there exists AOs that do not employ FAD as co-factor and have different properties than MAO-A and MAO-B. These AOs catalyze oxidation reactions which can result in toxic products that contributes to oxidative stress. They are called semicarbazide sensitive amine oxidase (SSAO) and derive their name from the fact that they are sensitive to inhibition by semicarbazide. SSAOs are copper containing enzymes and often make use of topa-quinine as co-factor. For the larger part, these enzymes are found on the cell surface and differ from FAD- containing AOs in their distribution, substrate specificity, inhibitors and function. SSAOs are also found in bacteria, yeast cells, plants and other higher eukaryotes (Jalkanen *et al.*, 2001).

The structure of a SSAO was elucidated by crystallizing a SSAO of *E.coli* . It was found that SSAOs are roughly mushroom shaped and consist of four regions with the active site located deeply within the molecule (Fig. 2.25). When a substrate binds to the enzyme, the coordination position of the copper changes along with a shift in position of the topa-quinine co-factor (Parsons *et al.*, 1995).

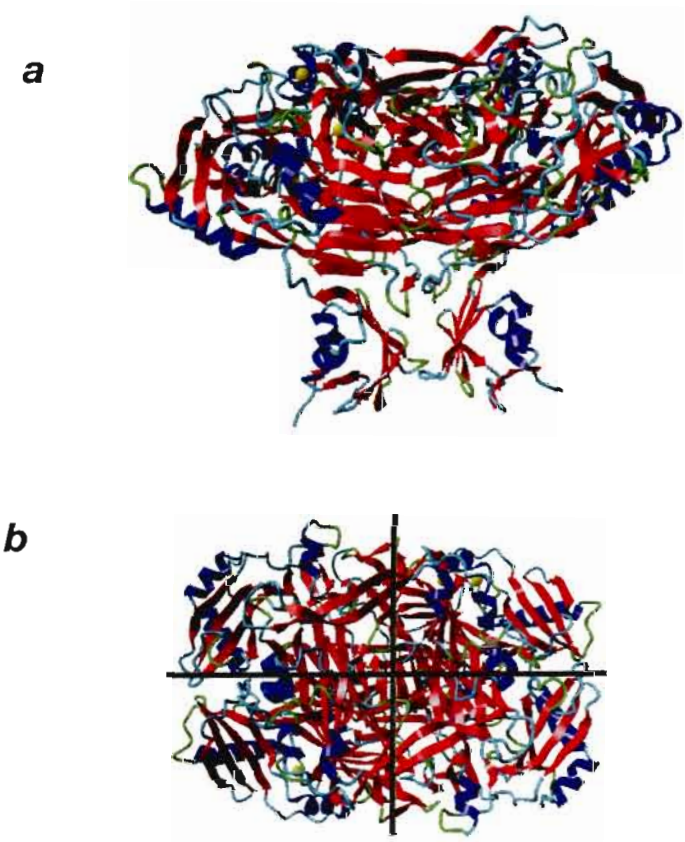

Figure 2.21 ***a***) The mushroom shaped protein structure of SSAO. ***b***) The four regions of SSAO viewed from the top.

This enzyme is mainly responsible for the oxidative deamination of primary amines through the formation of a Schiff base as intermediate product. Similar to FAD-containing AOs, oxidation reactions catalyzed by SSAOs result in the potentially harmful products, aldehydes and H_2O_2 along with ammonia, but in this case it is the topa-quinine that undergoes the reduction and re-oxidation process (Fig. 2.22) (Lee *et al.*, 2002).

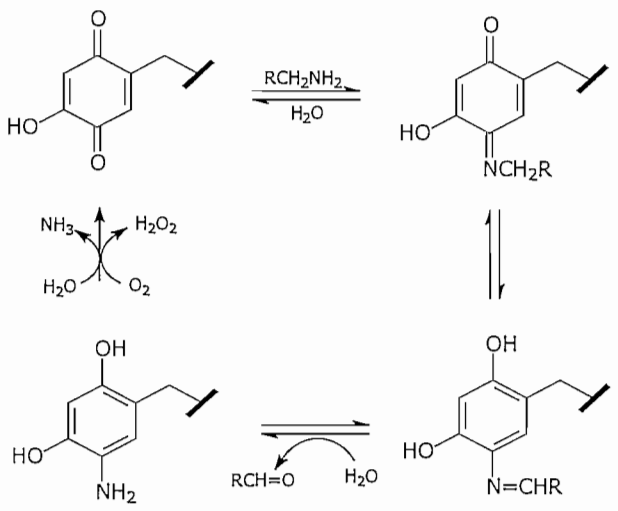

Figure 2.22 The catalytic cycle of topa-quinine.

There still remains uncertainty concerning the function of SSAO, but it is proposed that the enzyme plays a role in glucose metabolism in the adipocytes and the regulation of leukocyte trafficking in the endothelial cells. With regards to glucose metabolism it is thought that the H_2O_2 formed during SSAO oxidation regulates the glucose transporter, GLUT4. It is also believed that SSAO acts as an adhesion molecule for leukocytes through a multistep adhesion cascade.

SSAO can be subdivided into different classes, such as the soluble and membrane bound SSAOs. In the human it is supposed that the membrane bound enzyme undergoes proteolytic cleavage to form the soluble enzyme. Soluble SSAOs were found to be elevated in persons with liver diseases and diabetes. In diabetics SSAOs may cause the typical atherogenic lesions through elevated aldehyde production and ROS formation. Although SSAO occurs predominantly as an extracellular enzyme, there are a few intracellular varieties, for example, diamine oxidase. Diamine oxidase plays a role in the regulation of inflammation due to its ability to oxidize histamine. Another example of a SSAO is lysyl oxidase, a smaller enzyme that utilizes lysyl tyrosylquinone as co-factor. During extracellular matrix formation, lysyl oxidase plays a role in the cross linking of collagen and

elastin. The fact that this enzyme lacks certain features typical of other SSAOs has brought lysyl oxidase's classification as a SSAO under dispute (Jalkanen *et al.*, 2001).

2.4 Enzyme kinetics

2.4.1 Introduction

Enzyme kinetics play a key role in the determination of inhibitor potency. The inhibitor potency is expressed by the inhibitor constant, K_i. The lower the value of K_i, the higher the inhibitor potency and *visa versa*. The method of determining K_i will be discussed and illustrated in this section. A general equation for a chemical reaction between a substrate and enzyme can be illustrated as:

$$S + E \xrightarrow{v_i} SE$$

where S is the substrate and E the enzyme. The velocity of the forward reaction is shown by v_i. In the case where the substrate is in excess compared to the enzyme, v_i will be directly proportionate to the enzyme concentration ($v_i \propto [E]$). As the substrate concentration increases, v_i will increase until V_{max} is reached where a further increase in substrate will have no effect on v_i (the enzyme is saturated). In this instance v_i is dependant on how quickly the substrate is released from the enzyme for another reaction.

2.4.2 The Michaelis-Menten equation and Lineweaver-Burk plot

The Michaelis-Menten equation describes the relationship between v_i and [S], the substrate concentration:

$$v_i = \frac{V_{max}[S]}{K_m + [S]}$$

K_m is the Michaelis constant and can be described as the substrate concentration where v_i equals half of V_{max} (Fig. 2.23).

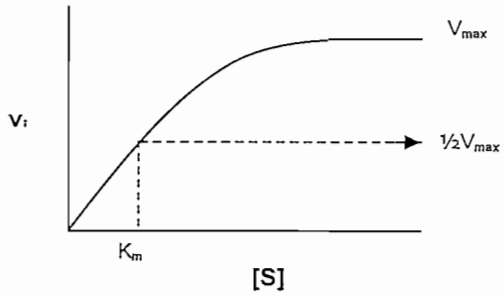

Figure 2.23 A graph of the influence of the substrate concentration on v_i. The K_m value equals the substrate concentration at $\frac{1}{2}V_{max}$.

There are three conditions under which the Michaelis-Menten equation can be evaluated:
(1) when [S] is much less than K_m then K_m + [S] can be set equal to K_m:

$$v_i = \frac{V_{max}[S]}{K_m}$$

(2) when [S] is greater than K_m then K_m + [S] can be set equal to [S]:

$$v_i = V_{max}$$

(3) when [S] equals K_m then v_i can be set equal to $V_{max}/2$:

$$v_i = \frac{V_{max}}{2}$$

Rearranging the Michaelis-Menten equation into an equation for a straight line results in the following equation:

$$\frac{1}{v_i} = \left(\frac{K_m}{V_{max}}\right)\frac{1}{[S]} + \frac{1}{V_{max}}$$

This equation can now be used to create a graph called the Lineweaver-Burk plot. The value of K_m can be calculated from the x-intercept, where $x = -1/K_m$ (Fig. 2.24).

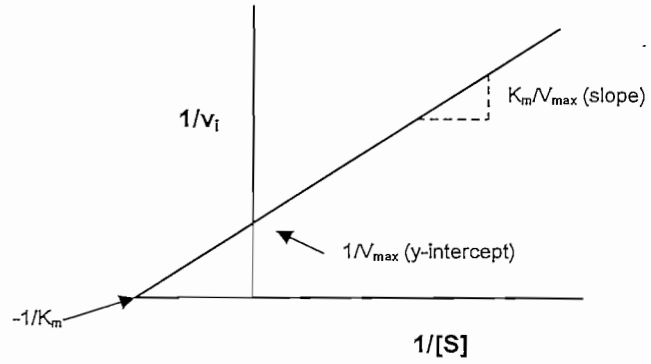

Figure 2.24 Lineweaver-Burk plot.

During competitive inhibition of an enzyme, the inhibitor competes with the substrate for binding at the active site. Typical competitive inhibition shows that two lines plotted on the Lineweaver-Burk plot, one in the presence of an inhibitor and one in the absence of an inhibitor, have a common intercept on the y-axis (Fig. 2.25).

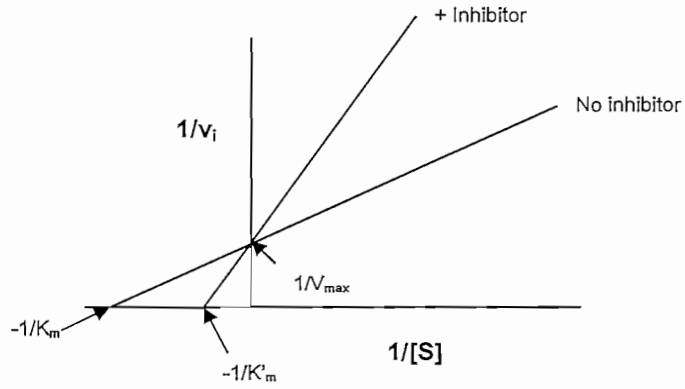

Figure 2.25 Competitive inhibition

Thus, competitive inhibition has no effect on the V_{max} value, but increases the apparent K_m value. By calculating the K_m value in the absence of the inhibitor, the K_i value can now be calculated by using the following equation:

$$x = \frac{-1}{K_m}\left(1 + \frac{[I]}{K_i}\right)$$

Lineweaver-Burk plots of non-competitive inhibition typically exhibits a constant K_m value, while V_{max} decreases (Fig. 2.26) (Murray *et al.*, 2003).

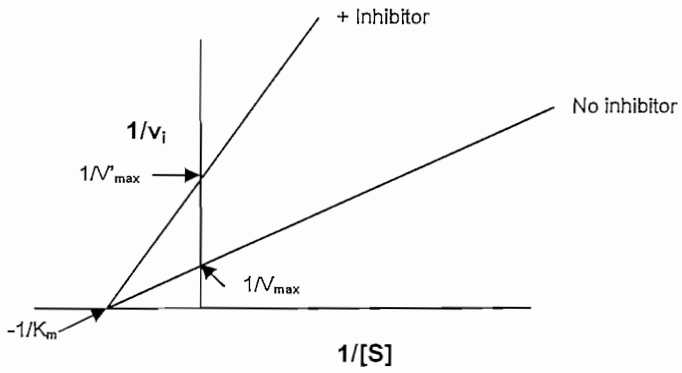

Figure 2.26 Non - competitive inhibition

According to Dixon (1952) there is an easier way to determine K_i. This is achieved by plotting $1/v_i$ against the inhibitor concentration ([I]) while the substrate concentration remains constant. Two lines are plotted for two different substrate concentrations. These two lines intercept each other left of the y-axis and the x-coordinate of interception equals $-K_i$ (Fig. 2.27).

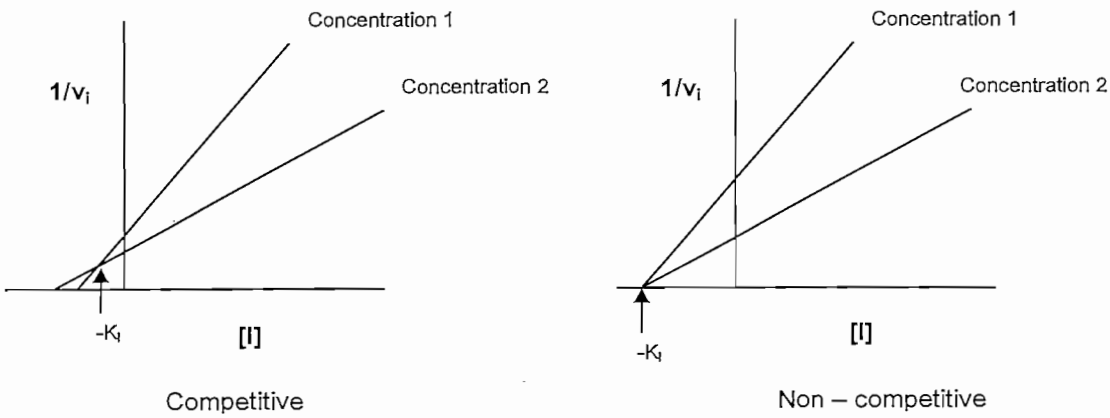

Figure 2.27 Dixon's method for determining K_i for competitive and non-competitive inhibition.

2.4.3 IC_{50} value calculation

Another way of expressing inhibitor potency is with the IC_{50} value. The IC_{50} value represents the concentration of a drug that is required for 50% inhibition *in vitro* (Fig. 2.28).

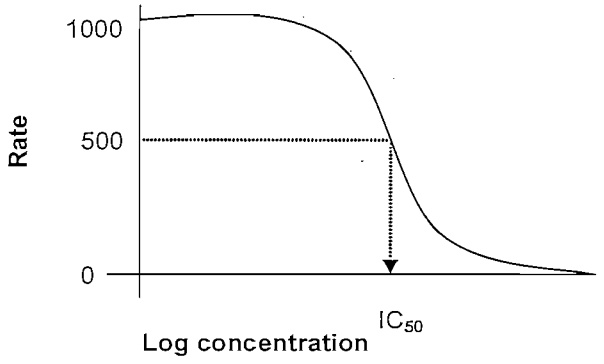

Figure 2.28 Graphical representation of the IC_{50} value.

The relationship between the K_i and the IC_{50} value can be expressed by the following eqaution: $K_i = IC_{50} / (1+[S]/K_m)$ (Cheng *et al.*, 1973).
For the study presented here, the values of [S] and K_m were as follows:

Enzyme	Substrate	Substrate concentration (μM)	K_m
Baboon MAO-B	MMTP	50	68.3 ± 1.6 μM (Pretorius *et al.*, 2008)
Human MAO-B	Kynuramine	45	52.9 ± 3.4 μM (Naoi *et al.*, 1988)
Human MAO-A	Kynuramine	30	29 ± 2 μM (Novaroli *et al.*, 2005)
Recombinant human MAO-A	Kynuramine	30	16.1 ± 0.21 μM[a]
Recombinant human MAO-B	Kynuramine	45	22.66 ± 0.72 μM[a]

[a] These K_m values were obtained experimentally as described in section 4.4.

Chapter 3

Synthesis

3.1 Introduction

The compounds that were prepared and evaluated as MAO-B and MAO-A inhibitors in this study are illustrated in table 3.1.

Table 3.1 Illustration of the compounds that will be synthesized in this study.

-R	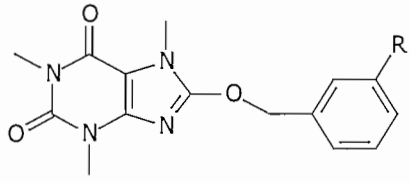
-H	**1a** 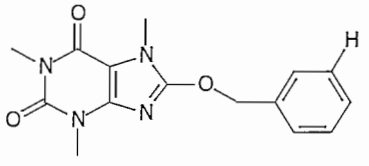
-Cl	**1b** 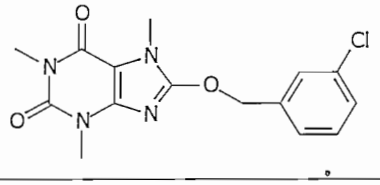
-Br	**1c** 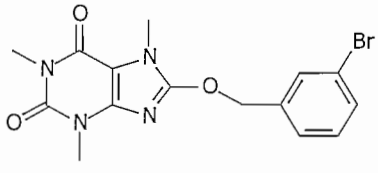
-F	**1d** 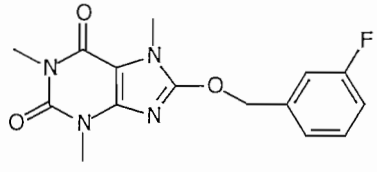

$-CF_3$	**1e**	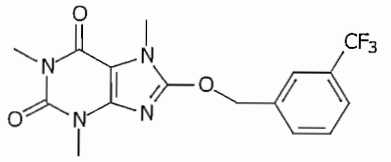
$-CH_3$	**1f**	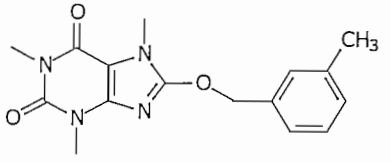
$-OCH_3$	**1g**	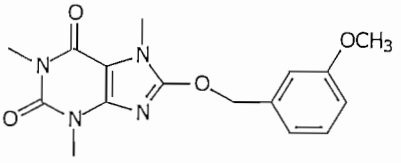

The synthesis of the unsubstituted analogue of 8-benzyloxycaffeine have previously been reported (Huston *et al.*, 1934) and was prepared by condensing 8-chlorocaffeine (**3**) (Fig. 3.1) with benzylalcohol (**2a**) (Fig. 3.1) at high temperatures in the presence of metallic sodium. In this study the same method was used to prepare the target benzyloxycaffeine analogues (**1a-g**) illustrated in table 3.1.

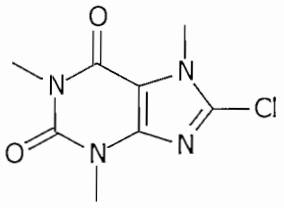

3

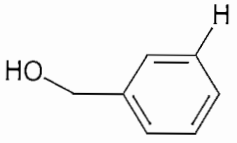

2a

Figure 3.1 The chemical structures of 8-chlorocaffeine (**3**) and benzylalcohol (**2a**).

3.2 Materials and instrumentation

Materials:

All compounds used in this study were obtained from Sigma-Aldrich.

Thin layer chromatography (TLC):

To determine that reactions were complete, TLC was used before terminating the syntheses. In the instances where silica gel were used, the mobile phase was a mixture of 80% ethyl acetate and 20% petroleum ether. Where aluminium oxide were used, 80% chloroform and 20% ethyl acetate served as the mobile phase. An UV-lamp was used to observe the thin layer platelets at a wavelength of 254 nm.

Melting points:

The melting points for all of the synthesized compounds were measured with a Stuart SMP10 apparatus and are uncorrected. The melting points of previously reported compounds (if available) were compared to the measured melting points of the inhibitors to confirm the identity of the compounds synthesized.

Mass spectra:

An Autospec ETOF (Micromass) mass spectrometer was used to determine the mass spectra of all compounds. The measured mass/charge (m/z) ratio were then compared to the calculated molar mass to confirm the identity of the compounds.

Nuclear magnetic resonance (NMR):

Proton (^{1}H) and carbon (^{13}C) spectra were recorded with a Varian Gemini 300 and a Bruker Avance III 600 apparatus. ^{1}H NMR were recorded at 600 MHz and ^{13}C NMR at 150 MHz. The chemical shifts are reported in parts per million (δ) downfield from the signal of tetramethylsilane dissolved in deuterated chloroform. Spin multiplicities are given as s (singlet), d (doublet), t (triplet), q (quartet), dd (doublet of doublets) or m (multiplet). The coupling constants (J) are expressed in hertz (Hz).

3.3 Synthesis of 8-benzyloxycaffeine analogues

An amount of 0.02 g of metallic sodium was weighed, cut into small pieces and added to the appropriate substituted benzylalcohol (24.65 mmol) (**2a-g**). When the sodium has completely reacted to yield the sodium alkoxide an equivalent amount of dry 8-chlorocaffeine (1.75 mmol)(**3**) was added to the mixture (Fig. 3.2).

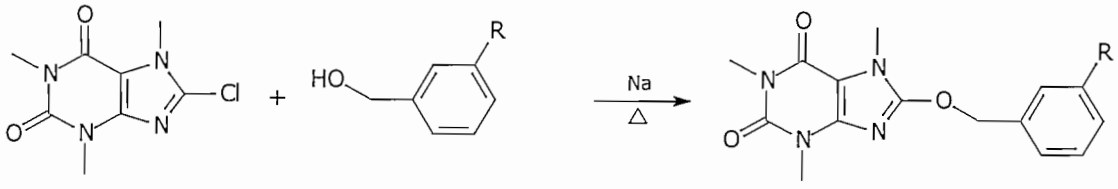

3

2a:	R = 3-H	**1a:**	R = 3-H
2b:	R = 3-Cl	**1b:**	R = 3-Cl
2c:	R = 3-Br	**1c:**	R = 3-Br
2d:	R = 3-F	**1d:**	R = 3-F
2e:	R = 3-CF_3	**1e:**	R = 3-CF_3
2f:	R = 3-CH_3	**1f:**	R = 3-CH_3
2g:	R = 3-OCH_3	**1g:**	R = 3-OCH_3

Figure 3.2 An illustration of the synthesis of 8-benzyloxycaffeine analogues.

The resulting mixture was heated under reflux on an oil bath with occasional shaking for a half hour to 5 hours depending on the rate of the reaction. It is important to note that the reaction temperature should be kept between 150 and 170 °C due to decomposition of the target compound at higher temperatures (Huston *et al.*, 1934). While the solution was still hot, it was filtered to remove the sodium chloride that has formed during the reaction. The sodium chloride was washed with small quantities of the benzylalcohol that was used in the reaction. After the mixture was cooled, the 8-benzyloxycaffeine analogues were obtained by crystallization. Crystallization was enhanced by the addition of 40 – 50% ethanol and cooling the mixture to 4 °C. Clusters of very small 8-benzyloxycaffeine crystals formed. Since 8-chlorocaffeine is not commercially available it was synthesized according to the following procedure.

Synthesis of 8-chlorocaffeine:

Following the method of Fischer *et al.* (1883), 8-chlorocaffeine (**3**) was prepared by heating 2.5 g dry caffeine (**4**) in 20 ml chloroform under reflux until all the caffeine has dissolved. Dry chlorine gas was subsequently bubbled through the solution. It is extremely important that no water is introduced to the reaction. For this reason the chlorine gas was dried by first passing it through sulphuric acid. During the reaction, hydrochloric acid (HCl) is formed. After a short interval a precipitate formed (the HCl salt of caffeine), but the reaction was continued until the precipitate again dissolved and the formation of HCl ceased. In this manner 50 g of caffeine can be chlorinated in 30 minutes (Fig. 3.3). The chloroform was removed via distillation using a rotary avaporater and the crystals were freed from the residual chloroform by heating it with a small amount of water. White 8-chlorocaffeine crystals were obtained in high yield (95 – 100%)

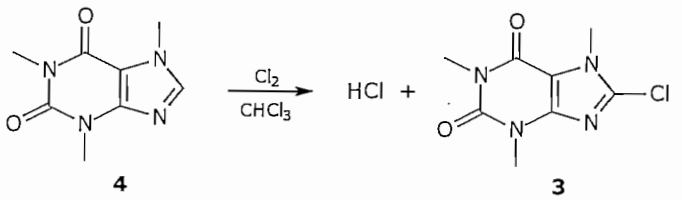

4 **3**

Figure 3.3 The synthesis of 8-chlorocaffeine

The chlorine gas used in the synthesis was prepared in the laboratory since only small quantities were needed for this synthetic procedure.

Synthesis of chlorine gas:

Chlorine gas was prepared by the reaction between HCl and potassium permanganate ($KMnO_4$) by using the apparatus in figure 3.4.

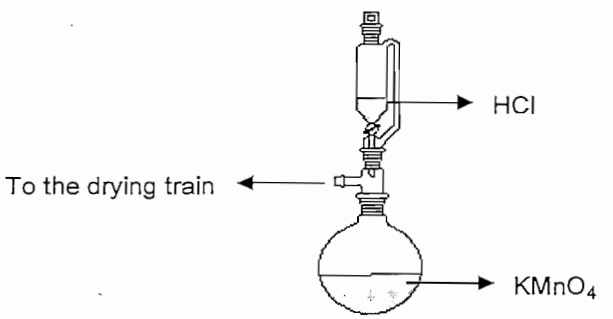

Figure 3.4 The apparatus used for the synthesis of chlorine gas.

It is important that this reaction should be carried out in a fume cupboard as chlorine is toxic and an irritant. The required quantity of $KMnO_4$ (0.367 g $KMnO_4$ for the production of 0.412 g Cl_2) was placed in a round-bottomed flask and 20.17 ml of concentrated HCl (32%) was placed in a pressure equalizing funnel which was secured by an elastic band. The HCl was slowly dropped onto the $KMnO_4$ while the flask was occasionally shaken. A flask containing water was connected to the device and the formed Cl_2 gas was passed through the water to remove hydrogen chloride from the chlorine. The Cl_2 gas was passed through another flask containing concentrated sulphuric acid to dry the gas. An empty flask was finally used as safety measure between the reaction vessel and the dry chlorine generating source.

After half of the acid has been dropped onto the $KMnO_4$ crystals, the formation of chlorine begins to recede and the flask was warmed slightly. When all the acid has been added the mixture was boiled to complete the formation of chlorine (Fig. 3.5) (Vogel *et al.*, 1989). The equipment was aranged in such a manner that the chlorine gas could be directly used for the 8-chlorocaffeine synthesis (Fig. 3.6).

$$2KMnO_4 + 16HCl \longrightarrow 2MnCl_2 + 2KCl + 8H_2O + 5Cl_2$$

Figure 3.5 The chemical reaction for the synthesis of chlorine gas.

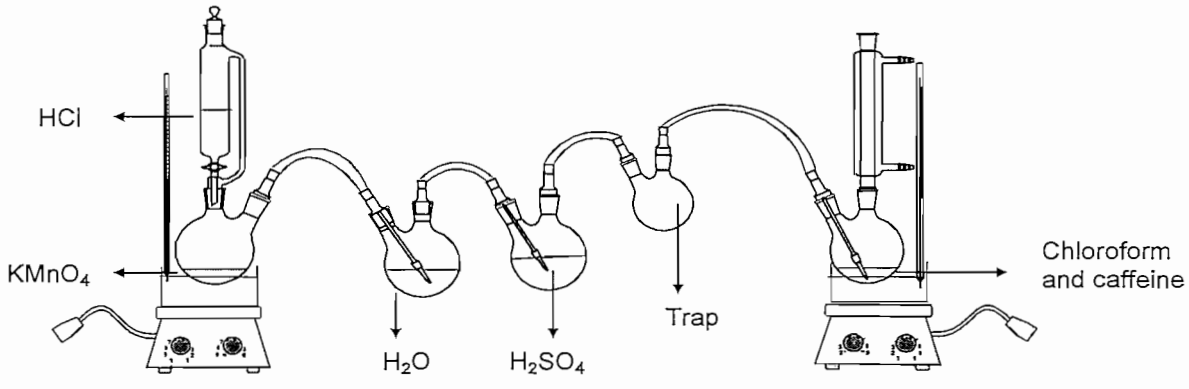

Figure 3.6 Experimental setup of the chlorine and 8-chlorocaffeine synthesis.

3.4 Results

The NMR spectrums for all the compounds synthesized can be viewed in appendix A.

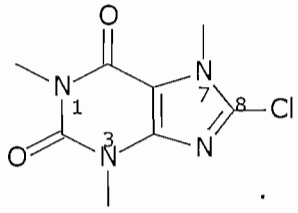

3

8-Chlorocaffeine (**3**) was prepared from caffeine (**4**) and chlorine gas in a yield of 100%: mp 188 °C; ^{1}H NMR ($CDCl_3$) δ 3.34 (s, 3H), 3.51 (s, 3H), 3.91 (s, 3H); ^{13}C NMR ($CDCl_3$) δ 26.93 (CH_3), 29.76 (CH_3), 32.63 (CH_3), 108.17 (C), 138.91 (C), 146.99 (C), 151.2 (C), 154.49 (C); HRMS calculated 228.64 ($M^{\cdot+}$), found: 228 ($M^{\cdot+}$).

^{1}H NMR:

- The three methyl groups at N1, N3 and N7 correspond to the singlets at 3.34, 3.51 and 3.91 ppm (the signals integrate for 3 protons each)

^{13}C NMR:

- Methyl groups at N1, N3 and N7 are represented by signals at 26.93, 29.76 and 32.63 ppm
- C8 and the remaining carbons resonate at 108.17, 138.91, 146.99, 151.2 and 154.49 ppm

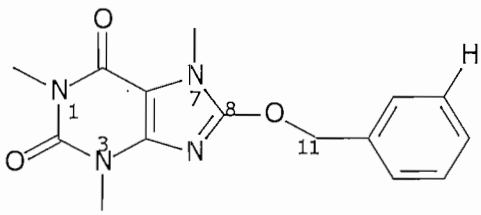

1a

8-Benzyloxycaffeine (**1a**) was prepared from 8-chlorocaffeine (**3**) and benzyl alcohol (**2a**) in a yield of 29%: mp 173 °C; ^{1}H NMR ($CDCl_3$) δ 3.36 (s, 3H), 3.52 (s, 3H), 3.69 (s, 3H), 5.47 (s, 2H), 7.32 – 7.46 (m, 5H); ^{13}C NMR ($CDCl_3$) δ 29.8 (CH_3), 29.71 (CH_3), 27.68 (CH_3), 72.52 (CH_2), 103.532 (C), 135 (CH), 128.84 (CH), 128.66 (CH), 128.41 (CH), 155.51 (C), 154.8 (C), 151.66 (C), 146.16 (C); HRMS calculated 300.32 ($M^{\cdot+}$), found: 300 ($M^{\cdot+}$).

^{1}H NMR:

- The three methyl groups at N1, N3 and N7 correspond to the singlets at 3.36, 3.52 and 3.69 ppm (the signals integrate for 3 protons each)
- The methylene group at C11 is represented by the singlet at 5.47 ppm (the signal integrates for 2 protons)
- Aromatic protons on the phenyl ring correspond with the multiplets at 7.32 – 7.46 ppm (the multiplets integrate for 5 protons).

^{13}C NMR:

- Methyl groups at N1, N3 and N7 are represented by signals at 29.8, 29.71 and 27.68 ppm
- The methylene C11 signal is at 72.52 ppm
- C8 corresponds to the signal at 103.532 ppm
- Aromatic carbons are represented by signals at 135, 128.84, 128.66 and 128.41 ppm
- The remaining carbons resonate at 155.51, 154.8, 151.66 and 146.16 ppm

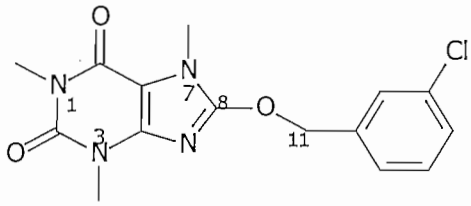

1b

8-(3-Chlorobenzyloxy)caffeine (**1b**) was prepared from 8-chlorocaffeine (**3**) and 3-chlorobenzyl alcohol (**2b**) in a yield of 22%: mp 174 °C; ^{1}H NMR ($CDCl_3$) δ 3.35 (s, 3H), 3.5 (s, 3H), 3.68 (s, 3H), 5.42 (s, 2H), 7.45 (s, 1H), 7.3 (m, 3H); ^{13}C NMR ($CDCl_3$) δ 29.85 (CH_3), 29.7 (CH_3), 27.7 (CH_3), 71.5 (CH_2), 103.631 (C), 126.34, 128.44, 128.96, 129.96, 134.58, 136.96, 146.03, 151.62, 154.8, 155.17; HRMS calculated 334.76 ($M^{\cdot+}$), found: 334 ($M^{\cdot+}$).

^{1}H NMR:

- The three methyl groups at N1, N3 and N7 correspond to the singlets at 3.35, 3.5 and 3.68 ppm (the signals integrate for 3 protons each)
- The methylene group at C11 is represented by the singlet at 5.42 ppm (the signal integrates for 2 protons)
- Aromatic protons on the phenyl ring correspond with the singlet at 7.45 which integrates for one proton and the multiplet at 7.3 ppm which integrates for 3 protons

^{13}C NMR:

- Methyl groups at N1, N3 and N7 are represented by signals at 29.85, 29.7 and 27.7 ppm
- The methylene C11 signal is at 71.5 ppm
- C8 corresponds to the signal at 103.631 ppm
- Aromatic carbons are represented by signals at 126.34, 128.44, 128.96, 129.96, 134.58 and 136.93 ppm
- The remaining carbons resonate at 146.03, 151.62, 154.8 and 155.17 ppm

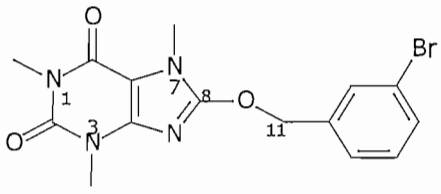

1c

8-(3-Bromobenzyloxy)caffeine (**1c**) was prepared from 8-chlorocaffeine (**3**) and 3-bromobenzyl alcohol (**2c**) in a yield of 33%: mp 169 °C; ^{1}H NMR ($CDCl_3$) δ 3.34 (s, 3H), 3.49 (s, 3H), 3.68 (s, 3H), 5.4 (s, 2H), 7.6 (s, 1H), 7.48 (d, 1H), 7.36 (d, 1H), 7.2 – 7.28 (t, 1H); ^{13}C NMR ($CDCl_3$) δ 29.86 (CH_3), 29.71 (CH_3), 27.7 (CH_3), 71.43 (CH_2), 103.636 (C), 126.85, 130.23, 131.41, 131.9, 122.66, 137.18, 146.03, 151.62, 154.8, 155.15; HRMS calculated 379.21 ($M^{\cdot+}$), found: 378 ($M^{\cdot+}$).

^{1}H NMR:

- The three methyl groups at N1, N3 and N7 correspond to the singlets at 3.34, 3.49 and 3.68 ppm (the signals integrate for 3 protons each)
- The methylene group at C11 is represented by the singlet at 5.4 ppm (integrates for 2 protons)
- Aromatic protons on the phenyl ring correspond with the singlet at 7.6 which integrates for one proton, two doublets at 7.48 and 7.36 which integrates for one proton each and a triplet at 7.2 – 7.28 which integrates for one proton.

^{13}C NMR:

- Methyl groups at N1, N3 and N7 are represented by signals at 29.86, 29.71 and 27.7 ppm
- The methylene C11 signal is at 71.43 ppm
- C8 corresponds to the signal at 103.636 ppm
- Aromatic carbons are represented by signals at 126.85, 130.23, 131.41, 131.9, 122.66 and 137.18 ppm
- The remaining carbons resonate at 146.03, 151.62, 154.8 and 155.15 ppm

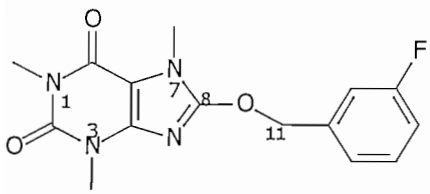

1d

8-(3-Fluorobenzyloxy)caffeine (**1d**) was prepared from 8-chlorocaffeine (**3**) and 3-fluorobenzyl alcohol (**2d**) in a yield of 44%: mp 185 °C; ^{1}H NMR ($CDCl_3$) δ 3.35 (s, 3H), 3.5 (s, 3H), 3.69 (s, 3H), 5.43 (s, 2H), 6.98 - 7.08 (m, 1H), 7.1 – 7.22 (m, 2H), 7.3 – 7.38 (m, 1H); ^{13}C NMR ($CDCl_3$) δ 29.83 (CH_3), 29.7 (CH_3), 27.69 (CH_3), 71.51 (CH_2), 103.62 (C), 115.3, 115.86, 123.74, 130.33, 137.45, 155.2, 146.05, 151.62, 161.18, 164.46; HRMS calculated 318.31 ($M^{\cdot+}$), found: 318 ($M^{\cdot+}$).

^{1}H NMR:

- The three methyl groups at N1, N3 and N7 correspond to the singlets at 3.35, 3.5 and 3.69 ppm (the signals integrate for 3 protons each)
- The methylene group at C11 is represented by the singlet at 5.43 ppm (integrates for 2 protons)
- Aromatic protons on the phenyl ring correspond with the multiplets at 6.98 – 7.08 (integrates for 1 proton), 7.1 – 7.16, 7.16 – 7.22 (integrate for 2 protons) and 7.3 – 7.38 (integrates for 1 proton)

^{13}C NMR:

- Methyl groups at N1, N3 and N7 are represented by signals at 29.83, 29.7 and 27.69 ppm
- The methylene C11 signal is at 71.51 ppm
- C8 corresponds to the signal at 103.62 ppm
- Aromatic carbons are represented by signals at 115.3, 115.86, 123.74, 130.33, 137.45 and 155.2 ppm
- The remaining carbons resonate at 146.05, 151.62, 161.18 and 164.46 ppm

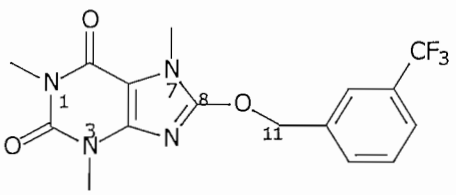

1e

8-(3-Ttrifluoromethyl)benzyloxy)caffeine (**1e**) was prepared from 8-chlorocaffeine (**3**) and 3-(trifluoromethyl)benzyl alcohol (**2e**) in a yield of 22%: mp 146 °C; ^{1}H NMR ($CDCl_3$) δ 3.34 (s, 3H), 3.56 (s, 3H), 3.69 (s, 3H), 5.5 (s, 2H), 7.27 – 7.51 (m, 4H); ^{13}C NMR ($CDCl_3$) δ 29.85 (CH_3), 29.66 (CH_3), 27.69 (CH_3), 71.52 (CH_2), 103.67 (C), 129.23, 131.26, 335.96, 125.65, 131.26, 122.93, 125.65, 146.01, 151.62, 154.81, 155.09; HRMS calculated 368.32 ($M^{\cdot+}$), found: 368 ($M^{\cdot+}$).

^{1}H NMR:

- The three methyl groups at N1, N3 and N7 correspond to the singlets at 3.34, 3.56 and 3.69 ppm (the signals integrate for 3 protons each)
- The methylene group at C11 is represented by the singlet at 5.5 ppm (integrates for 2 protons)
- Aromatic protons on the phenyl ring correspond with the multiplets at 7.51 – 7.27 ppm (integrates for 4 protons)

^{13}C NMR:

- Methyl groups at N1, N3 and N7 are represented by signals at 27.69, 29.66 and 29.85 ppm
- The methylene C11 signal is at 71.52 ppm
- C8 corresponds to the signal at 103.67 ppm
- Aromatic carbons are represented by signals at 129.23, 131.26, 335.96, 125.65, 131.26 and 122.93 ppm
- The remaining carbons resonate at 125.65, 146.01, 151.62,154.81 and 155.09 ppm

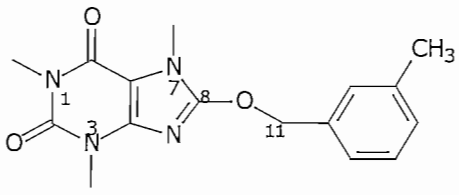

1f

8-(3-Methylbenzyloxy)caffeine (**1f**) was prepared from 8-chlorocaffeine (**3**) and 3-methylbenzyl alcohol (**2f**) in a yield of 13%: mp 145 °C; ^{1}H NMR ($CDCl_3$) δ 3.42 (s, 3H), 3.58 (s, 3H), 3.74 (s, 3H), 2.43 (s, 3H), 5.5 (s, 2H), 7.24 – 7.34 (m, 4H); ^{13}C NMR ($CDCl_3$) δ 21.3 (CH_3), 27.64 (CH_3), 29.66 (CH_3), 29.77 (CH_3), 72.59 (CH_2), 103.47 (C), 125.48, 128.54, 129.13, 129.56, 134.87, 138.37, 146.15, 151.63, 154.75, 155.54; HRMS calculated 314.34 ($M^{\cdot+}$), found: 314 ($M^{\cdot+}$).

^{1}H NMR:

- The three methyl groups at N1, N3 and N7 correspond to the singlets at 3.42, 3.58 and 3.74 ppm (the signals integrate for 3 protons each)
- The methyl on the phenyl ring corresponds with a singlet at 2.43 ppm which integrates for 3 protons
- The methylene group at C11 is represented by the singlet at 5.5 ppm (integrates for 2 protons)
- Aromatic protons on the phenyl ring correspond with multiplets at 7.24 – 7.34 ppm which integrates for 4 protons

^{13}C NMR:

- Methyl groups at N1, N3, N7 and on the phenyl ring are represented by signals at 21.3, 27.64, 29.66 and 29.77 ppm
- The methylene C11 signal is at 72.59 ppm
- C8 corresponds to the signal at 103.47 ppm
- Aromatic carbons are represented by signals at 125.48, 128.54, 129.13, 129.56, 134.87 and 138.37 ppm
- The remaining carbons resonate at 146.15, 151.63, 154.75 and 155.54 ppm

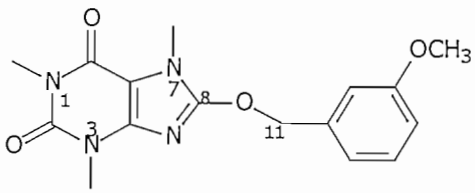

1g

8-(3-Methoxybenzyloxy)caffeine (**1g**) was prepared from 8-chlorocaffeine (**3**) and 3-methoxybenzyl alcohol (**2g**) in a yield of 30%: mp 144 °C; ^{1}H NMR ($CDCl_3$) δ 3.3 (s, 3H), 3.4 (s, 3H), 3.6 (s, 3H), 3.8 (s, 3H), 5.5 (s, 2H), 6.9 – 7.5 (m, 4H); ^{13}C NMR ($CDCl_3$) δ 29.85 (CH_3), 29.75 (CH_3), 27.72 (CH_3), 55.27 (CH_3), 72.38 (CH_2), 103.56 (C), 114.14, 114.07, 120.56, 129.79, 136.48, 146.16, 151.68, 154.80, 155.49, 159.8; HRMS calculated 330.34 ($M^{\cdot+}$), found: 330 ($M^{\cdot+}$).

^{1}H NMR:

- The four methyl groups at N1, N3, N7 and the methyl group on the phenyl ring correspond to the singlets at 3.3, 3.4, 3.6 and 3.8 ppm (the signals integrate for 3 protons each)
- The methylene group at C11 is represented by the singlet at 5.5 ppm (integrates for 2 protons)
- Aromatic protons on the phenyl ring correspond with multiplets at 6.9 – 7.5 ppm which integrates for 4 protons

^{13}C NMR:

- Methyl groups at N1, N3 and N7 are represented by signals at 29.85, 29.75 and 27.72 ppm
- The carbon in the methoxy group on the phenyl ring resonates at 55.27 ppm
- The methylene C11 signal is at 72.38 ppm
- C8 corresponds to the signal at 103.56 ppm
- Aromatic carbons are represented by signals at 114.14, 114.07, 120.56, 129.79, 136.48 and 146.16 ppm
- The remaining carbons resonate at 151.68, 154.80, 155.49 and 159.8 ppm

Chapter 4

Enzymology

4.1 Approaches to the measurement of *in vitro* catalytic activity of MAO

There are several ways in which the activity of MAO can be measured *in vitro.* The most common method used is the spectrophotometric measurement of the products formed during MAO oxidation (Inoue *et al.*, 1999; Zhou *et al.*, 1996). There are various other assay techniques, apart from spectrophotometry, to determine MAO activity:

Radiometric – This is a method that relies on the formation of radio labeled aldehydes. It is a widely used, discontinuous method with a high level of sensitivity and specificity. The availability of radio labeled physiological substrates also made this a popular method. (Holt *et al.*, 1997; Nicotra *et al.*, 1999).

Ammonia detection –In this assay the production of ammonia during amine oxidation is measured continuously. Unfortunately not all amines form ammonia during their oxidation by MAO-B (Holt *et al.*, 1997; Nicotra *et al.*, 1999).

Polarographic – With this method, oxygen consumption is measured as an indicator of the extent to which oxidation takes place. This is an accurate and reproducible method, but it lacks sensitivity and specificity (Holt *et al.*, 1997; Meyerson *et al.*, 1978).

Luminometric - This is a highly specific and accurate method developed by O' Brien *et al.* (1993) where it is described how H_2O_2 (a product of MAO-B oxidation) catalyses a reaction that transforms luminol into a substance that emits light. Measuring the extent of light emission directly correlates with MAO-B activity. The substrate chosen must not be oxidized by H_2O_2 more readily than luminol.

During this study two techniques were used : Spectrophotometry with MMTP as substrate and a fluorometric assay with kynuramine as substrate.

4.1.1 Spectrophotometric assay

In this assay the extent to which MMTP is oxidized by MAO-B to $MMDP^+$ (Fig. 4.1) in the presence of the inhibitors is measured spectrophotometrically. Production of $MMDP^+$ is measured at a wavelength of 420 nm where neither the substrate (MMTP) nor the inhibitors absorb light. Advantages of using MMTP are its stability and solubility in water. The disadvantage of using MMTP is the toxicity of the substance (Inoue *et al.*, 1999). $MMDP^+$ is very stable *in vitro* and does not undergo further oxidation. IC_{50} values can hence be calculated to compare inhibition potencies of the inhibitors (Vlok *et al.*, 2006). The enzyme used for the MMTP assay is obtained from baboon liver due to its rich content of MAO-B.

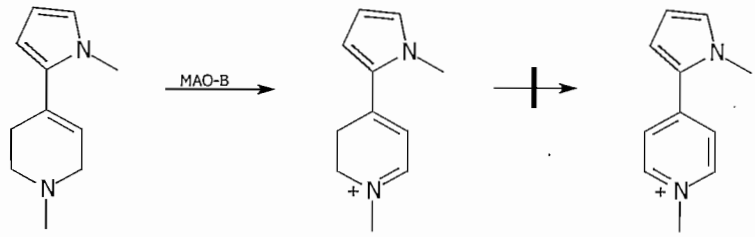

Figure 4.1 Oxidation of MMTP to $MMDP^+$ by MAO-B

Method:

The Baboon liver mitochondrial fraction was isolated as described by Salach *et al.* (1987) and stored at -70 °C. An equal amount of sodium phosphate buffer (100 mM, pH 7.4) which contains glycerol (50%, w/v) was added to the mitochondrial fraction. The protein concentration was determined using the method of Bradford with bovine serum albumin as reference standard (Bradford *et al.*, 1976).

All the reactions were prepared in sodium phosphate buffer (100 mM, pH 7.4). The incubations contained various concentrations of the test inhibitor (0 – 100 µM), 50 µM MMTP (substrate) and enzyme (0.15 mg/ml) resulting in a final incubation volume of 500 µL. The stock solution of the test inhibitors were prepared to give a 4% (v/v) concentration of DMSO in the final solution for incubation. A higher DMSO concentration can cause MAO-B inhibition (Gnerre *et al.*, 2000).

The reactions were incubated at 37 °C for 10 minutes and stopped with 10 µL perchloric acid (70%). It was found that $MMDP^+$ production is linear for the first 10 minutes under these conditions (Pretorius *et al.*, 2008). The incubations were centrifuged at 16 000 g for 10 minutes. $MMDP^+$ concentrations in the supernantant were measured spectrophotometrically a wavelenghth of 420 nm (ε = 25,000 M^{-1}) using a Shimadzu UV2100 apparatus.

IC_{50} values were calculated by plotting the initial oxidation rate versus the logarithm of the inhibitor concentration and then obtaining the sigmoidal dose–response curve. These data were fitted into the one site competition model using the Prism 4 software package (GraphPad Software Inc.). The IC_{50} values were determined in duplicate and are expressed as mean ± standard error of the mean (SEM).

4.1.2 Fluorometric assay

This method is based on the fact that certain MAO-B substrates are oxidized to fluorescent products. The substrate used in this study was kynuramine which is oxidized to 4-hydroxyquinoline (Fig. 4.2). The generation of this product can subsequently be measured with a fluorescence spectrophotometer. (Zhou *et al.*, 1996; Nicotra *et al.*, 1999). Inhibitor potencies are expressed as an IC_{50} value for each inhibitor. This fluorometric method is frequently used to determine the activities of recombinant human MAO-A and MAO-B. The fluorometric method has the advantage that it is more sensitive than the spectrophotometric method (Matsumoto *et al.*, 1985) and is therefore more suitable to measure activities of recombinant human MAO-A and MAO-B which displays relative low activities compared to baboon liver mitochondrial MAO-B. The spectrophotometric method was therefore used to measure activities of baboon liver MAO-B while the fluorometric method was used to determine the activities of recombinant human MAO-A and MAO-B.

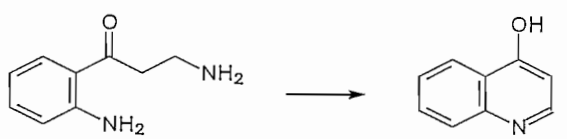

Kynuramine 4-Hydroxy quinoline

Figure 4.2 The oxidation of kynuramine

Method:

Recombinant human MAO-A (5 mg/ml) and MAO-B (5 mg/ml) were obtained from Sigma-Aldrich, pre-aliquoted and stored at -70 °C. Before use MAO-A was diluted to 0.075 mg/ml and MAO-B was diluted to 0.15 mg/ml in a potassium phosphate buffer (100 mM, pH 7.4).

All reactions were prepared in potassium phosphate buffer (100 mM, pH 7.4) containing various concentrations of the test inhibitor (0 – 100 µM), kynuramine (substrate) and the respective enzyme. The kynuramine added to the incubations resulted in final concentrations of 45 µM for MAO-A and 30 µM for MAO-B. The final volume of the incubations were 500 µL. Stock solutions of the test inhibitors were prepared to give a 4% (v/v) concentration of DMSO in the final incubations. The final concentration of MAO-A in each incubation was 0.0075 mg/ml while the final concentration of MAO-B was 0.015 mg/ml.

The reactions were incubated for 20 minutes at 37 °C and terminated with 200 µL NaOH (2 N). 1200 µL distilled water were added to each incubation before it was centrifuged for 10 minutes at 16 000 g. The concentration of 4-hydroxyquinoline in each incubation was determined by measuring the fluorescence of the supernatant at an excitation wavelength of 310 nm and an emission wavelength of 400 nm. For this purpose a Varian Cary Eclipse fluorescence spectrophotometer was used. The PMT voltage was set to medium with an excitation and emission slit width of 5 mm each.

IC_{50} values were determined by plotting the initial rate of oxidation versus the logarithm of the inhibitor concentration and obtaining a resulting sigmoidal dose–response curve. A calibration curve was prepared for each data set by measuring the fluorescence of increasing concentrations of 4-hydroxyquinoline (0.188 -6.25 µM) in a mixture of DMSO (4%) and potassium phosphate (500 µL).To each calibrated standard a volume of 200 µL NaOH (2N) and 1200 µL distilled water was added. The values obtained for the calibration curve should bracket the fluorescence values obtained for the test inhibitor and it should also display linearity. The inhibition data were fitted to an one site competition model using the Prism 4 software package. The IC_{50} values were determined in duplicate and are expressed as mean ± SEM.

4.1.3 Results

All the IC_{50} values obtained for the various MAO enzymes are listed in table 4.1 and are expressed in µM. The most potent inhibition value (lowest IC_{50}) for each enzyme is highlighted in grey. 8-(3-Trifluorobenzyloxy)caffeine proved to be the most potent inhibitor for baboon MAO-B with an IC_{50} of 112 nM. The calculated K_i value using the equation in 2.4.3 is therefore 64.7 nM. This is approximately twofold more potent than the lead compound, CSC, which inhibits MAO-B with a K_i value of 128 nM (Vlok *et al.*, 2006).

Table 4.1 IC_{50} values for the inhibition of baboon liver MAO-B, human MAO-B and MAO-A by 8-benzyloxycaffeine analogues.

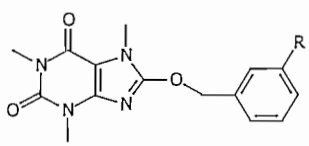	IC_{50} MAO-B (baboon) µM	IC_{50} MAO-B (human) µM	IC_{50} MAO-A (human) µM
-H	2.49 ± 0.029	1.77 ± 0.151	1.24 ± 0.035
-Cl	0.120 ± 0.031	0.107 ± 0.013	0.666 ± 0.011
-Br	0.113 ± 0.005	*0.068 ± 0.003*	0.941 ± 0.007
-F	0.534 ± 0.065	0.542 ± 0.042	1.07 ± 0.092
-CF_3	*0.112 ± 0.016*	0.152 ± 0.003	3.72 ± 0.179
-CH_3	0.698 ± 0.007	0.546 ± 0.022	*0.397* ± 0.013
-OCH_3	1.59 ± 0.431	1.01 ± 0.196	3.15 ± 0.017

A typical graph for the measurement of IC_{50} values is shown in figure 4.3. The catalytic rate of the enzyme is plotted against the logarithm of the inhibitor concentration. The IC_{50} value is obtained as explained earlier by calculating the concentration of the inhibitor which results in a reduction of 50% of the rate obtained in the absence of inhibitor. This graph is for 8-(3-bromobenzyloxy)caffeine which was the most potent inhibitor for human MAO-B with an IC_{50} of 0.068 ± 0.003 µM.

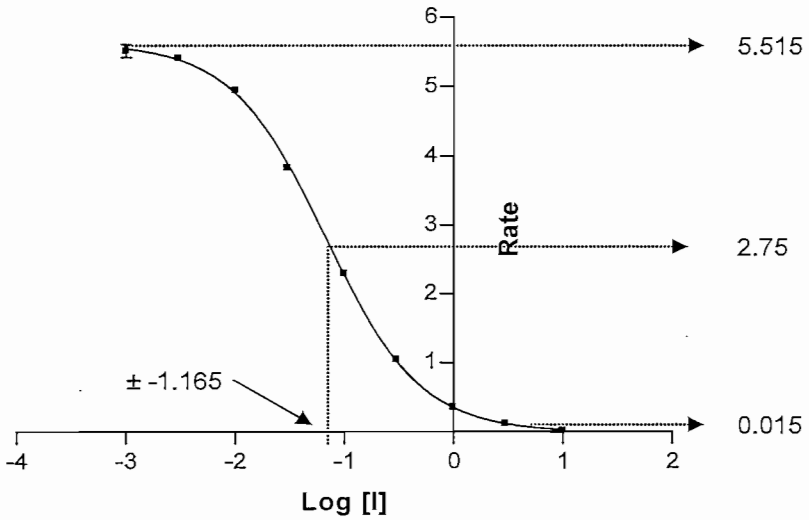

Figure 4.3 The IC_{50} calculation of 8-(3-bromobenzyloxy)caffeine towards human MAO-B: Log [I] = -1.165, which is equal to [I] = 0.068 µM. The rate is expressed as nmol product formed/min/mg protein.

The 8-benzyloxycaffeine analogues were not only potent MAO-B inhibitors, but inhibited MAO-A as well. The most potent MAO-A inhibitor was 8-(3-methylbenzyloxy)caffeine with an IC_{50} value of 0.397 ± 0.013 µM (figure 4.4). This compound was also a relatively good MAO-B inhibitor and can therefore be used as lead where dual MAO-A and -B inhibition may be required.

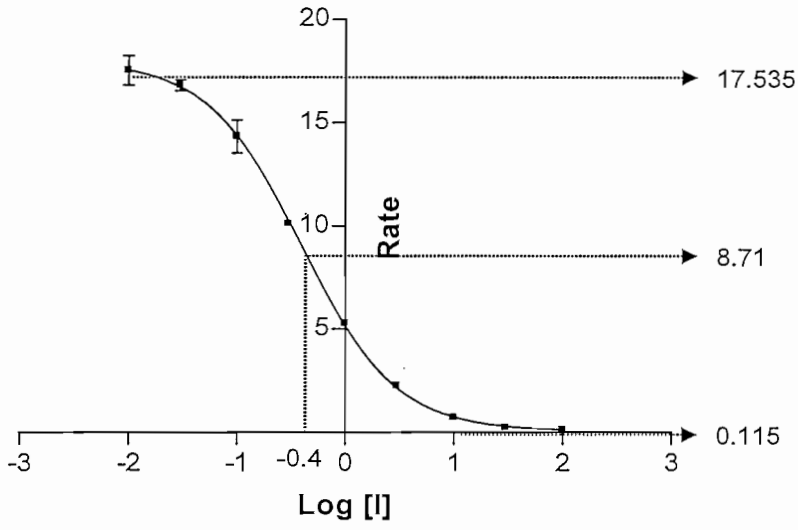

Figure 4.4 The IC_{50} calculation of 8-(3-methylbenzyloxy)caffeine towards human MAO-A: Log [I] = -0.4, which is equal to [I] = 0.397 µM. The rate is expressed as nmol product formed/min/mg protein.

4.2 K_m determination

In order to select appropriate substrate concentrations for the inhibition studies in 4.1 K_m values were determined for the oxidation of kynuramine by recombinant human MAO-A and –B. The K_m values can also be used to calculate the K_i values for the inhibition of the recombinant human enzymes by **1a-g**. The K_i values can be used to calculate inhibitor selectivities between MAO-A and –B. In this study the oxidation rate of various concentrations of kynuramine by recombinant human MAO-A and –B was measured in order to determine the K_m value.

4.2.1 Method

The oxidation rate of kynuramine were measured at 6 different concentrations ranging from 2.5 µM to 80 µM. For MAO-A the final enzyme concentration in the incubations was 0.00375mg/ml while the final concentration for MAO-B was 0.0075mg/ml. All the incubations were prepared in a buffer of potassium phosphate (100 mM, pH 7.4) and were incubated for 20 minutes at 37 °C. The reactions were stopped with 200 µL NaOH (2N) and 1200 µL distilled water was added before they were centrifuged for 10 minutes at 16 000 g. The incubations were carried out in duplicate.

A calibration curve was prepared for each data set by measuring the fluorescence of increasing concentrations of 4-hydroxyquinoline (0.188 – 6.25 µM) in a mixture of DMSO (4%) and potassium phosphate (100 mM, pH 7.4). To each calibration standard a volume of 200 µL NaOH (2N) and 1200 µL distilled water was added. The concentration of 4-hydroxyquinoline in each incubation and calibration standard were determined fluorometrically by measuring the fluorescence of the supernatant at an excitation wavelength of 310 nm and an emission wavelength of 400 nm. The PMT voltage was set to medium with an excitation and emission slit width of 5 mm each. The data obtained were fitted to a Michaelis-Menten equation by plotting the initial rates of substrate oxidation as a function of the kynuramine concentration.

4.2.2 Results

Recombinant human MAO-A:

A K_m value of 16.1 ± 0.21 µM (figure 4.5) was obtained for the oxidation of kynuramine by recombinant human MAO-A.

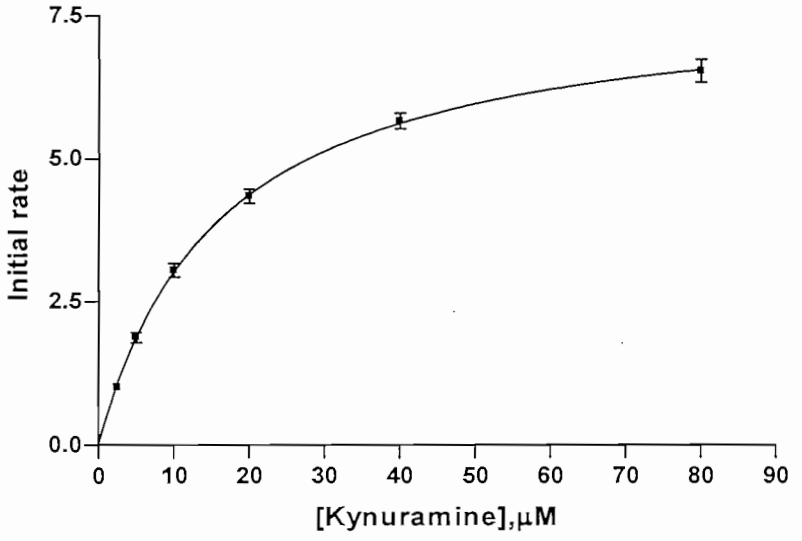

Figure 4.5 The determination of the K_m value of kynuramine oxidation by recombinant human MAO-A. The initial rates are expressed as nmol-mg protein^{-1}min^{-1} of 4-hydroxyquinoline formed.

Recombinant human MAO-B:

A K_m value of 22.66 ± 0.72 μM (figure 4.6) was obtained for the oxidation of kynuramine by recombinant human MAO-B.

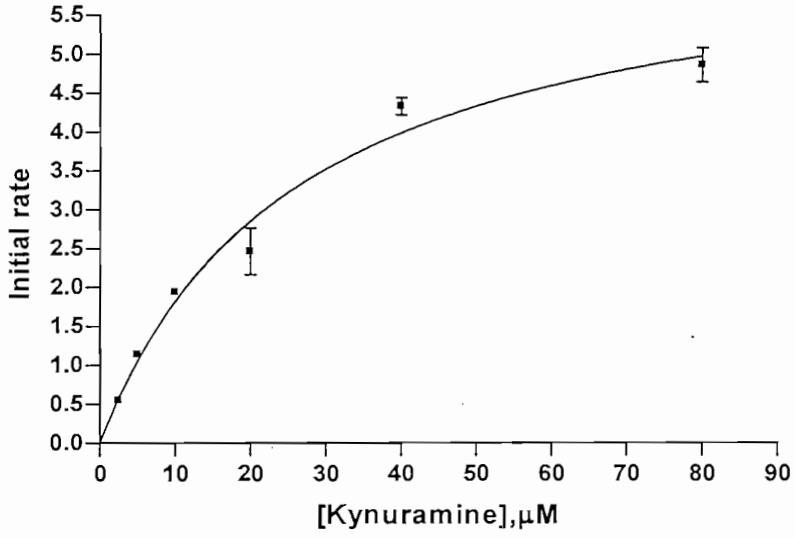

Figure 4.6 The determination of the K_m value of kynuramine oxidation by recombinant human MAO-B. The initial rates are expressed as nmol-mg protein^{-1}min^{-1} of 4-hydroxyquinoline formed.

4.3 K_i determination and calculation

In this study the inhibitor activities are expressed as IC_{50} values. However as mentioned earlier, inhibitor potency can also be expressed as the K_i value. We have experimentally measured the value of one inhibitor, 8-(3-trifluoromethylbenzyloxy)caffeine (**1e**), for baboon liver MAO-B as well as for recombinant human MAO-A and MAO-B. The purpose of this study was to determine whether the 8-benzyloxycaffeine inhibitors investigated exhibit a competitive mode of inhibition by constructing Lineweaver-Burk plots. As discussed earlier, an intersecting set of Lineweaver-Burk plots are an indication of competitive inhibition.

4.3.1 Method

Spectrophotometrically:

The baboon liver mitochondrial isolate was prepared and stored as described in 4.1. MMTP (K_m = 68.3 ± 1.6 µM for baboon liver MAO-B) was used as substrate.

The reactions were prepared in sodium phosphate buffer (100 mM, pH 7.4) with 30, 60, 90 and 120 µM MMTP, baboon liver mitochondria and various concentrations of the test inhibitors (0, 32.5, 65, 130 nM). The enzyme was added to the incubations so that the final concentration mitochondria present is 0.15 mg protein. A final volume of 500 µL were obtained for each incubation. The stock solutions of the inhibitors were prepared with DMSO with a resulting DMSO concentration of 4% in the incubations.

The reactions were incubated for 10 minutes at 37 °C and terminated with 10 µL of perchloric acid (70%). The incubations were centrifuged at 16 000 g for 10 minutes and the $MMDP^+$ concentrations in the supernatant were measured spectrophotometrically at 420 nm.

Initial oxidation rates of four different substrate concentrations (30 – 120 µM) in the absence and presence of three inhibitor concentrations (32.5 – 130 nM) were calculated and presented as Lineweaver-Burk plots. A replot of the slopes of the Lineweaver-Burk plots versus the inhibitor concentration was used to determine the K_i value from the x-axis intercept.

Fluorometrically:

Recombinant human MAO-A and MAO-B were prepared as described in 4.1. Kynuramine (K_m = 29 ± 2 µM for human MAO-A, K_m = 52.9 ± 3.4 for human MAO-B) was used as substrate.

All reactions were prepared in potassium phosphate buffer (100 mM, pH 7.4) with kynuramine concentrations of 15, 30, 60 and 90 µM, the respective recombinant human enzyme and various inhibitor concentrations. For human MAO-A the final enzyme concentration was 0.0075 mg/ml and for human MAO-B it was 0.015 mg/ml. The inhibitor

concentrations for MAO-A were 0, 0.931, 1.861 and 3.722 nM while the concentrations for MAO-B were 0, 32.5, 65 and 130 nM. Stock solutions of the test inhibitors were prepared in DMSO. A final volume of 500 µL for each incubation was obtained. The reactions were incubated for 10 minutes at 37 °C and terminated with 200 µL NaOH (2 N). 1200 µL Distilled water was added to each incubation before it was centrifuged for 10 minutes at 16 000 g.

The concentration of 4-hydroxyquinoline in each incubation was determined fluorometrically by measuring the fluorescence of the supernatant at an excitation wavelength of 310 nm and an emission wavelength of 400 nm. The PMT voltage was set to medium with an excitation and emission slit width of 5 mm each. A Varian Eclipse fluorescence spectrophotometer was used.

Initial oxidation rates of the four substrate concentrations were calculated in the absence and in the presence of three different inhibitor concentrations. A calibration curve was prepared for each data set by measuring the fluorescence of increasing concentrations of 4-hydroxyquinoline (0.188 – 6.25 µM) in a mixture of DMSO (4%) and potassium phosphate. To each calibrated standard a volume of 200 µL NaOH (2N) and 1200 µL distilled water was added. The values obtained for the calibration curve should bracket the fluorescence values obtained for the test inhibitor and display linearity. Lineweaver-Burk plots were constructed from the data sets and the slopes were replotted against the inhibitor concentration. Using this graph the K_i value could be obtained from the x intercept.

4.3.2 Results

Baboon liver MAO-B:

Classical Lineweaver-Burk plots were obtained for **1e** (Fig. 4.7), which indicated that inhibition of baboon liver MAO-B by 8-benzyloxycaffeine analogues are competitive. As discussed in 2.4.2, competitive inhibition is caracterized by the interception of the Lineweaver-Burk plots at or close to the y-axis.

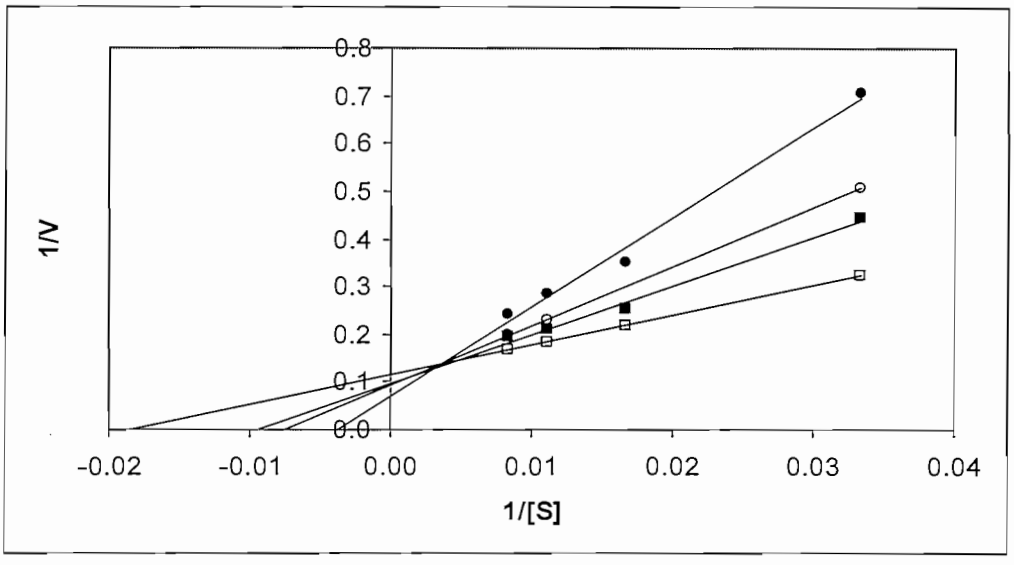

Figure 4.7 Lineweaver-Burk plots of the oxidation of MMTP by baboon liver MAO-B in the absence (open squares) and presence of various concentrations of **1e** (filled squares, 32.5 nM; open circles, 65 nM and filled circles, 130 nM). The rate (V) is expressed as nmol product/min/mg protein.

A replot of the slopes versus the inhibitor concentrations results in a linear graph that can be used to calculate the K_i value since the K_i equals the negative of the x-axis intercept (Fig. 4.8).

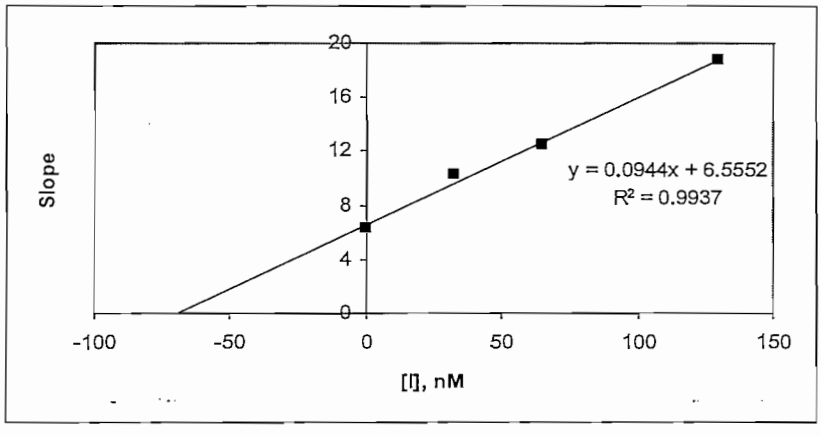

Figure 4.8 Graph of the slopes of the Lineweaver-Burk plots against inhibitor concentration.

Thus, the K_i value can be calculated using the equation: y = 0.094x + 6.561. Since the x-axis intercept is -69.8 nM the K_i value for the inhibition of baboon liver mitochondria MAO-B is 69.8 nM.

Recombinant human MAO-B:

The Lineweaver-Burk plots for inhibition of human MAO-B by **1e** indicated that the inhibition is competitive (Fig. 4.9). It can be concluded that 8-benzyloxycaffeine and its analogues inhibit recombinant human MAO-B competitively.

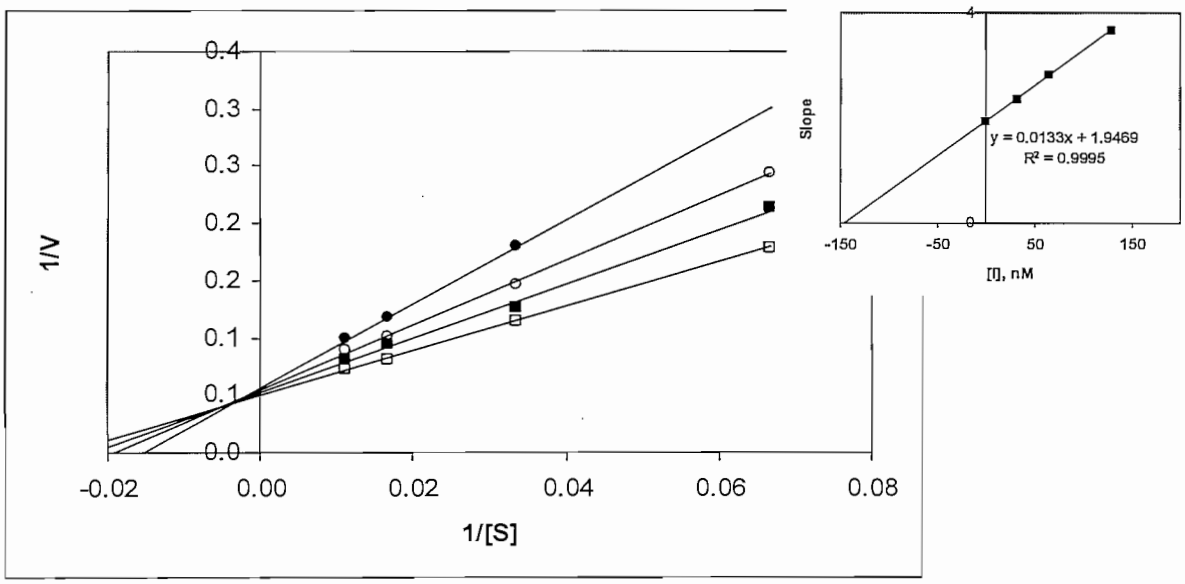

Figure 4.9 Lineweaver-Burk plots of the oxidation of kynuramine by recombinant human MAO-B in the absence (open squares) and presence of various concentrations of **1e** (filled squares, 32.5 nM; open circles, 65 nM and filled circles, 130 nM). The inset is the replot of the slopes versus the inhibitor concentration. The rate (V) is expressed as nmol product formed/min/mg protein.

Recombinant human MAO-A :

Competitive inhibition was observed for recombinant human MAO-A by **1e**. The Lineweaver-Burk plots imply that 8-benzyloxycaffeine analogues inhibit human MAO-A competitively (Fig. 4.10).

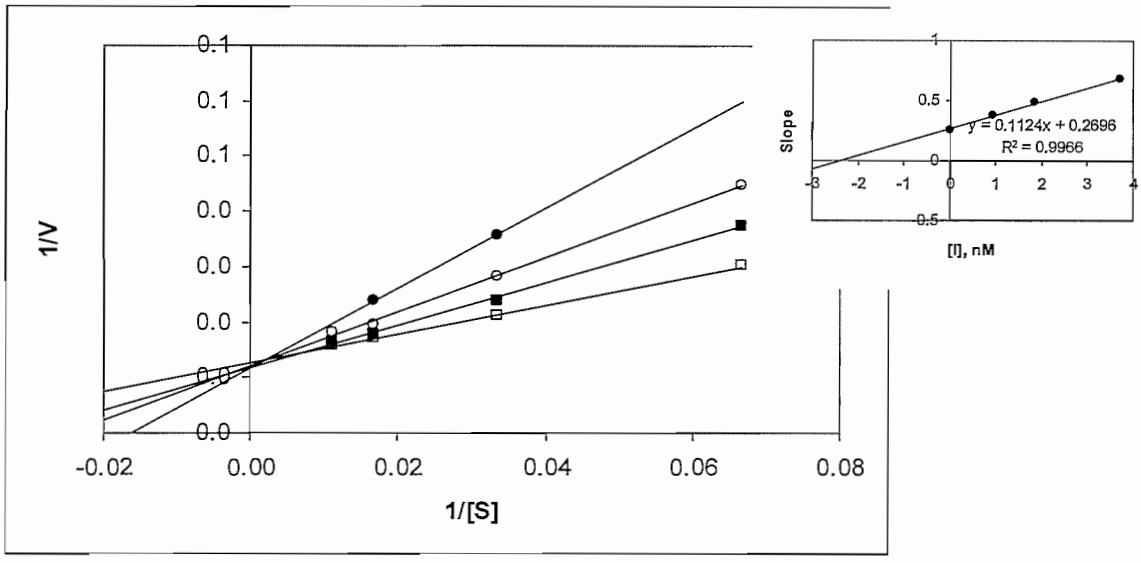

Figure 4.10 Lineweaver-Burk plots of the oxidation of kynuramine by recombinant human MAO-A in the absence (open squares) and presence of various concentrations of **1e** (filled squares, 931 nM; open circles, 1861 nM and filled circles, 3722 nM). The inset is the replot of the slopes versus the inhibitor concentration. The rate (V) is expressed as nmol product formed/min/mg protein.

4.3.3 K_i calculations

The K_i values for the inhibition of mitochondrial baboon liver MAO-B and recombinant human MAO-A and –B by **1a-g** were calculated with the following equation:

$$K_i = IC_{50} / (1 + [S] / K_m)$$

The substrate concentrations used were 30 μM for human MAO-A, 45 μM for human MAO-B and 50 μM for baboon liver MAO-B. The selectivities of the test inhibitors between human MAO-A and –B were determined. The higher the selectivity value, the more selective the inhibitor is for MAO-A. In the literature selectivity is often calculated by using the IC_{50} values. However, it is more appropriate to use the K_i value for this calculations since the K_i value accounts for the different affinities of the substrate (kynuramine) for MAO-A and MAO-B. The calculated K_i values are presented in Table 4.2.

Table 4.2 The calculated K_i values for the inhibition of human MAO-A, -B and baboon liver MAO-B by 8-benzyloxycaffeine analogues **1a-g**.

Compounds	Recombinant human MAO-A K_i (μM)	Recombinant human MAO-B K_i (μM)	Mitochondrial baboon liver MAO-B K_i (μM)[a]	Selectivity[b]
1a	0.43	0.59	1.44	1.37
1b	0.23	0.04	0.07	0.17
1c	0.33	0.02	0.07	0.06
1d	0.37	0.18	0.31	0.49
1e	1.30	0.05	0.06	0.04
1f	0.14	0.18	0.40	1.29
1g	1.10	0.34	0.92	0.31

[a] The K_m value of baboon liver MAO-B with MMTP as substrate is reported in section 2.4.3.
[b] K_i(MAO-B)/K_i(MAO-A) ratio

From the data it can be concluded that compound **1e** is very selective for human MAO-B and would be a suitable lead compound were selective inhibition of MAO-B is needed. Compounds **1a** and **1f** are the least selective of the inhibitors and would be lead compounds where dual inhibition of MAO-A and –B is required. Overall the test inhibitors **1a-g** inhibit MAO-B more potently than MAO-A. The values obtained for baboon liver MAO-B and human MAO-B compared very well.

4.4 Reversibility study

For safety considerations, reversibility is an important requirement for MAO inhibitors. One inhibitor, 8-(3-chlorobenzyloxy)caffeine (**1b**), was chosen as the representative inhibitor in the reversibility studies with baboon liver MAO-B, human MAO-A and –B. In this study the inhibitor was pre-incubated with the enzyme for various periods of time and the rate of substrate oxidation will subsequently be measured. The rate of substrate oxidation versus the range of pre-incubation times was plotted on a bar graph. A constant oxidation rate for all of

the incubation times is an indication of inhibitor reversibility. In contrast, an irreversible inhibitor will exhibit a time-dependant decrease in the rate of enzyme catalysis.

4.4.1 Method

Spectrophotometrically:

The baboon liver mitochondrial isolate was prepared and stored as described in 4.1.1 MMTP (K_m = 68.3 ± 1.6 µM for baboon liver MAO-B) was used as substrate.

Baboon liver mitochondrial fractions (0.326 mg protein/ml) were pre-incubated with 0.28 µM of **1b** for periods of 0, 15, 30 and 60 minutes at 37 °C. The incubations were prepared in sodium phosphate buffer (100 mM, pH 7.4). A final concentration of 50 µM MMTP were incubated at 37 °C for 15 minutes with the pre-incubated enzyme complex. The final volume of the incubations were 500 µL. After the incubation period the reactions were stopped with 10 µL of perchloric acid (70%). The incubations were centrifuged at 16 000 g for 10 minutes and the $MMDP^+$ concentrations in the supernatant were measured spectrophotometrically at 420 nm. This experiment was carried out in triplicate.

Fluorometrically:

Recombinant human MAO-A and MAO-B were prepared as described in 4.1. Kynuramine (K_m = 29 ± 2 µM for human MAO-A, K_m = 52.9 ± 3.4 for human MAO-B) was used as substrate.

Human recombinant MAO were pre-incubated with **1b** for periods of 0, 15, 30 and 60 minutes at 37 °C. MAO-A were used in concentrations of 0.0163 mg/ml with 1.3 µM of **1b** while 0.0326 mg/ml MAO-B was incubated with 0.23 µM of the inhibitor. The incubations were prepared in potasium phosphate buffer (100 mM, pH 7.4). A final concentration of 45 µM kynuramine for MAO-A and 30 µM for MAO-B were incubated at 37 °C for 15 minutes with the pre-incubated enzyme complex. The final volume of the incubations were 500 µL. After the incubation period the reactions were stopped with 200 µL of NaOH (2 N). 1200 µL distilled water was added to each incubation before it was centrifuged for 10 minutes at 16 000 g.

The concentration of 4-hydroxyquinoline in each incubation was determined fluorometrically by measuring the fluorescence of the supernatant at an excitation wavelength of 310 nm and an emission wavelength of 400 nm. The PMT voltage was set to medium with an excitation and emission slit width of 5 mm each. This experiment was carried out in triplicate. A calibration curve was prepared for each data set as described in the inhibition studies.

4.4.2 Results

Baboon liver MAO-B:

The graph of the oxidation rate of MMTP versus the different incubation times (Fig. 4.11) illustrated that inhibition of baboon liver MAO-B by **1b** is reversible. Since there is no decrease in MMTP oxidation rate over incubation time it can be concluded that 8-benzyloxycaffeine analogues are reversible inhibitors of mitochondrial baboon liver MAO-B.

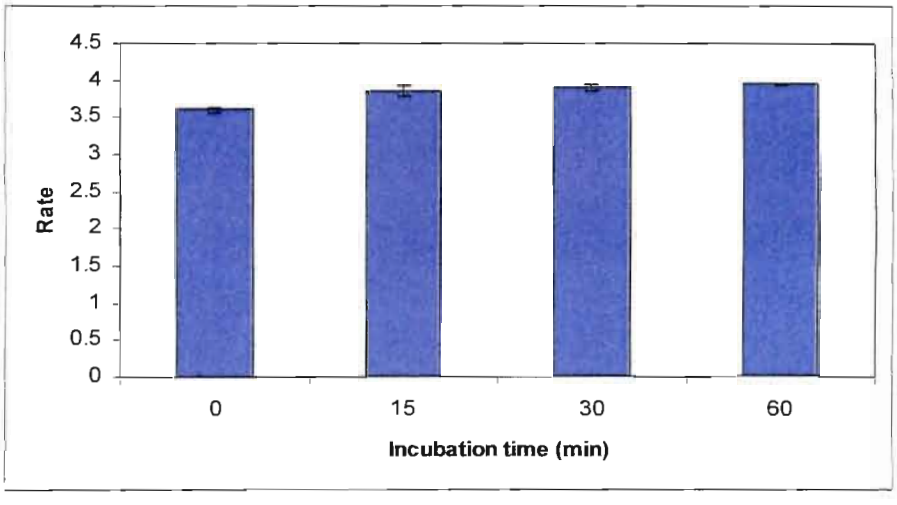

Figure 4.11 Rate of MMTP oxidation by baboon liver MAO-B for each of the pre-incubation periods (0 – 60 minutes). The rate (V) is expressed as nmol product formed/min/mg protein.

Recombinant human MAO-B:

Reversible inhibition of human MAO-B by **1b** was observed. The graph showed no decline in the rate of kynuramine oxidation as a function of incubation time (Fig. 4.12). Inhibition of human MAO-B by 8-benzyloxycaffeine analogues are therefore reversible.

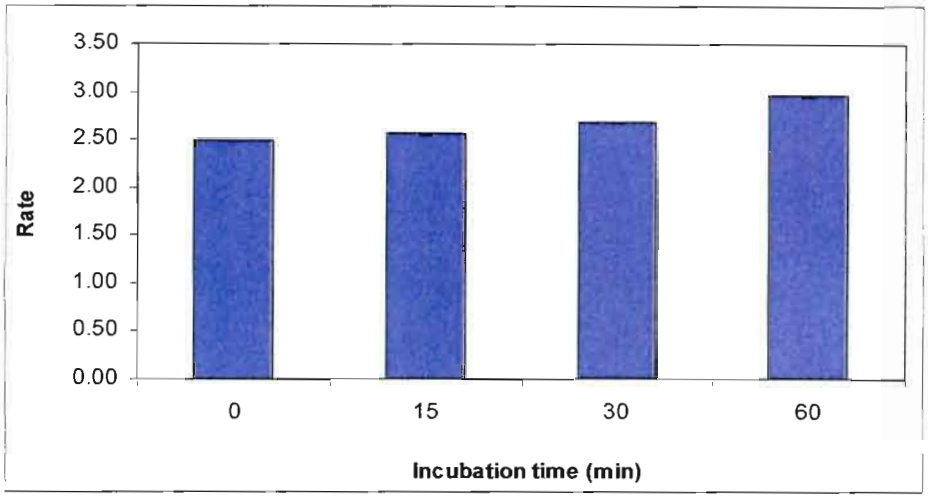

Figure 4.12 Rate of kynuramine oxidation by recombinant human MAO-B for each of the pre-incubation periods (0 – 60 minutes). The rate (V) is expressed as nmol product formed/min/mg protein.

Recombinant human MAO-A:

The graph in figure 4.13 illustrates that inhibition of human MAO-B by **1b** is reversible. No decline in kynuramine oxidation rate is observed over incubation time and it can thus be concluded that 8-benzyloxycaffeine analogues inhibit recombinant human MAO-A reversibly.

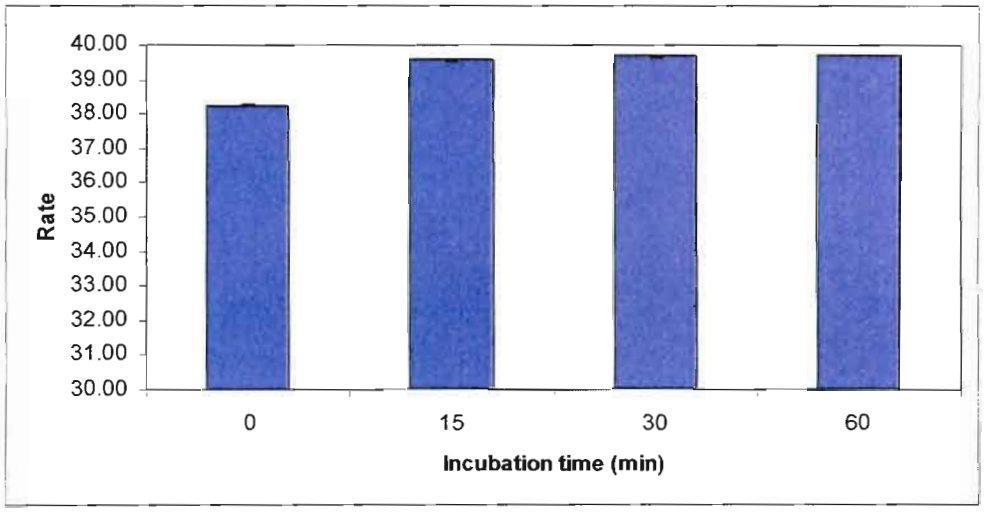

Figure 4.13 Rate of kynuramine oxidation by recombinant human MAO-A for each of the pre-incubation periods (0 – 60 minutes). The rate (V) is expressed as nmol product formed/min/mg protein.

4.5 Hansch-type structure-activity relationship studies

Hansch-type structure-activity relationship (SAR) studies quantifies the relationship between biological activity, for example MAO-B inhibitor activity (IC_{50}), and the physiochemical properties of substituents on a phenyl ring, while the rest of the structure is ignored. There are many parameters that describe these physiochemical properties. Among these are the Van der Waals volume (V_w) and Taft steric parameter (E_s), which represents the bulkiness of a substituent, while lipophilicity is described by the Hansch constant (π). Electronic parameters are described by the classical Hammett constant (σ_m or σ_p) and the Swain-Lupton constant (F). These physiochemical parameters can be obtained from various literature sources.

MAO-B inhibitor activity (expressed as the logarithm of IC_{50}) is correlated to the physiochemical parameters through linear regression and the correlation constant (R^2) is calculated. It is possible to predict which physiochemical property of the substituent will influence the inhibitor potency. The closer the value of R^2 is to 1, the better the correlation between the inhibitor's potency and the physiochemical parameter. For example, in figure 4.14 lipophilicity of the phenyl substituent is plotted against inhibitor activity (log IC_{50}) with a R^2 of 0,98. The high value of the correlation value means that there is a definite relationship between inhibitor potency and lipophilicity. In this case the inhibitor potency will decrease if the lipophilicity of the concerned substituent increases. This makes it possible to predict which substituents will increase inhibitor potency (Vlok *et al.*, 2006; Van den Berg *et al.*, 2007; Gnerre *et al.*, 2000). A critical *F* value (F_{max}) relates the R^2 to the error variance. The higher F_{max} the better the fit. F_{max} can be calculated as described by Livingstone (2005). A F_{max} value higher than the critical *F* value is deemed significant. The critical F value for 95% significance for models containing seven logIC_{50} values and two out of a possible five parameters (V_w, E_s, π, σ and F) was calculated to be 30.18 while F_{max} for one out of five parameters is 25.32.

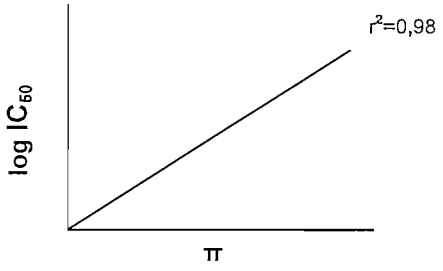

Figure. 4.14 A general illustration of a graph correlating inhibitor potency (log IC_{50}) with lipophilicity (π).

In this study, a Hansch-type SAR analysis was carried out in order to determine the effect of the substituents at C-3 of the phenyl ring on the inhibition activities (IC_{50} values) of the 8-benzyloxycaffeine analogues. Unfortunately no correlations were obtained for the inhibition of MAO-A by the 8-benzyloxycaffeine analogues. All the values of the parameters used in this study was obtained from the literature (Hansch *et al.*, 1995, Van de Waterbeemb *et al.*, 1987)

4.5.1 Results and discussion

Results of the statistical analysis for both mitochondrial baboon liver MAO-B and recombinant human MAO-B are shown in tables 4.3 and 4.4, respectively.

Table 4.3 Correlations of baboon liver MAO-B inhibition ($logIC_{50}$) by 8-benzyloxycaffeine analogues with steric, electronic and hydrophobic descriptors of the substituents at C-3 of the phenyl ring[a]

Parameter	Slope	y-intercept	R^2	*F*	Significance[b]
σ	-2.247 ± 0.684	0.121 ± 0.202	0.62	10.79	0.022
F	-1.963 ± 0.89	0.175 ± 0.303	0.39	4.866	0.079
V_w	-0.488 ± 0.44	0.045 ± 0.455	0.02	1.132	0.337
π	-1.288 ± 0.244	0.19 ± 0.142	0.82	27.82	0.003
E_s	0.528 ± 0.223	0.126 ± 0.268	0.44	5.614	0.065
$\sigma + \pi$	-1.227 ± 0.19 -0.933 ± 0.098	0.308 ± 0.05	0.98	147.3	0.003 0.0007
$F + \pi$	-1.122 ± 0.194 -1.066 ± 0.097	0.411 ± 0.064	0.98	120.6	0.005 0.0004

[a] The logarithm of the IC_{50} values (expressed in μM) was used in the linear regression anlysis.
[b] The significance is the fractional probability that the coefficient of the added variable is zero.

Table 4.4 Correlations of recombinant human MAO-B inhibition ($logIC_{50}$) by 8-benzyloxycaffeine analogues with steric, electronic and hydrophobic descriptors of the substituents at C-3 of the phenyl ring[a]

Parameter	Slope	y-intercept	R^2	*F*	Significance[b]
σ	-2.139 ± 0.711	0.01 ± 0.233	0.51	7.308	0.043
F	-1.973 ± 0.922	0.071 ± 0.314	0.37	4.579	0.085
V_w	-0.562 ± 0.429	0.024 ± 0.444	0.11	1.716	0.247
π	-1.269 ± 0.293	0.075 ± 0.17	0.75	18.76	0.008
E_s	0.446 ± 0.265	0.061 ± 0.318	0.23	2.828	0.153
$\sigma + \pi$	-1.098 ± 0.541 -0.951 ± 0.278	0.18 ± 0.143	0.84	17.3	0.112 0.027
$F + \pi$	-1.151 ± 0.419 -1.042 ± 0.21	0.302 ± 0.139	0.89	25.414	0.052 0.008

[a] The logarithm of the IC_{50} values (expressed in μM) was used in the linear regression anlysis.
[b] The significance is the fractional probability that the coefficient of the added variable is zero.

For baboon liver MAO-B the Hansch constant (π) showed good correlation with the log IC_{50} values and had a R^2 of 0.82. The *F* value for this correlation was found to be 27.82 which is higher than the critical *F* value (F_{max} = 25.32) for 95% significance. Even better correlations were found if a second parameter was added. A combination of the Hammett constant (σ) and π gave the best correlation with a R^2 of 0.98 and a *F* of 147.3 (F_{max} = 30.18) (Fig. 4.15). For this correlation the probability that σ and π are zero is 0.3% and 0.07%, respectively. The best mathematical description for the binding affinity of 8-benzyloxycaffeine analogues (**1a-g**) to baboon liver MAO-B is therefore:

$$\mathbf{Log IC_{50} = -1.227(\pm 0.19)\sigma - 0.933(\pm 0.098)\pi + 0.308(\pm 0.05)}$$
$$\mathbf{R^2 = 0.98 \text{ and } F = 147.3} \qquad \mathbf{(1)}$$

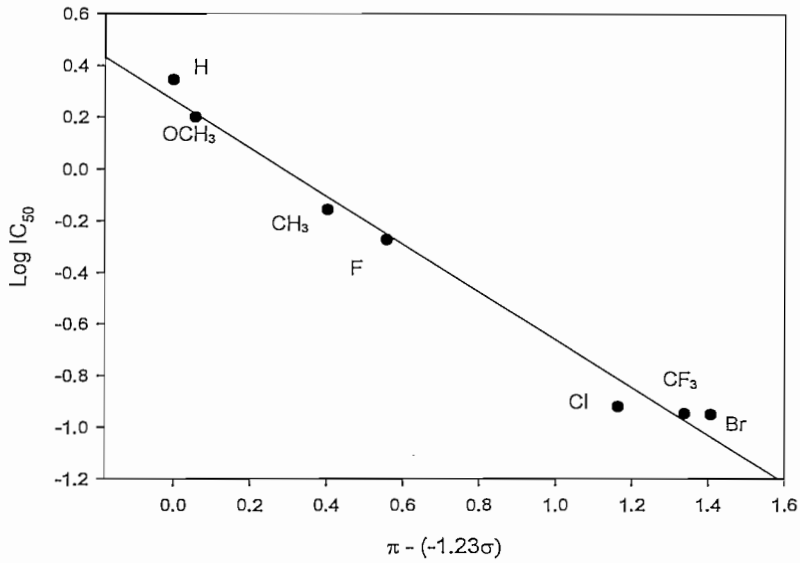

Figure 4.15 Correlations of the log IC_{50} values for the inhibition of baboon liver MAO-B by **1a-g** with the Hansch constant (π) of the substituents at C-3 of the phenyl ring. The π values were adjusted by the contribution of the Hammett constant (σ) as indicated on the x-axis titles. The linear regression line is a representation of equation 1.

The Swain-Lupton constant and π also correlated very well with the inhibition potency (log IC_{50}) and had a R^2 of 0.98 while the *F* value was 120.6 (F_{max} = 30.18). The negative correlation between log IC_{50} and F(-1.122 ± 0.194) and σ (-1.227 ± 0.19) is an indication that inhibition potency of 8-benzyloxycaffeine analogues towards baboon liver MAO-B can

be enhanced by substitution with electron withdrawing groups on C-3 of the phenyl ring. A negative correlation was found for the π constant (-1.288 ± 0.244) which indicates that lipophilic substituents on C-3 of the phenyl ring can result in more potent inhibitors.

For recombinant human MAO-B, π had the best correlation with the inhibition potencies (log IC_{50}). This correlation had a R^2 of 0.75 and *F* value of 18.76 (F_{max} = 25.32). Similar to the baboon liver MAO-B, better correlations were obtained with a combination of two parameters. A combination of F and π gave a correlation with a R^2 of 0.89 and a *F* of 25.41 (F_{max} = 30.18) (Fig. 4.16). For this correlation the probability that F and π are zero is 5.2% and 0.8%, respectively. The best mathematical description for the binding affinity of 8-benzyloxycaffeine analogues (**1a-g**) to recombinant human MAO-B is therefore:

$$\text{Log } IC_{50} = -1.15(\pm 0.42)F - 1.04(\pm 0.21)\pi + 0.302(\pm 0.14)$$
$$R^2 = 0.89 \text{ and } F = 25.414 \qquad (2)$$

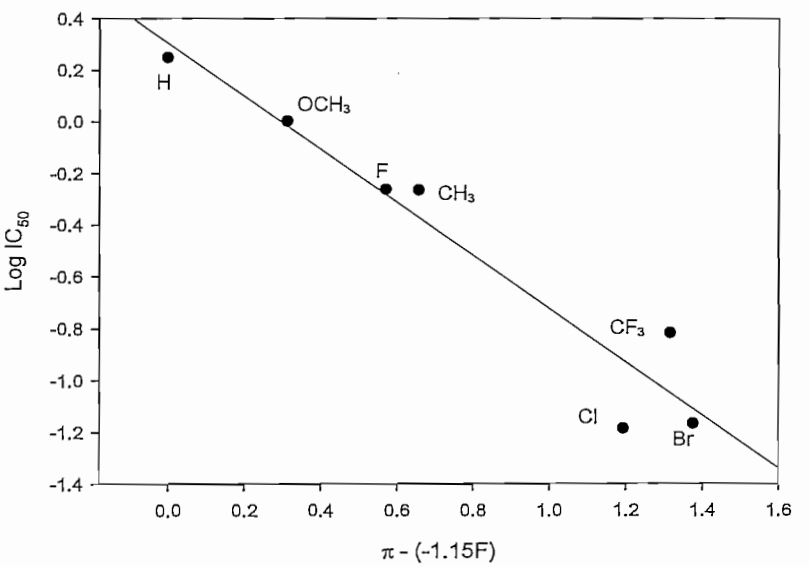

Figure 4.16 Correlations of the log IC_{50} values for the inhibition of recombinant human MAO-B by **1a-g** with the Hansch constant (π) of the substituents at C-3 of the phenyl ring. The π values were adjusted by the contribution of the Swain-Lupton constant (F) as indicated on the x-axis titles. The linear regression line is a representation of equation 2.

Another combination, π and σ also correlated very well with the inhibition potencies and had a R^2 of 0.84 while the *F* value was 17.3 (F_{max} = 30.18). Similarly to the baboon liver MAO-B, negative correlations were found for F, σ and π with the IC_{50} values obtained with the human MAO-B. This indicates that substituents on C-3 of the phenyl ring which is lipophilic and electron withdrawing result in more potent inhibitors.

Summary

It can be concluded that 8-benzyloxycaffeine analogues are competitive, reversible inhibitors of MAO-A and –B. The SAR study showed that for these compounds to be potent inhibitors of MAO-B (human and baboon liver) they should contain lipophilic and electron withdrawing groups on C-3 of the phenyl ring of the benzyloxy side chain.

Chapter 5

Molecular docking studies

5.1 Introduction

The development and discovery of new drugs for therapeutic application can be done by designing ligands for a specific receptor target. This is done by way of structural and computational chemistry. Molecular docking is the process of computationally fitting a ligand to a receptor or enzyme.

Docking studies are not only employed to identify new drugs, but can be used to examine the interaction between the active site of an enzyme and the docked inhibitor. Due to an increasing availability of high resolution structural data on enzymes and other protein receptors, docking studies are becoming an integral part of drug discovery (Knegtel *et al.*, 1997). In combination with SAR studies, docking studies can be used to identify critical structural features of inhibitors for optimal activity towards a specific enzyme.

All the target compounds in this study (**1a-g**) were computationally docked within models of MAO-B and MAO-A. CSC and harmine were used as control compounds for MAO-B and MAO-A respectively.

5.2 Experimental

The molecular docking studies were carried out in Windows based Discovery Studios 1.7. All the inhibitors were drawn in DS Visualizer Pro and prepared for docking with the 'Prepare Ligands' protocol within Discovery Studios. The MAO-A (2Z5X.pdb) and MAO-B (2V5Z.pdb) enzyme models were obtained from Brookhaven Protein Data Bank, co-crystallized with harmine and safinamide, respectively. After the enzymes were prepared with the 'Clean Protein' function they were typed with the CHARMm forcefield. A series of three minimizations were carried out on each enzyme while the backbone was kept fixed. The first minimization was

the steepest descent minimization followed by the conjugate gradient and adopted basis NR minimizations. During the minimizations the implicit distance-dependant dielectrics solvent model was used with the dielectric constant set to 4. Existing ligands were erased from the enzyme and the backbone constraints removed. The binding site was identified within the enzyme before the ligands were docked using the 'Ligandfit' protocol. In situ ligand minimization was used on the docked ligand with the 'Smart Minimizer' algorithm. Ten possible docking poses were calculated for each inihibitor.

5.3 Results and discussion

MAO-B:

All the 8-benzyloxycaffeine analogues traversed both the entrance and binding site cavities. It was shown that 8-benzyloxycaffeine and its analogues bind to MAO-B with the caffeine moiety oriented towards the FAD co-factor while the benzyloxy side chain protrudes into the entrance cavity (Fig. 5.1). This is a similar orientation to that of CSC, a potent inhibitor of MAO-B. The Ile-199 residue which acts as a gate was in an open conformation. Hydrogen bonding occurred between the oxygens on the caffeine ring and Tyr-435, a water molecule and FAD.

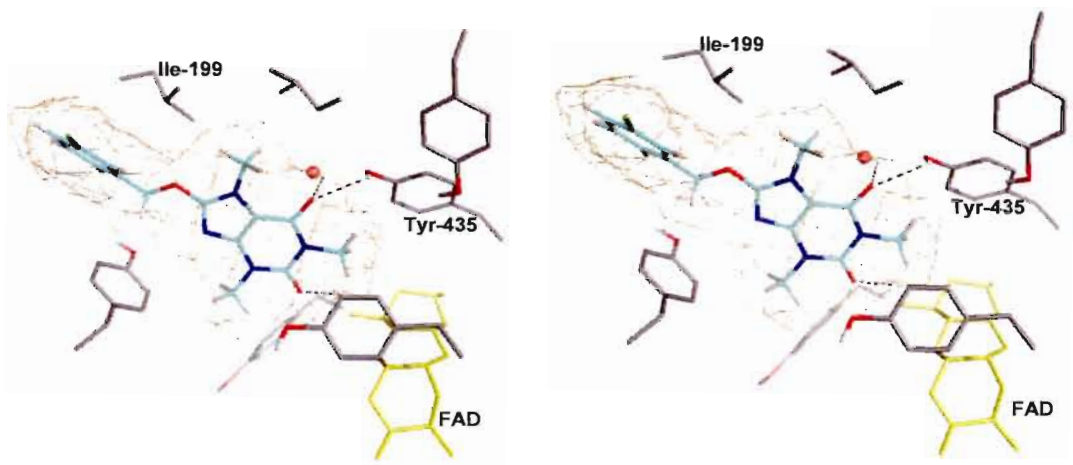

Figure 5.1 Stereo view representation of 8-(3-chlorobenzyloxy)caffeine docked within MAO-B. The inhibitor is displayed in cyan, the FAD co-factor in yellow and hydrogen bonds in black. The red sphere represents a water molecule.

MAO-A:

Harmine is a potent inhibitor of MAO-A. It is a small molecule which fits easily within the active site cavity of MAO-A (Fig. 5.2) where it interacts with the FAD co-factor. Smaller molecules are thought to be better MAO-A inhibitors since MAO-A does not have an entrance cavity to accommodate larger molecules (De Colibus *et al.*, 2005; Son *et al.*, 2008).

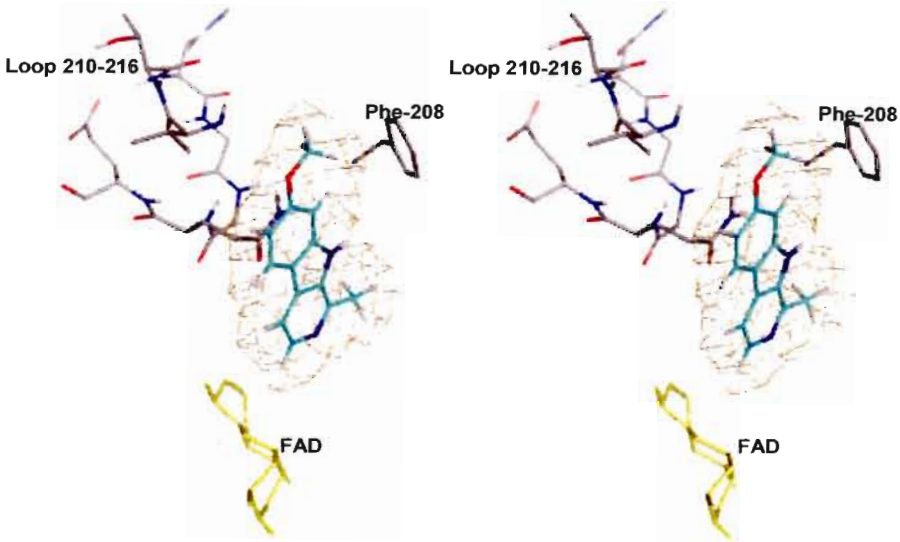

Figure 5.2 Stereo view representation of harmine docked within MAO-A. The inhibitor is displayed in cyan and the FAD co-factor in yellow.

However, 8-benzyloxycaffeine analogues seem to be able to bind within the MAO-A active site by rotating the benzyloxy side chain at an angle to circumnavigate the Phe-208 residue (Fig. 5.3). This flexibility can be attributed to the sp^3-hybridized oxygen and carbon atoms linking the phenyl and caffeine rings of 8-benzyloxycaffeine. The caffeine moiety is oriented towards the FAD co-factor. Hydrogen bonding occurs between the FAD and an oxygen on the caffeine ring.

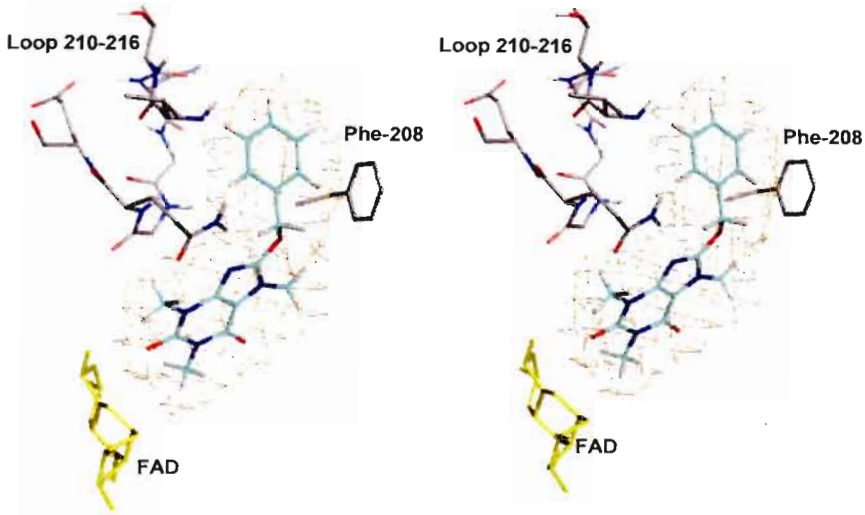

Figure 5.3 Stereo view of 8-benzyloxycaffeine docked within MAO-A. The inhibitor is displayed in cyan, the FAD co-factor in yellow and hydrogen bonds in black.

The docking studies revealed that 8-benzyloxycaffeine analogues possess affinity for both MAO-A and MAO-B. MAO-A inhibitory activity is probably made possible by the inhibitor's ability to rotate its side chain to avoid unfavourable interactions with Phe-208. The binding mode of 8-benzyloxycaffeine analogues to MAO-B and MAO-A are similar in that the caffeine moiety is always oriented towards the FAD co-factor where hydrogen bonding may occur.

Chapter 6

Discussion and conclusion

In this study 8-benzyloxycaffeine analogues (**1a-g**) were successfully synthesized and tested as inhibitors of baboon liver MAO-B and recombinant human MAO-A and –B. It was found that **1c** inhibits MAO-B approximately twofold more potently than CSC. The test inhibitors displayed similar potencies toward baboon liver MAO-B and human MAO-B. This is an indication that human and mitochondrial baboon liver MAO-B have similar active sites and inhibitor specificities. Inhibition of recombinant human MAO-A was also observed for the 8-benzyloxycaffeine analogues.

Compounds **1a-g** were found to be reversible and competitive in their inhibition of baboon liver MAO-B and human MAO-A and –B, giving these inhibitors a better safety profile. A Hansch-type SAR analysis indicated that substituents on C-3 of the phenyl ring of the benzyloxy side chain have a distinct effect on the inhibition potencies of the 8-benzyloxycaffeine analogues toward MAO-B. Substituents which are more hydrophobic and electron withdrawing have the ability to increase inhibition potencies.

Docking studies gave better insight into the binding mode of compounds **1a-g** within the active sites of MAO-A and –B. It was found that 8-benzyloxycaffeine analogues traverse both cavities of MAO-B. The caffeine moiety is oriented towards the FAD co-factor in the substrate cavity while the benzyloxy side chain extends into the entrance cavity. This mode of binding is thought to be necessary for the selective inhibition of MAO-B since larger molecules are not able to bind within the smaller active site of MAO-A. Further docking studies of 8-benzyloxycaffeine analogues within MAO-A provided a possible explanation for the occurence of MAO-A inhibition by these compounds. The test inhibitors bind within MAO-A with the caffeine ring oriented toward the FAD in the active site while the benzyloxy side chain is rotated into a conformation which avoids unfavourable intractions with the Phe-208 residue. This flexibility can be attributed to the presence of the sp^3-hybridized oxygen and methylene linker in the benzyloxy side chain.

Thus, 8-benzyloxycaffeine analogues are non-selective MAO inhibitors with competitive and reversible binding modes. These qualities make compounds **1a-g** ideal drug candidates for the future treatment of PD.

APPENDIX A

List of ^{1}H and ^{13}C NMR spectrums:

^{13}C NMR

8-Chlorocaffeine (3)

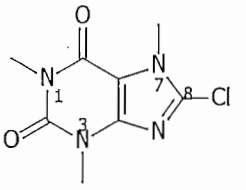

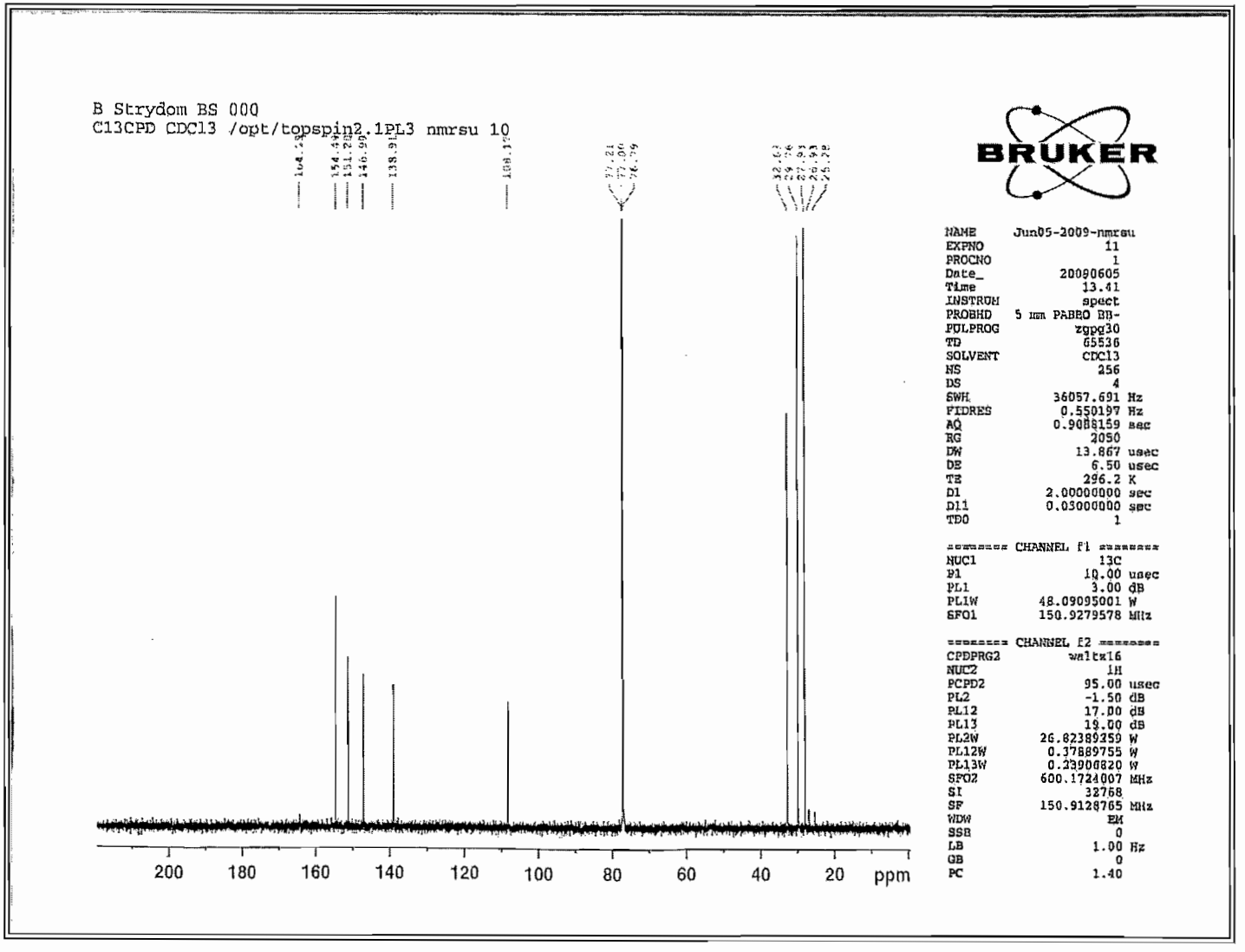

^{1}H NMR

8-Chlorocaffeine (3)

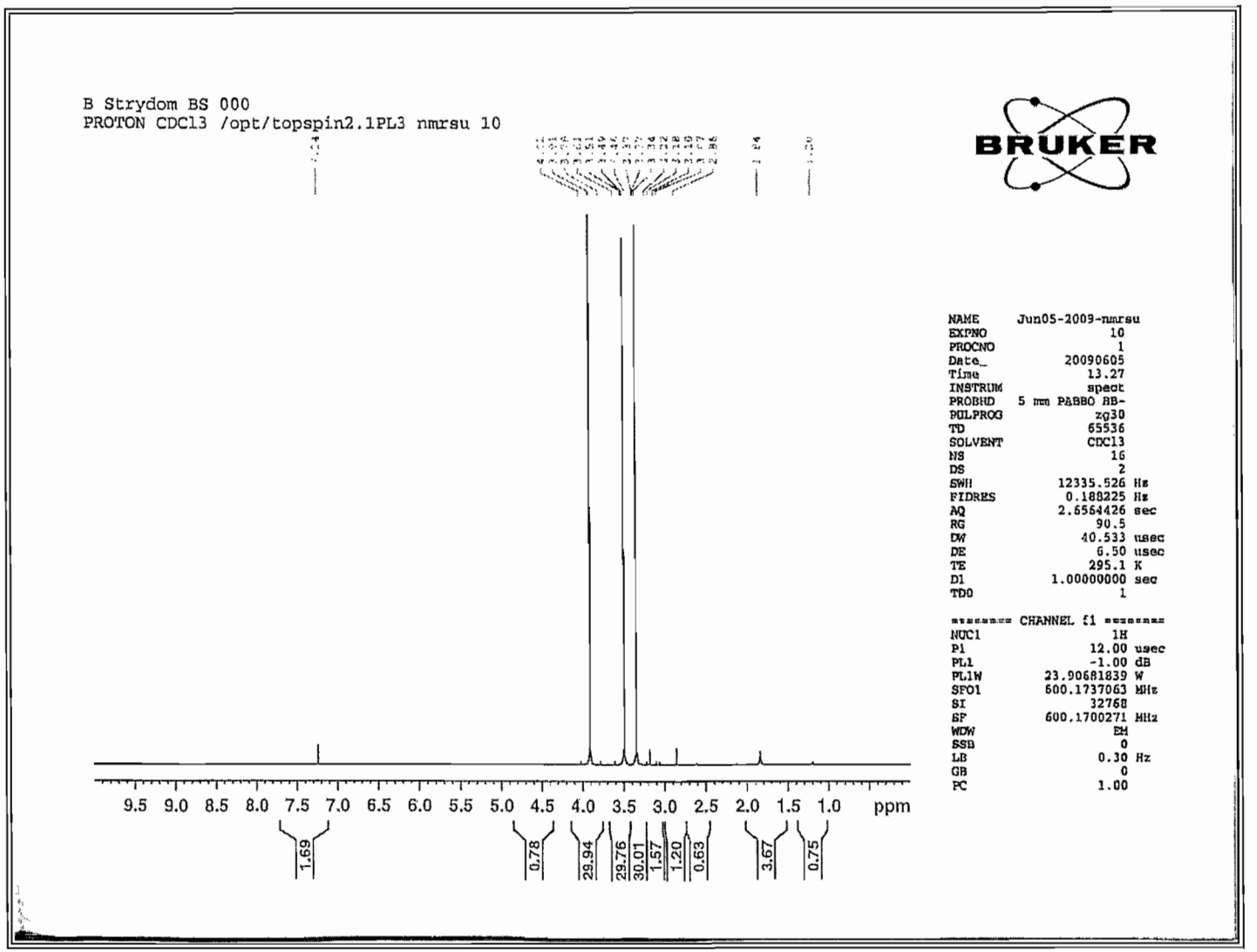

^{13}C NMR

8-Benzyloxycaffeine (1a)

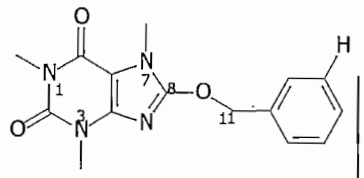

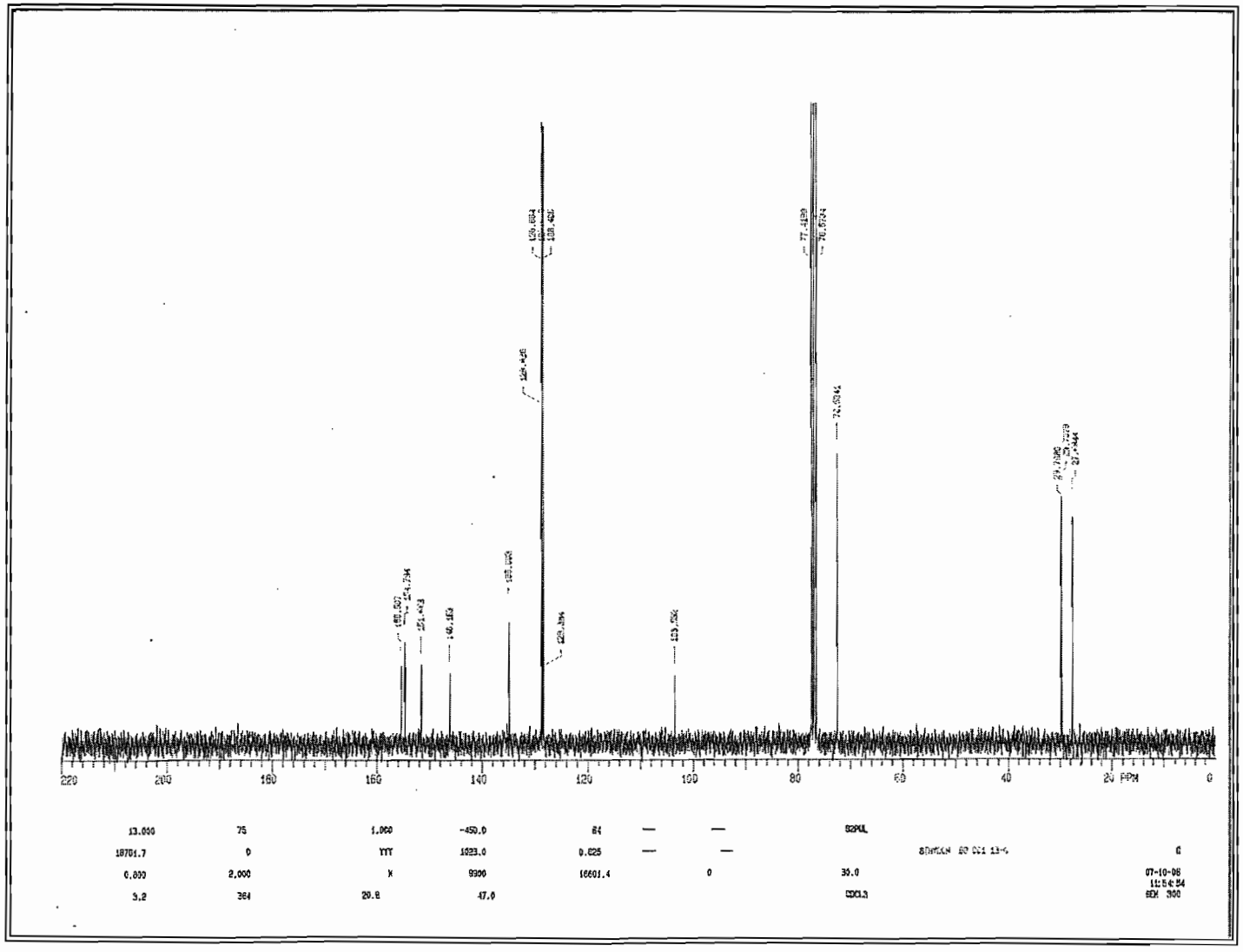

^{1}H NMR

8-Benzyloxycaffeine (1a)

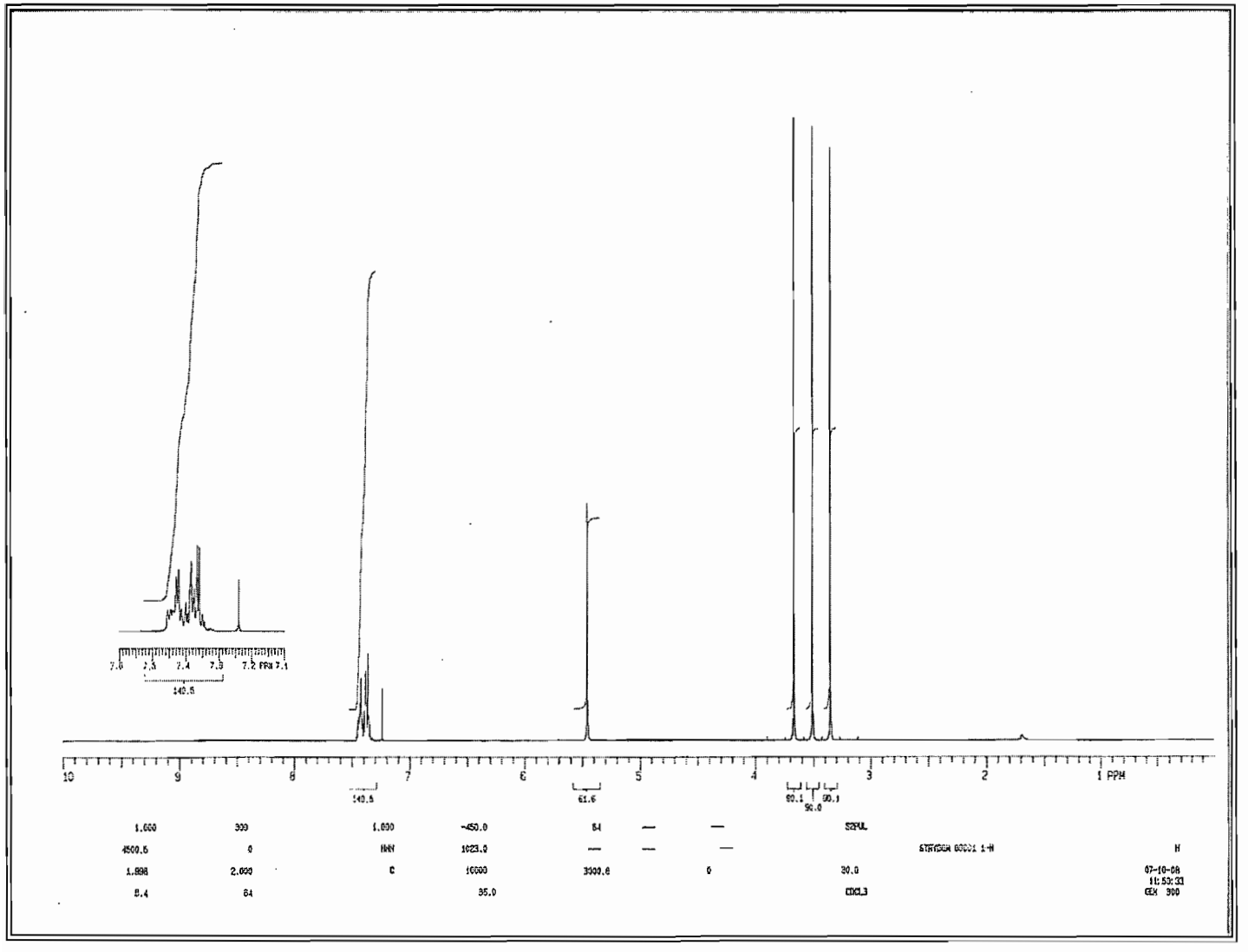

^{13}C NMR

8-(3-Chlorobenzyloxy)caffeine (1b)

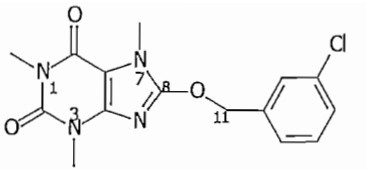

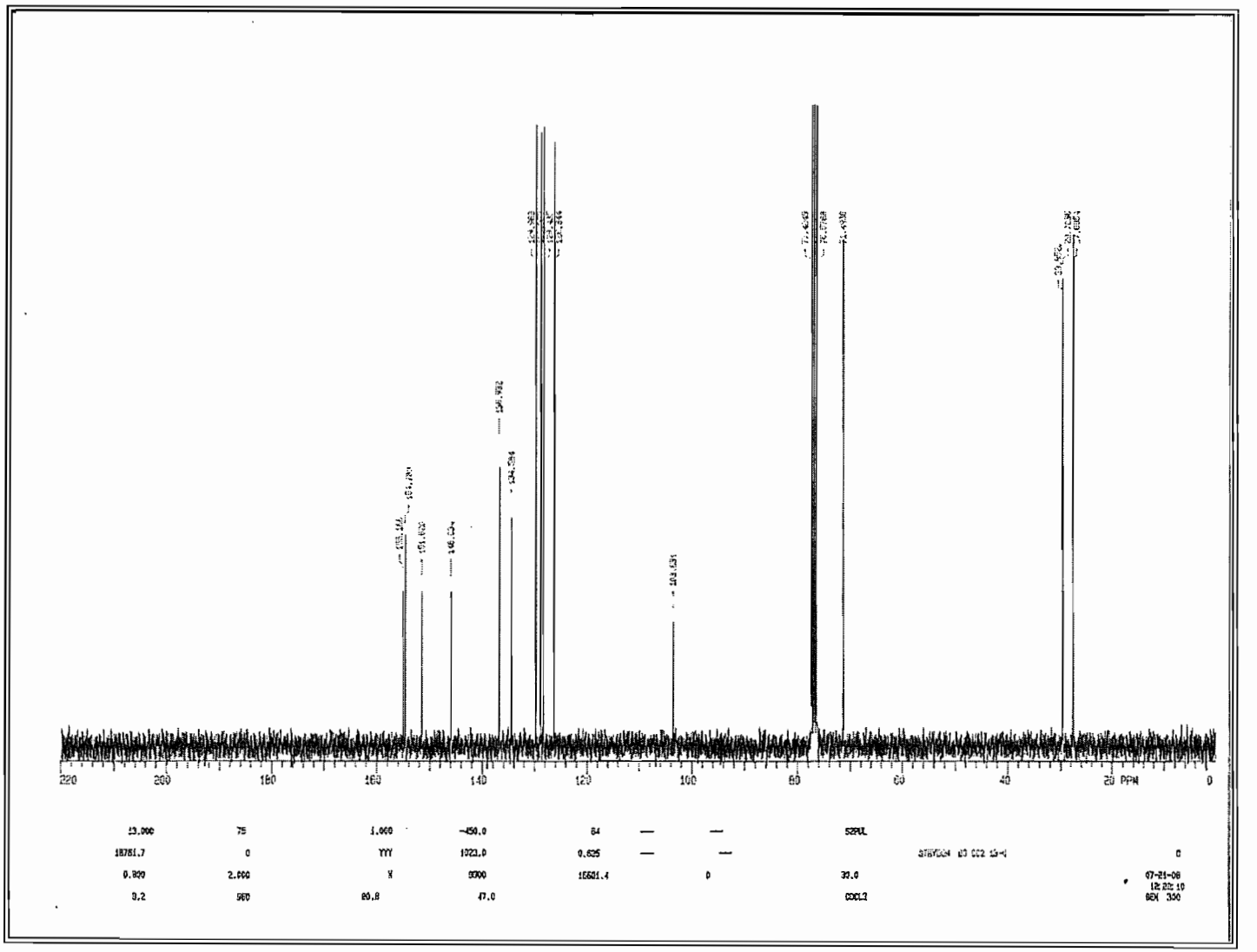

^{1}H NMR

8-(3-Chlorobenzyloxy)caffeine (1b)

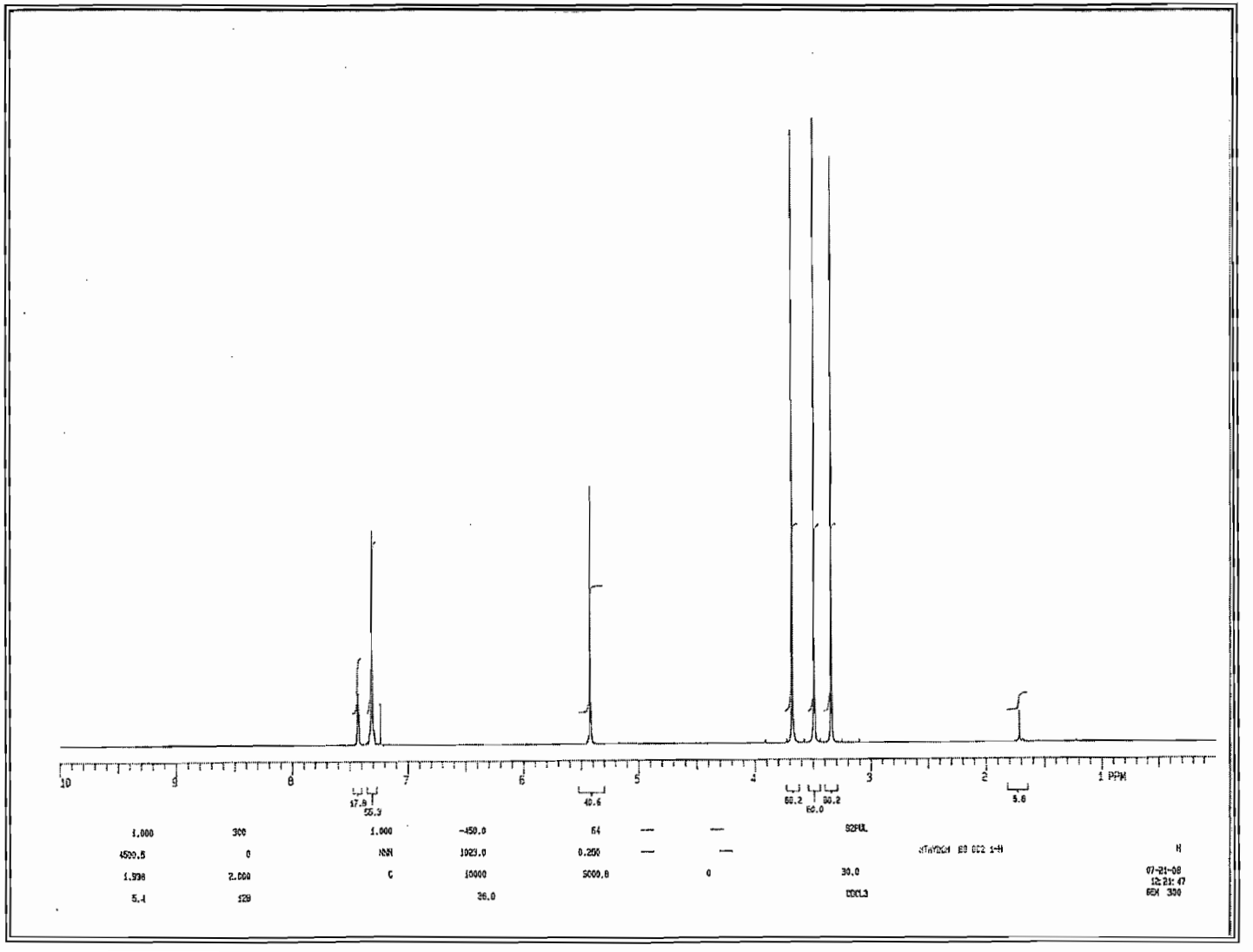

^{13}C NMR

8-(3-Bromobenzyloxy)caffeine (1c)

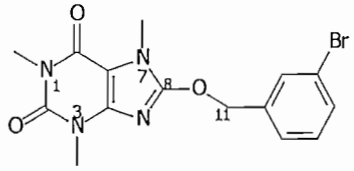

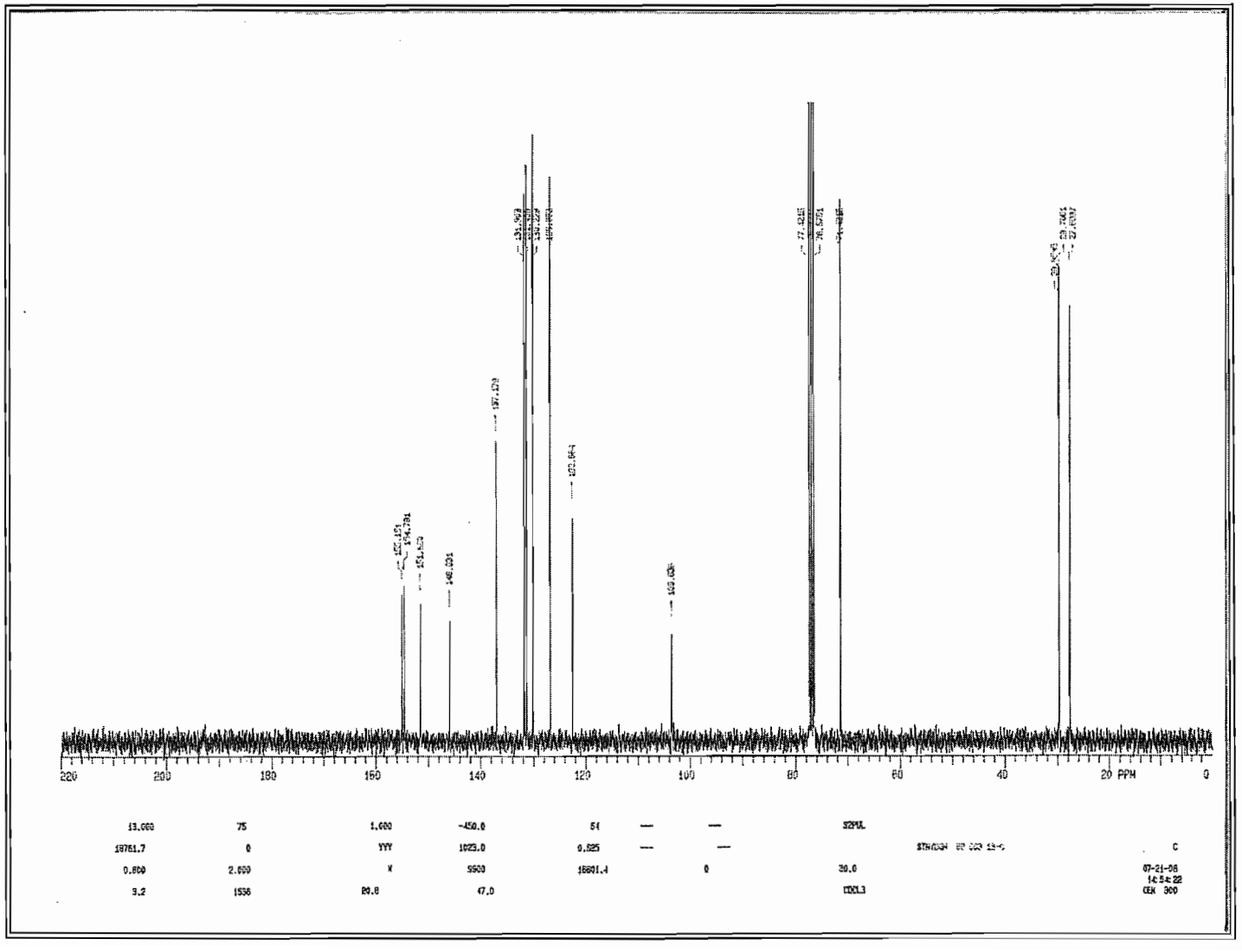

^{1}H NMR

8-(3-Bromobenzyloxy)caffeine (1c)

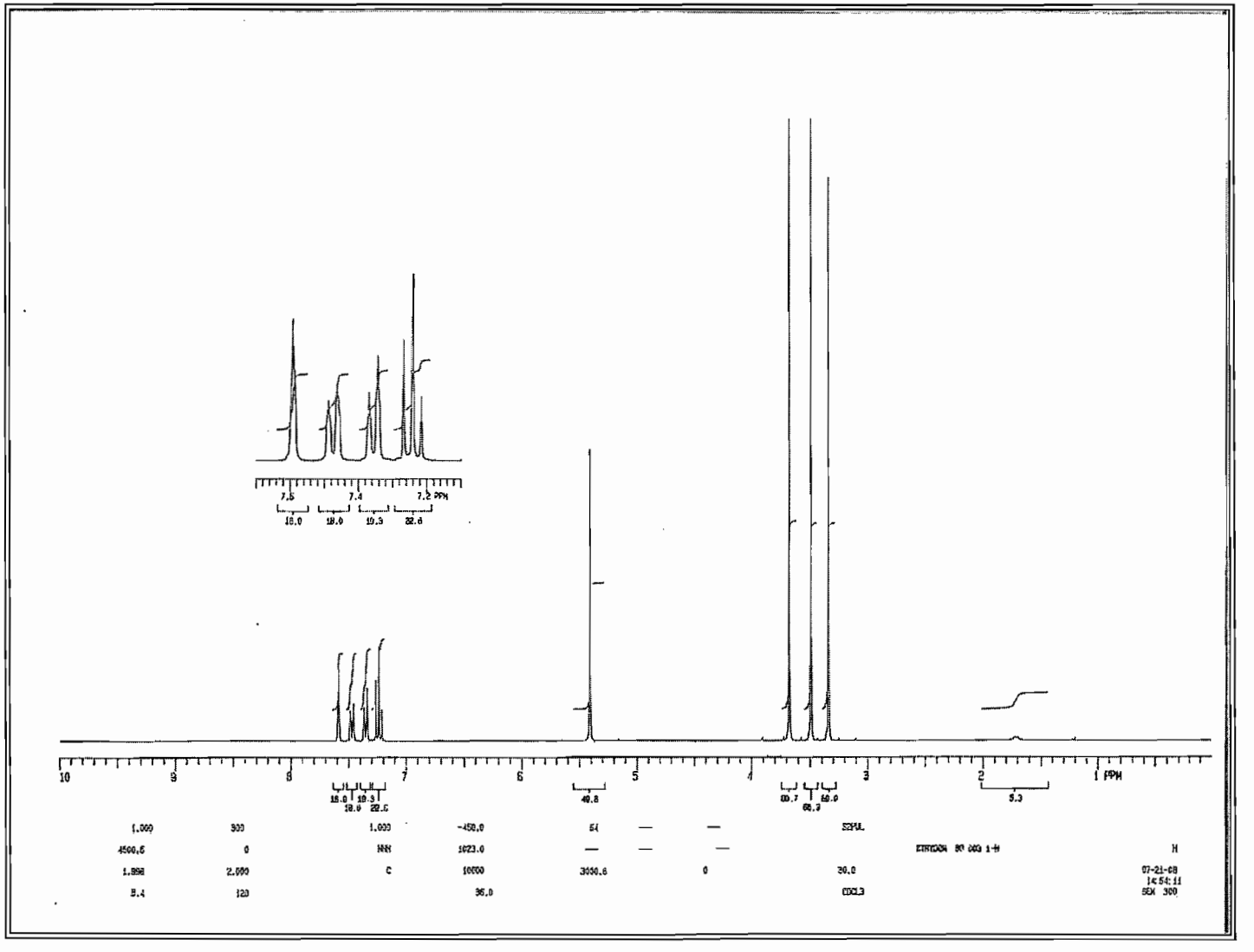

^{13}C NMR

8-(3-Fluorobenzyloxy)caffeine (1d)

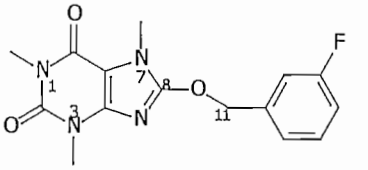

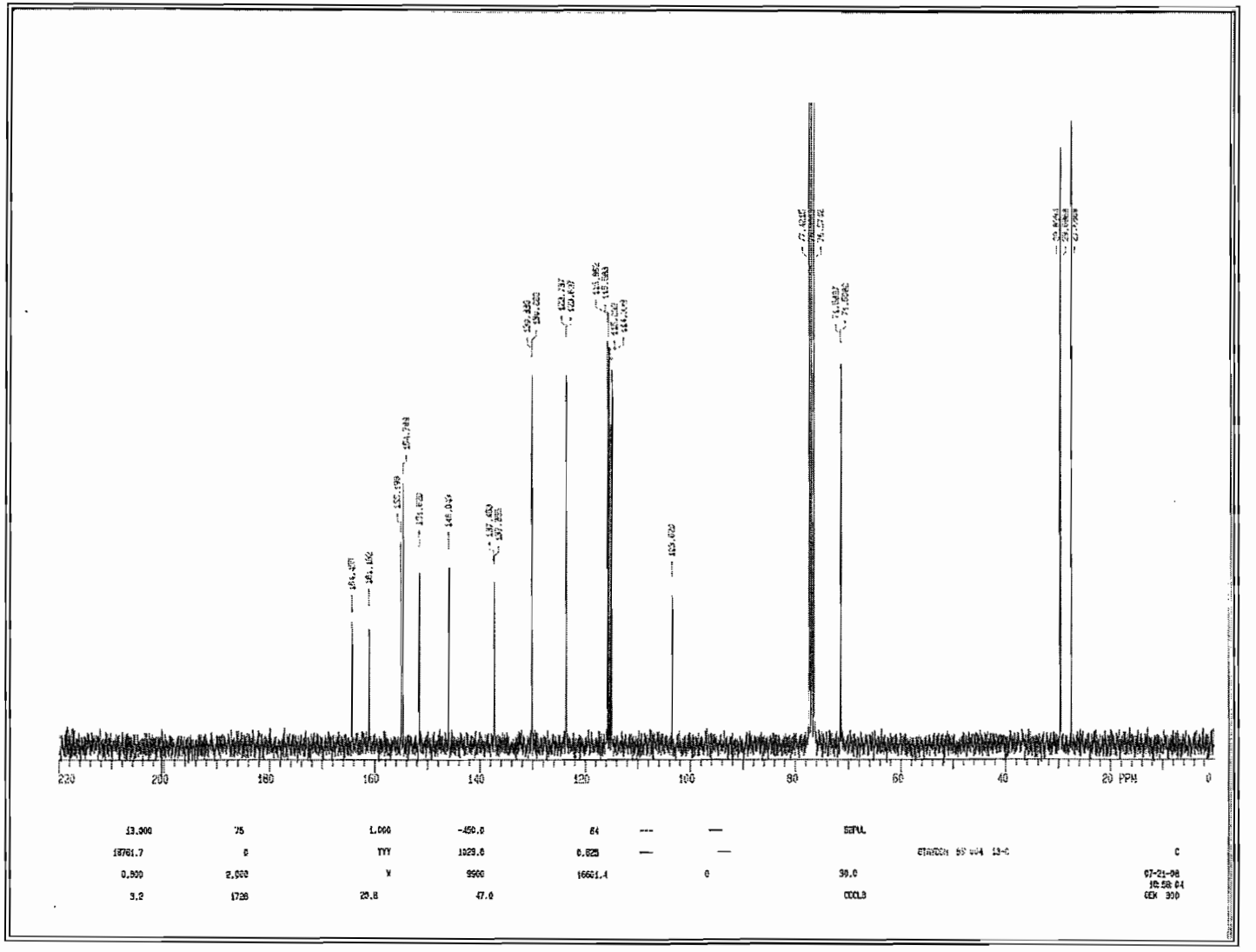

^{1}H NMR

8-(3-Fluorobenzyloxy)caffeine (1d)

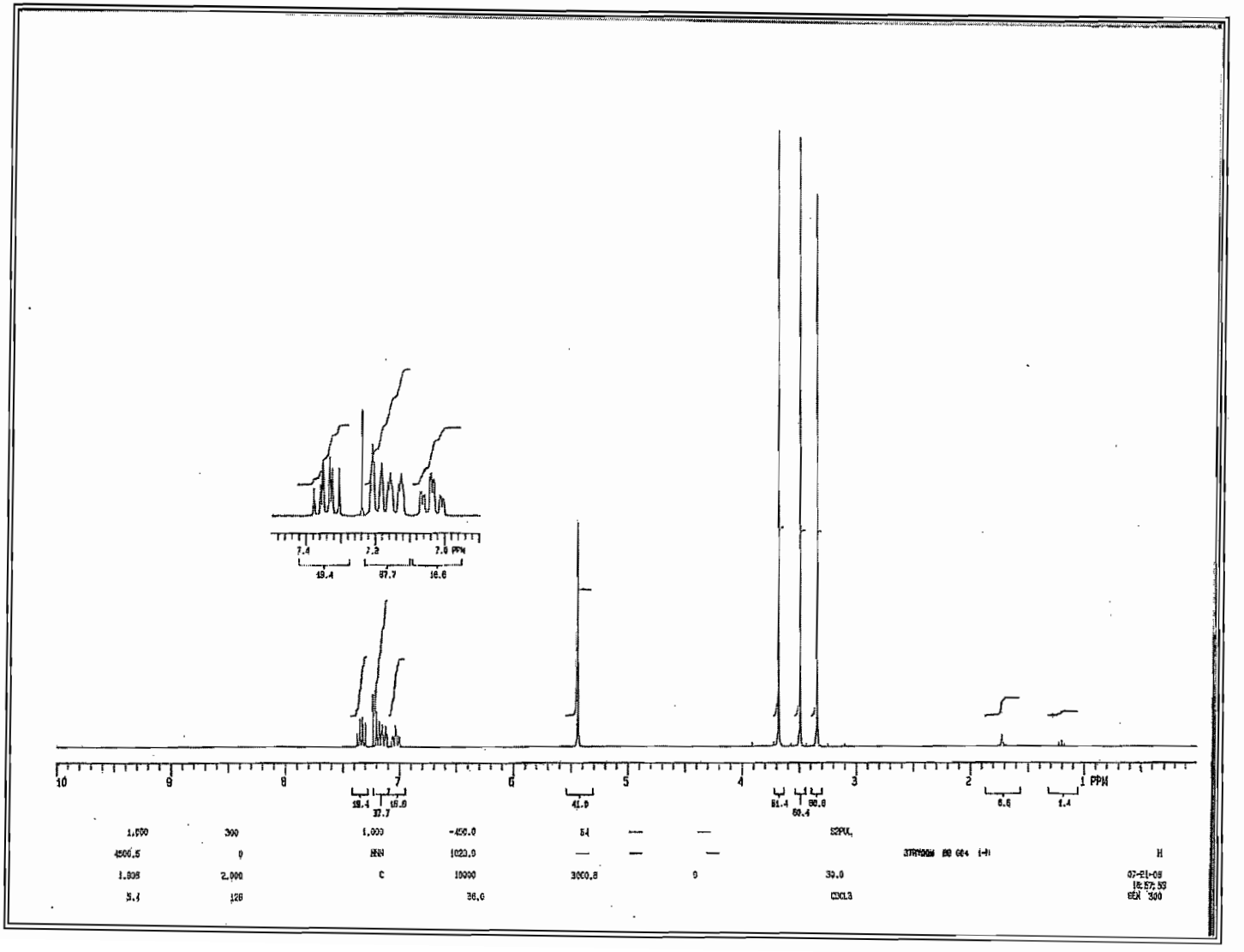

^{13}C NMR

8-(3-Trifluoromethylbenzyloxy)caffeine (1e)

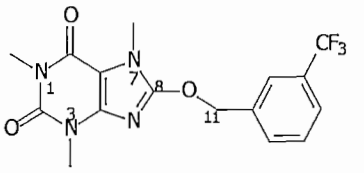

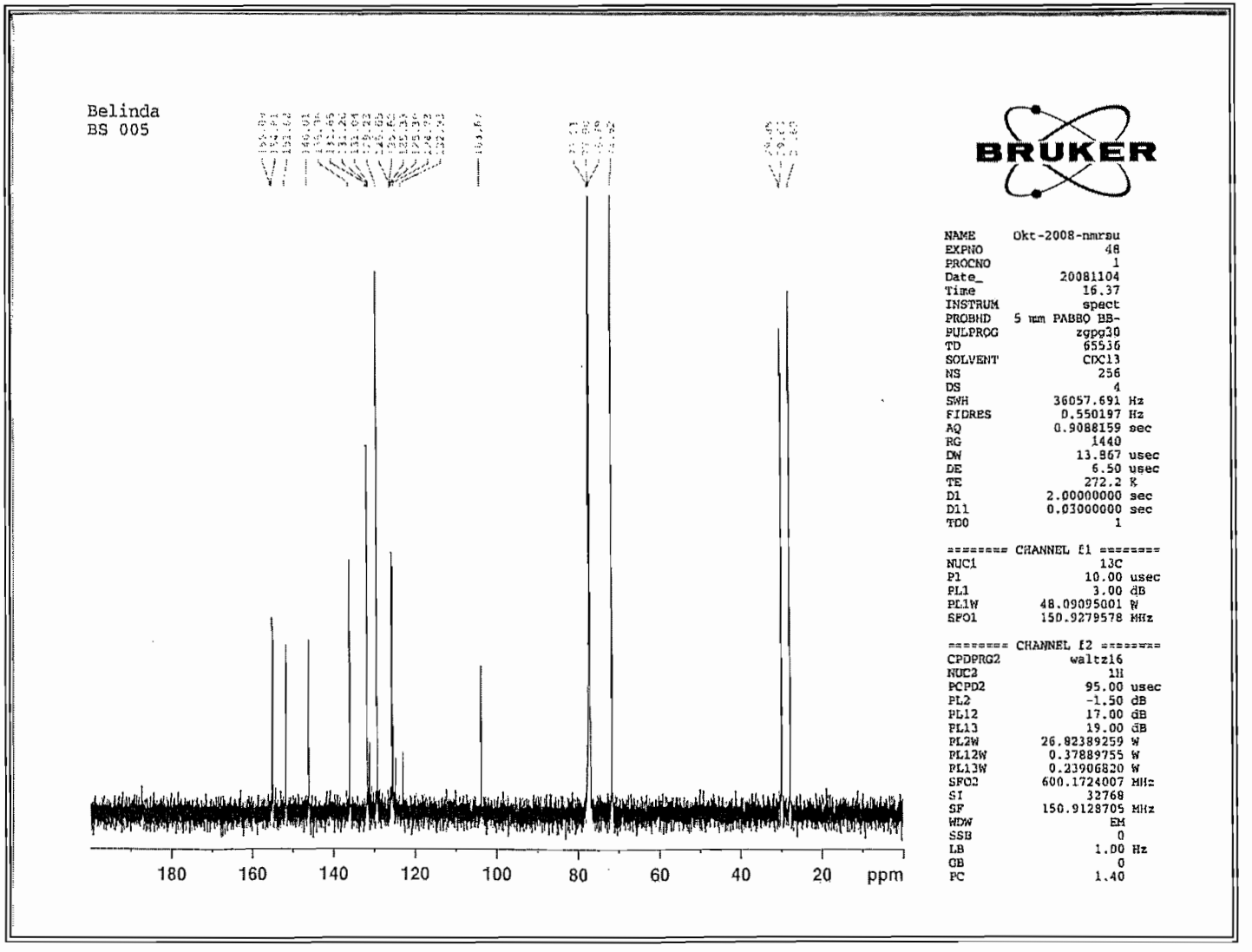

NAME	Okt-2008-nmrsu
EXPNO	48
PROCNO	1
Date_	20081104
Time	16.37
INSTRUM	spect
PROBHD	5 mm PABBO BB-
PULPROG	zgpg30
TD	65536
SOLVENT	CDCl3
NS	256
DS	4
SWH	36057.691 Hz
FIDRES	0.550197 Hz
AQ	0.9088159 sec
RG	1440
DW	13.867 usec
DE	6.50 usec
TE	272.2 K
D1	2.00000000 sec
D11	0.03000000 sec
TD0	1
======== CHANNEL f1 ========	
NUC1	13C
P1	10.00 usec
PL1	3.00 dB
PL1W	48.09095001 W
SFO1	150.9279578 MHz
======== CHANNEL f2 ========	
CPDPRG2	waltz16
NUC2	1H
PCPD2	95.00 usec
PL2	-1.50 dB
PL12	17.00 dB
PL13	19.00 dB
PL2W	26.92389259 W
PL12W	0.37889755 W
PL13W	0.23906820 W
SFO2	600.1724007 MHz
SI	32768
SF	150.9128705 MHz
WDW	EM
SSB	0
LB	1.00 Hz
GB	0
PC	1.40

^{1}H NMR

8-(3-Trifluoromethylbenzyloxy)caffeine (1e)

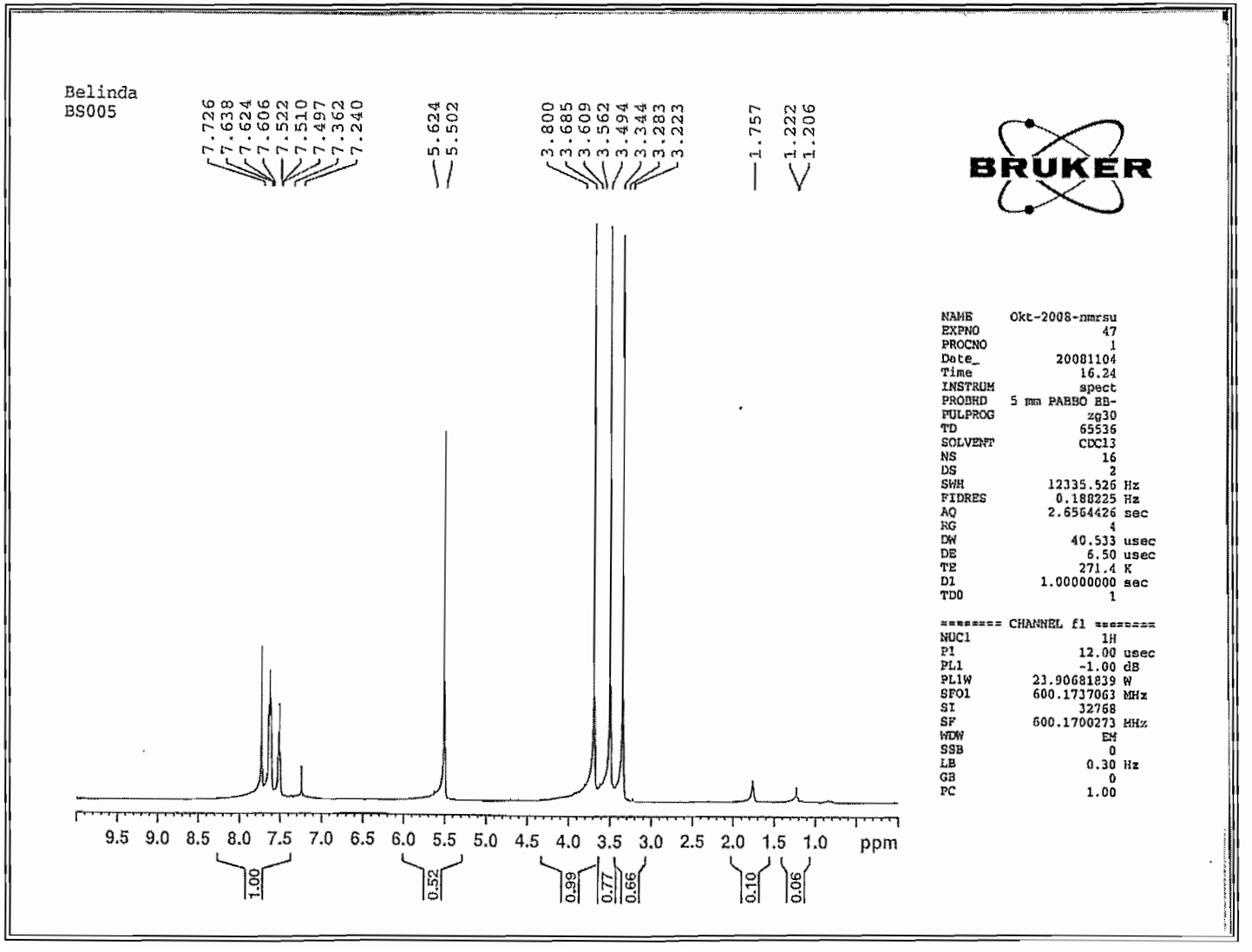

^{13}C NMR

8-(3-Methylbenzyloxy)caffeine (1f)

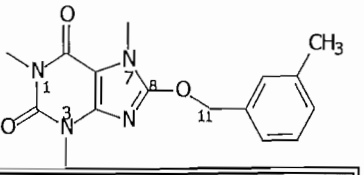

Belinda
BS 006

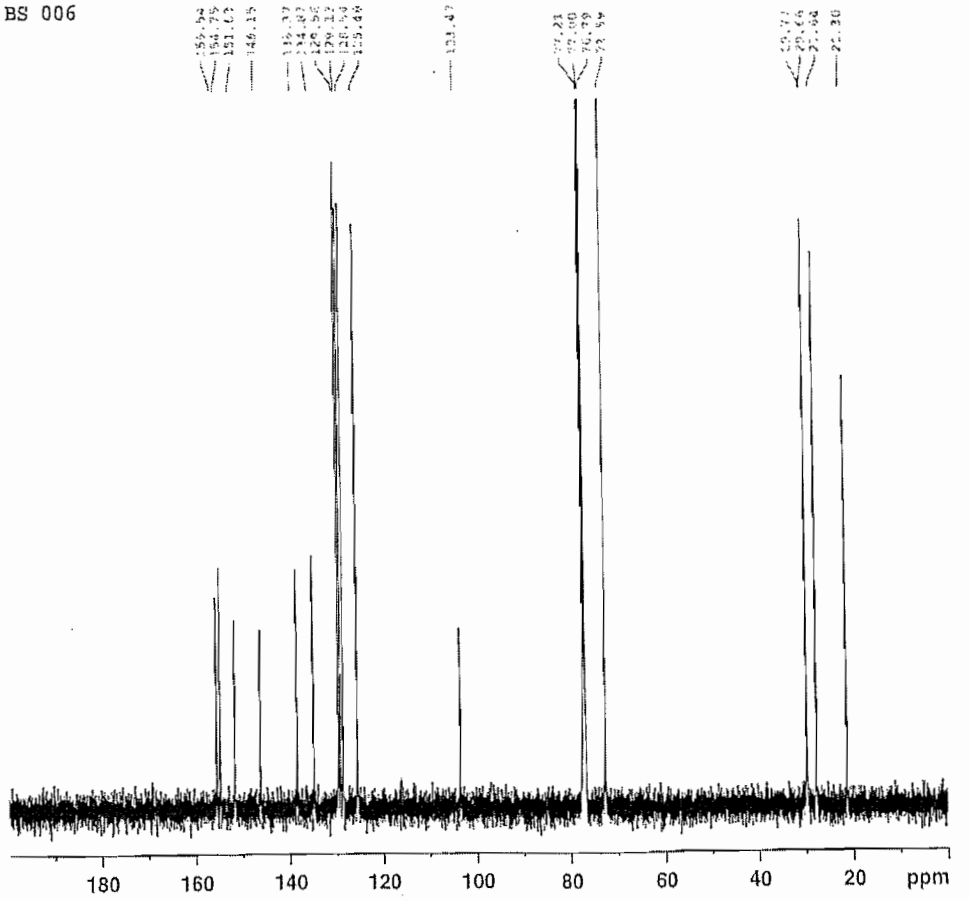

BRUKER

NAME	Okt-2008-nmrau
EXPNO	46
PROCNO	1
Date_	20081104
Time	16.14
INSTRUM	spect
PROBHD	5 mm PABBO BB-
PULPROG	zgpg30
TD	65536
SOLVENT	CDCl3
NS	256
DS	4
SWH	36057.691 Hz
FIDRES	0.550197 Hz
AQ	0.9088159 sec
RG	1150
DW	13.867 usec
DE	6.50 usec
TE	273.1 K
D1	2.00000000 sec
D11	0.03000000 sec
TD0	1
======== CHANNEL f1 ========	
NUC1	13C
P1	10.00 usec
PL1	3.00 dB
PL1W	48.09095001 W
SFO1	150.9279578 MHz
======== CHANNEL f2 ========	
CPDPRG2	waltz16
NUC2	1H
PCPD2	95.00 usec
PL2	-1.50 dB
PL12	17.00 dB
PL13	19.00 dB
PL2W	26.82389259 W
PL12W	0.37889755 W
PL13W	0.23906820 W
SFO2	600.1724007 MHz
SI	32768
SF	150.9138751 MHz
WDW	EM
SSB	0
LB	1.00 Hz
GB	0
PC	1.40

^{1}H NMR

8-(3-Methylbenzyloxy)caffeine (1f)

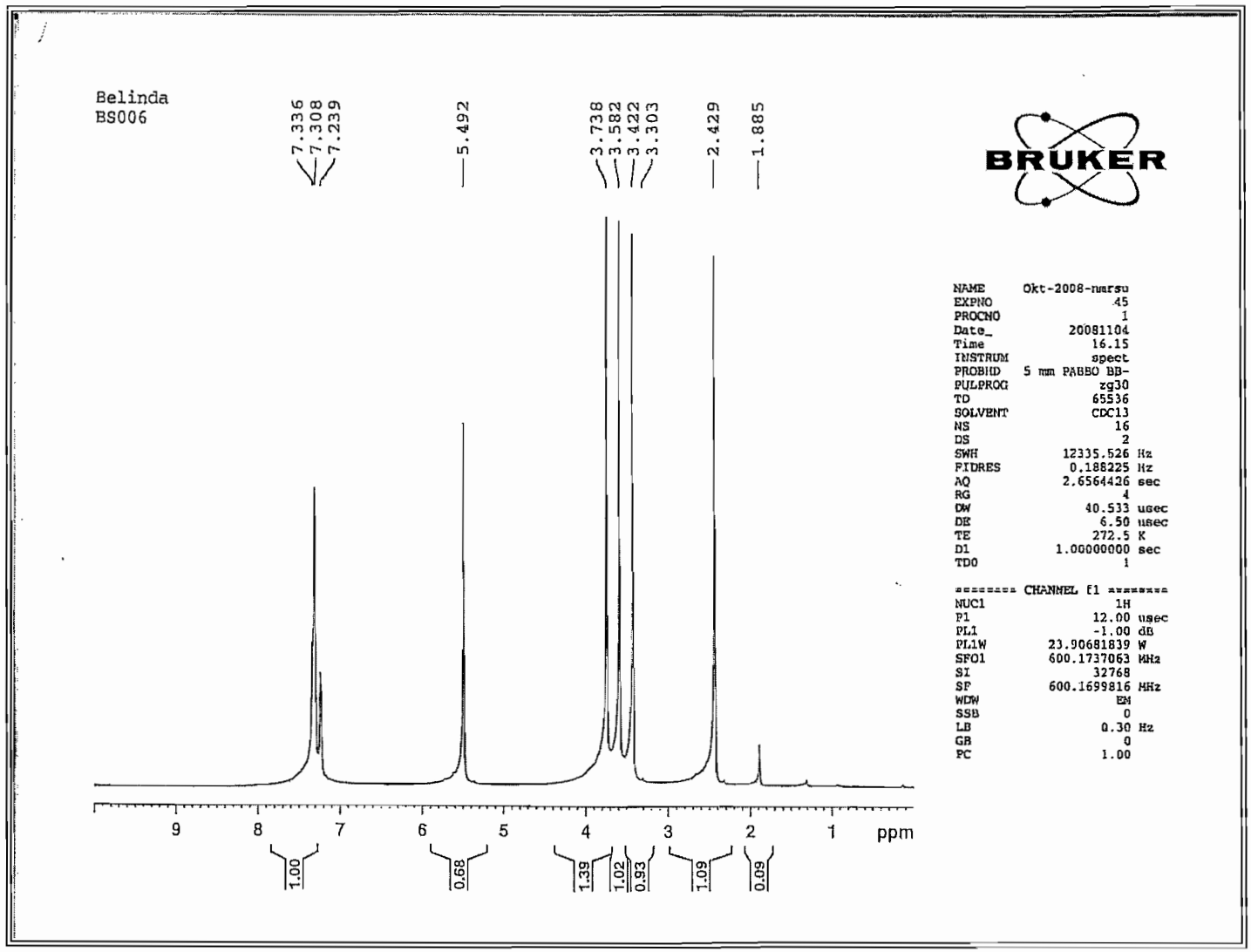

^{13}C NMR

8-(3-Methoxybenzyloxy)caffeine (1g)

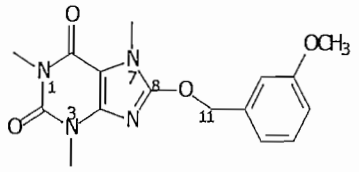

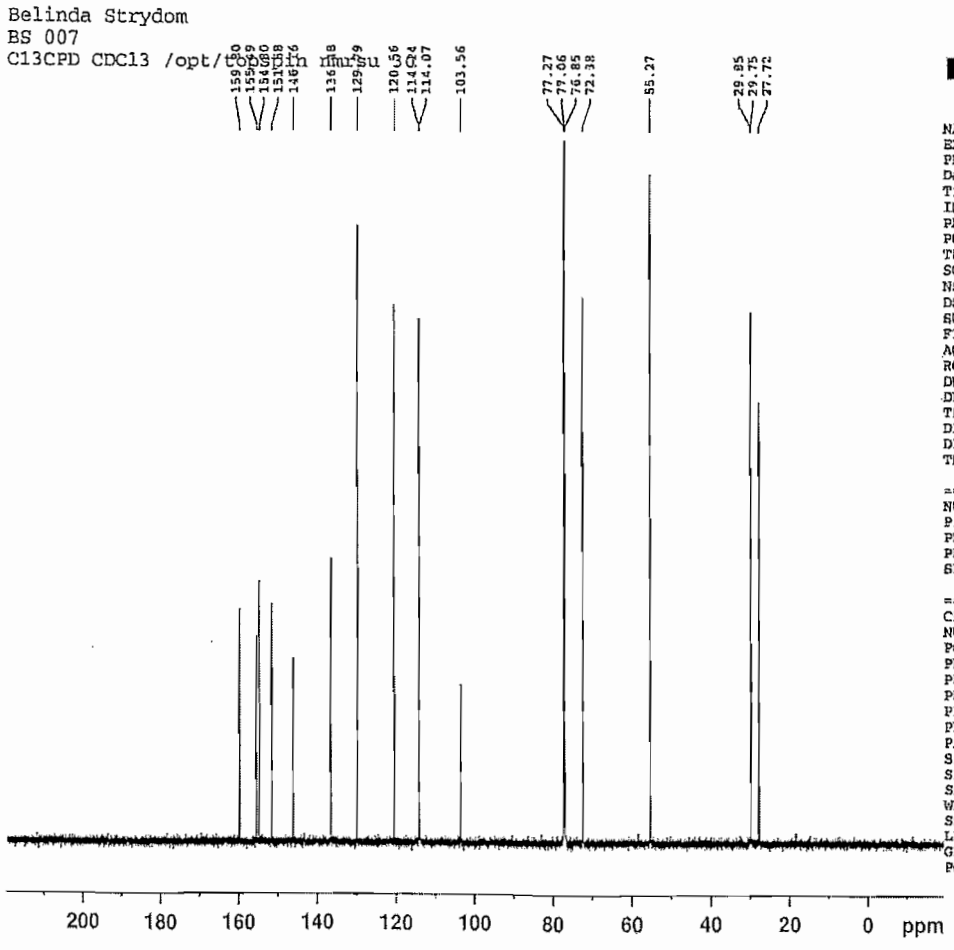

BRUKER

NAME	Aug26-2008-nmrsu
EXPNO	31
PROCNO	1
Date_	20080826
Time	14.25
INSTRUM	spect
PROBHD	5 mm PABBO BB-
PULPROG	zgpg30
TD	65536
SOLVENT	CDCl3
NS	512
DS	4
SWH	36057.691 Hz
FIDRES	0.550197 Hz
AQ	0.9088159 sec
RG	2050
DW	13.867 usec
DE	6.50 usec
TE	300.0 K
D1	2.00000000 sec
D11	0.03000000 sec
TD0	1
======== CHANNEL f1 ========	
NUC1	13C
P1	10.00 usec
PL1	3.00 dB
PL1W	48.09095001 W
SFO1	150.9279578 MHz
======== CHANNEL f2 ========	
CPDPRG2	waltz16
NUC2	1H
PCPD2	95.00 usec
PL2	-1.50 dB
PL12	17.00 dB
PL13	19.00 dB
PL2W	26.82389259 W
PL12W	0.37889755 W
PL13W	0.23906820 W
SFO2	600.1724007 MHz
SI	32768
SF	150.9128670 MHz
WDW	EM
SSB	0
LB	1.00 Hz
GB	0
PC	1.40

^{1}H NMR

8-(3-Methoxybenzyloxy)caffeine (1g)

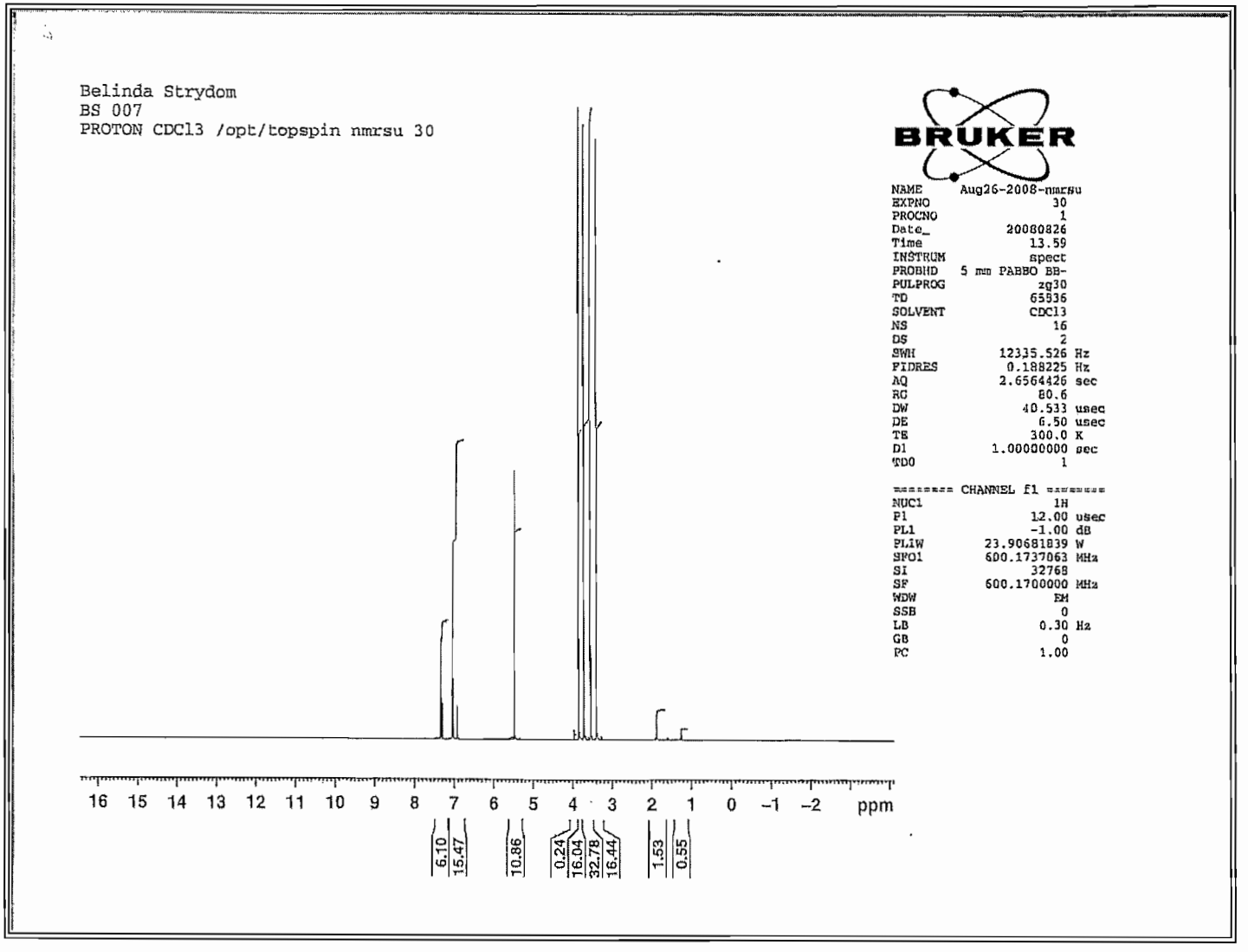

APPENDIX B

Concept article:

Inhibition of monoamine oxidase by 8-benzyloxycaffeine analogues

Belinda Strydom [a], Sarel F. Malan [a], Neal Castagnoli Jr. [b], Jacobus J. Bergh [a], Jacobus P. Petzer [a,*]

[a] *Pharmaceutical Chemistry, School of Pharmacy, North-West University, Private Bag X6001, Potchefstroom, 2520, South Africa*

[b] *Department of Chemistry, Virginia Tech and Edward Via College of Osteopathic Medicine, Blacksburg, VA 24061, USA*

Abstract—Based on recent reports that several (*E*)-8-styrylcaffeinyl analogues are potent reversible inhibitors of monoamine oxidase B (MAO-B) a series of 8-benzyloxycaffeinyl analogues were synthesized and evaluated as inhibitors of baboon liver MAO-B and recombinant human MAO-A and –B. The 8-benzyloxycaffeinyl analogues were found to reversibly inhibit both MAO isoforms with enzyme-inhibitor dissociation constants (K_I values) ranging from 0.14 to 1.30 μM for the inhibition of human MAO-A, and 0.023 to 0.59 μM for the inhibition of human MAO-B. The analogues inhibited human and baboon MAO-B with similar potencies. A quantitative structure-activity relationship (QSAR) study indicated that the MAO-B inhibition potencies of the 8-benzyloxycaffeinyl analogues are dependent on the Hansch lipophilicity (π) and Hammett electronic (σ) constants of the substituents at C-3 of the benzyloxy ring. Electron-withdrawing substituents with a high degree of lipophilicity enhance inhibition potency. These results are discussed with reference to possible binding orientations of the inhibitors within the active site cavities of MAO-A and –B.

Keywords: Monoamine oxidase; Reversible inhibition; 8-Benzyloxycaffeine; Caffeine; Quantitative structure-activity relationship; Molecular docking.

* Corresponding author. Tel.: +27 18 2992206; fax: +27 18 2994243.

E-mail address: jacques.petzer@nwu.ac.za (J.P. Petzer).

1. Introduction

Monoamine oxidase A and B (MAO-A and –B) are flavin adenine dinucleotide (FAD) containing enzymes which catalyze the oxidation of a variety of endogenous and xenobiotic amines in the brain and peripheral tissues (Youdim & Bakhle, 2006). The two isoforms are attached to the outer mitochondrial membrane and have different substrate and inhibitor specificities (Youdim, Edmondson & Tipton, 2006). MAO-A preferentially utilizes serotonin and norepinephrine as substrates and is irreversibly inhibited by clorgyline while MAO-B preferentially utilizes benzylamine as substrate and is irreversibly inhibited by (*R*)-deprenyl. Both isoforms catalyze the oxidative deamination of dopamine (Youdim, Edmondson & Tipton, 2006). Due to their roles in the metabolism of neurotransmittor amines, inhibitors of MAO-A and –B have been used in the treatment of neurological disorders. MAO-A inhibitors are used to treat depressive illness (Youdim, Edmondson & Tipton, 2006) while MAO-B inhbitors are useful in the treatment of Parkinson's disease (PD) (Fernandez & Chen, 2007). In the basal ganglia, oxidation by MAO-B appears to be the major metabolic pathway of dopamine and inhibitors of this enzyme may therefore slow the depletion of dopamine stores in the PD brain and posssibly elevate the concentrations of endogenous dopamine and dopamine produced from administered levodopa (Collins et al., 1970; Youdim et al., 1972; Di Monte et al., 1996). In primates, MAO-B inhibitors have been shown to enhance the elevation of dopamine concentrations in the striatum following levodopa treatment (Finberg et al., 1998). As a consequence, MAO-B inhibitors are employed as adjuvants to levodopa in the symptomatic treatment of PD (Fernandez & Chen, 2007). MAO-B inhibitors may also exert a neuroprotective effect by reducing potentially toxic side-products associated with the metabolism of monoamines. These include H_2O_2 and aldehyde products which may be neurotoxic if not rapidly metabolized to inactive compounds (Youdim & Bakhle, 2006). Since MAO-B activity as well as density increases in most brain regions with age, MAO-B inhibition may be especially relevant as a treatment strategy in the aged parkinsonian brain (Nicotra et al., 2004; Fowler et al., 1997).

We have recently reported that several (*E*)-8-styrylcaffeinyl analogues (**1**) (Fig. 1) are potent reversible inhibitors of monoamine oxidase B (MAO-B) (Vlok et al., 2006; Van den Berg et al., 2007; Pretorius et al., 2008). The styryl side chain of these analogues is an important structural feature for inhibition since caffeine (**2**) is a weak inhibitor of MAO-B (Van der Walt et al., 2009). A possible explanation for this effect is that (*E*)-8-styrylcaffeinyl analogues may

exhibit a dual binding mode within MAO-B with the caffeine ring located in the substrate cavity of the enzyme while the styryl side chain extends into the entrance cavity (Vlok et al., 2006). This would allow for more productive binding interactions with the enzyme and hence more potent inhibition. In contrast, caffeine is predicted to bind to either the substrate or entrance cavity. This view is supported by crystal structures of MAO-B which show that several potent reversible inhibitors span both active site cavities. For example, in the complex between safinamide (**3**) (Fig. 2) and MAO-B, the 3-fluorobenzyloxy side chain of safinamide is located in the entrance cavity while the propanamide moiety binds within the substrate cavity (Binda et al., 2007). Similarly, the 3-chlorobenzyloxy side chain of 7-(3-chlorobenzyloxy)-4-formylcoumarin (**4**) binds in the entrance cavity of the enzyme with the coumarin ring occupying the substrate cavity (Binda et al., 2007). Based on these observations it can be concluded that the styryl side chain of (*E*)-8-styrylcaffeinyl analogues and the benzyloxy side chains of **3** and **4** likely exhibit similar binding modes within the entrance cavity of MAO-B and are essential in stabilizing the complexes between the enzyme and the respective inhibitors. Since the styryl and benzyloxy side chains appear to have similar biological properties with respect to binding to MAO-B, in the present study a series of 8-benzyloxycaffeinyl analogues (**5a–g**) were synthesized and evaluated as inhibitors of baboon liver MAO-B and recombinant human MAO-B. By comparing the inhibition potencies of these analogues with those of the corresponding (*E*)-8-styrylcaffeinyl analogues the efficacy by which the benzyloxy side chain enhances the affinity of inhibitors for the active site of MAO-B may be compared to that of styryl substitution. The 8-benzyloxycaffeinyl analogues were also evaluated as potential inhibitors of recombinant human MAO-A. Previous studies have suggested that structures with a relatively larger degree of conformational freedom may be better suited for binding to MAO-A than relatively rigid structures (Van der Walt et al., 2009). Since the benzyloxy side chain is relatively flexible and free to rotate about the carbon-oxygen ether bond, 8-benzyloxycaffeinyl analogues may be expected to also bind to the MAO-A active site. These studies may contribute to the discovery of a new class of potent reversible MAO inhibitors.

2. Results

2.1. Chemistry

The 8-benzyloxycaffeinyl analogues (**5a–g**) examined in this study were prepared according to a procedure previously reported for the synthesis of **5a** (Scheme 1) (Huston & Allen, 1934). The appropriate benzylalcohol derivatives (**6**) were heated with dry 8-chlorocaffeine (**7**) at

high temperatures (150–170 °C) in the presence of metallic sodium. The products so obtained were recrystallized from ethanol to give **5a–g** in low to fair yields (13–44%). 8-Chlorocaffeine in turn was synthesized in high yield by reacting chlorine with caffeine in chloroform (Fischer & Reese., 1883). The structures and purity of the target compounds were verified by mass spectrometry, ^{1}H NMR and ^{13}C NMR. For previously reported **5a**, the melting point obtained corresponded to the literature value as cited in the Experimental section.

2.2. General enzymology

The 8-benzyloxycaffeinyl analogues (**5a–g**) examined here were evaluated initially as inhibitors of baboon liver mitochondrial MAO-B and then as inhibitors of recombinant human MAO-B and MAO-A. For this purpose the IC_{50} values (concentration of the inhibitor that produces 50% inhibition) for the inhibition of MAO by each test compound were measured. Since the test inhibitors exhibited a competitive mode of inhibition (see below), the IC_{50} values were converted to the corresponding K_i values (enzyme–inhibitor dissociation constants) using the Cheng-Prusoff equation (Cheng & Prusoff, 1973; Pretorius et al., 2008). These K_i values enabled the calculation of MAO-A/B selectivity ratios.

To evaluate **5a–g** as potential inhibitors of baboon liver mitochondrial MAO-B, the enzyme activity measurements were based on the extent to which the MAO-A/B mixed substrate, 1-methyl-4-(1-methylpyrrol-2-yl)-1,2,3,6-tetrahydropyridine (MMTP), is oxidized to the corresponding dihydropyridinium metabolite ($MMDP^+$) (Inoue et al., 1999). The production of $MMDP^+$ was measured spectrophotometrically at a wavelength of 420 nm where neither the substrate (MMTP) nor the test inhibitors absorb light. Inactivation of the MAO-A isoform was deemed unnecessary since baboon liver mitochondrial fractions are devoid of MAO-A activity (Inoue et al., 1999). For the purpose of converting the IC_{50} values of the test inhibitors to K_i values, a K_m value of 68.3 μM for the oxidation of MMTP by baboon liver MAO-B was used (Pretorius et al., 2008).

To evaluate **5a–g** as potential inhibitors of recombinant human MAO-A and MAO-B, the enzyme activity measurements were based on the extent to which kynuramine is oxidized to 4-hydroxyquinoline by the MAO isoforms (Novaroli et al., 2005). The formation of 4-hydroxyquinoline was measured fluorometrically at excitation and emission wavelengths of 310 and 400 nm, respectively.

None of the test inhibitors fluoresced at this excitation/emission wavelength or quenched the fluorescence of 4-hydroxyquinoline at the concentrations used for the inhibition studies. This fluorometric protocol is considerably more sensitive than the spectrophotometric method describe above and was thus more suitable for the measurement of recombinant human MAO-A (0.0075 mg protein/mL) and MAO-B (0.015 mg protein/mL) activities, which were relatively low compared to the activity of baboon liver mitochondrial MAO-B (0.15 mg protein/mL) at the enzyme concentrations used for this study. For the purpose of converting the IC_{50} values of the test inhibitors to K_i values, K_m values for the oxidation of kynuramine by recombinant human MAO-A and MAO-B were determined (see Experimental) (Pretorius et al., 2008). These were to found to be 16.1 ± 0.21 μM and 22.7 ± 0.72 μM for MAO-A and –B, respectively (data not shown).

2.3. MAO-B inhibition studies

As shown in Table 1, all of the 8-benzyloxycaffeinyl analogues (**5a–g**) evaluated were found to be inhibitors of baboon liver and recombinant human MAO-B (Fig. 3). The most potent inhibitor was **5c** with an IC_{50} value of 0.068 μM for the inhibition of recombinant human MAO-B. This corresponds to a calculated K_i value of 0.023 μM (Table 2). For this series, the K_i values ranged from 0.023 to 0.59 μM, indicating that all the test compounds are relatively potent inhibitors. Since the unsubstituted homolog, **5a**, was the weakest inhibitor it can be concluded that substitution at C-3 of the benzyloxy ring enhances MAO-B inhibition potency. Also, the inhibition potencies recorded with baboon and human MAO-B were found to be relatively similar. Based on this observation it can be concluded that the interactions of reversible inhibitors with human and baboon MAO-B are similar. This implies that there are not many significant differences between the geometries and amino acid residues of the active sites of these two enzymes.

To determine the modes of inhibition, sets of lineweaver–Burk plots were constructed for the inhibition of baboon MAO-B by one representative inhibitor, compound **5e**. As illustrated by example in fig. 4, the lines of the Lineweaver-Burk plots intersected which indicates that the mode of inhibition is competitive and that inhibition is therefore reversible. Essentially the same result was obtained when using recombinant human MAO-B as enzyme source (data

not shown). These results are in accordance with expectation since (*E*)-8-styrylcaffeinyl analogues are also reported to inhibit MAO-B competitively (Vlok et al., 2006; Van den Berg et al., 2007; Pretorius et al., 2008). To further confirm that the test inhibitors bind reversibly in the active site of MAO-B, one representative inhibitor, compound **5b** was selected for reversibility studies. Baboon liver mitochondria were preincubated with **5b** (0.28 μM, approximately 2 × IC_{50}) for periods of 0, 15, 30, and 60 minutes and the rates of the MAO-B catalyzed oxidation of MMTP (50 μM) to $MMDP^+$ were measured (Khalil et al., 2000; Manley-King et al., 2009). As shown in fig. 5 there is no decrease of MAO-B catalytic rate with increased incubation time. Similarly, when **5b** (0.23 μM, approximately 2 × IC_{50}) was preincubated with recombinant human MAO-B for periods of 0, 15, 30, and 60 minutes, the rate of kynuramine (30 μM) oxidation did not decrease with increased incubation time (data not shown). From these analyses it can be concluded that **5b** interacts reversibly with the active sites of baboon and human MAO-B.

2.4. MAO-A inhibition studies

Interestingly, the 8-benzyloxycaffeinyl analogues (**5a–g**) were also inhibitors of recombinant human MAO-A. The most potent inhibitor was **5f** with an IC_{50} value of 0.397 μM (Table 1) which corresponds to a calculated K_i value of 0.14 μM (Table 2). The K_i values ranged from 0.14 to 1.30 μM, indicating that **5a–g** are moderate to potent inhibitors of MAO-A. In general, however, these analogues were better MAO-B inhibitors. Based on the selectivity indexes (Table 2), compound **5e** displayed the highest selectivity for MAO-B (25-fold). The most potent MAO-B inhibitor of the series **5c** also exhibited a high degree of selectivity for MAO-B (14-fold). Compounds **5a** and **5f** were essentially nonselective.

To determine the mode of MAO-A inhibition, sets of lineweaver–Burk plots were constructed for the inhibition of human MAO-A by compound **5e**, which was selected as a representative inhibitor. As illustrated by example in fig. 6, the lines of the Lineweaver-Burk plots intersected which indicates that, similar to the inhibition of MAO-B, the mode of inhibition of MAO-A is competitive and reversible. The reversibility of inhibition was further demonstrated by preincubating recombinant human MAO-A with compound **5b** (1.31 μM, approximately 2 × IC_{50}) for periods of 0, 15, 30, and 60 minutes followed by measuring the rates of MAO-B catalyzed oxidation of kynuramine (45 μM). As shown in fig. 7, MAO-B catalytic rate is not

reduced with increased incubation time which indicates that **5b** binds reversibly to the active site of human MAO-A.

2.5. Quantitative structure-activity relationship (QSAR) studies

The results of the MAO-B inhibition studies (Tables 1 and 2) indicate that substitution at C-3 of the benzyloxy ring enhances MAO-B inhibition potency. To further investigate the effect of the substituents on the MAO-B inhibitory activity, a Hansch-type QSAR study was carried out. Five parameters were used to describe the physiochemical properties of the substituents. The Van der Waals volume (V_w) (Van de Waterbeemb *et al.*, 1987) and Taft steric parameter (E_s) (Hansch *et al.*, 1995) served as descriptors of the bulkiness of the substituents, while the lipophilicities were described by the Hansch constant (π) (Hansch *et al.*, 1995). The electronic properties were described by the classical Hammett constant (σ_m) and the Swain-Lupton constant (F) (Hansch *et al.*, 1995). The values of these physicochemical parameters were obtained from standard compilations (Hansch *et al.*, 1995, Van de Waterbeemb *et al.*, 1987).

QSAR studies were carried out with the inhibition data obtained with baboon liver MAO-B and recombinant human MAO-B as enzyme sources and the results are summarized in tables 3 and 4, respectively. Using the data generated with baboon liver MAO-B, a meaningful correlation was observed between the lipophilicity constant, π, and the inhibition potency ($\log IC_{50}$) with an R^2 value of 0.82. The statistical *F* value for this correlation was 27.8, which is higher than F_{max} value (25.32) (Livingstone, 2005) for 95% significance. A higher *F* value indicates a better fit. Improved correlations were obtained with the addition of a second substituent parameter. A two-parameter fit with the Hammett electronic parameter (σ_m) and π versus the inhibition potency ($\log IC_{50}$) yielded the best correlation with an R^2 of 0.98 and a statistical *F* value of 147 (F_{max} = 30.18) (Fig. 8). For this correlation the probability that σ_m and π are zero is 0.3% and 0.07%, respectively. The best mathematical description for the binding affinity of 8-benzyloxycaffeinyl analogues (**5a–g**) to baboon liver MAO-B is therefore:

$$\log IC_{50} = -1.23(\pm 0.19)\sigma_m - 0.93(\pm 0.10)\pi + 0.31(\pm 0.05)$$
$$(R^2 = 0.98 \text{ and } F = 147)$$

A two-parameter fit with the Swain-Lupton constant (F) and π also yielded good correlations with the inhibition potency ($\log IC_{50}$) and R^2 and *F* values of 0.98 and 120 (F_{max} = 30.18),

respectively, were recorded. The negative signs of the F (–1.12 ± 0.19) and σ_m (–1.23 ± 0.19) parameter coefficients indicate that the inhibition potencies of **5a–g** towards baboon liver MAO-B may be enhanced by substitution with electron withdrawing groups at C-3 of the benzyloxy ring. The negative correlations of the inhibition potencies with the π constant indicate that substituents at C-3 of the benzyloxy ring with enhanced lipophilicity may result in more potent inhibitors.

Using the inhibition data generated with recombinant human MAO-B as enzyme source, the best correlation observed was between the lipophilicity constant, π, and the inhibition potency ($\log IC_{50}$). The R^2 and statistical *F* values of this correlation were 0.75 and 18.8 (F_{max} = 25.32), respectively. A slightly improved correlation was obtained with the addition of a second substituent parameter. A two-parameter fit of F and π versus the inhibition potency ($\log IC_{50}$) yielded a model with an R^2 value of 0.89 and a statistical *F* value of 25.4 (F_{max} = 30.18). Similarly, a two-parameter fit of σ_m and π versus the inhibition potency yielded a model with an R^2 value of 0.84 and a statistical *F* value of 17.3 (F_{max} = 30.18). Although these correlations are not statistically significant, the results are similar to those obtained with baboon liver MAO-B as enzyme sources and may be viewed as further support of the notion that the interactions of reversible inhibitors with human and baboon MAO-B are similar.

A similar analysis using the inhibition data obtained with recombinant human MAO-A as enzyme source, failed to yield meaningful correlations between the inhibition potencies and the substituent parameters.

2.6. Molecular modelling

In an attempt to obtain insights into the possible binding modes of the 8-benzyloxycaffeinyl analogues (**5a–g**) within the active sites of MAO-A and –B, molecular docking experiments were performed. The X-ray crystal structures of recombinant human MAO-A and MAO-B were obtained from the Brookhaven Protein Data Bank. The structures of MAO-A co-crystallized with harmine (PDB code: 2Z5X) (Son et al., 2008) and MAO-B co-crystallized with safinamide (PDB code: 2V5Z) (Binda et al., 2007) were selected. These models were selected based on the relatively high resolution the crystallographic structures and the observation that, in the complex between MAO-B and safinamide, the side chain of Ile-199 is rotated out of the normal conformation to allow for fusion of the entrance and substrate

cavities. This is the preferred conformation when relatively large inhibitors, which span both the entrance and substrate cavities, bind to the active site of MAO-B (Hubalek et al., 2005). In contrast, the active site of MAO-A consists of a single cavity.

For the purpose of the docking studies, the LigandFit application of the modelling software Discovery Studio 1.7 (Accelrys), was used according to a modification of a previously reported protocol (Ogunrombi et al., 2008; Van der Walt et al., 2009). The structures of **5a–g** were built and geometry optimized in Discovery Studio and prepared for docking with the Prepare Ligands protocol. Following the addition of hydrogen atoms and the correction of the valences of FAD cofactors and co-crystallized ligands, the protein structures were subjected to an energy minimization while the protein backbone was constrained (see Experimental). Subsequently, the energy-minimized structures were deprived of the co-crystallized ligands and the backbone constraints. Following the docking procedure, the docked ligand conformations were further refined using the Smart Minimizer algorithm. Ten possible docking poses were calculated for each inhibitor.

The best-ranked docking solutions obtained with the structure of MAO-B showed one prevailing pose for all of the 8-benzyloxycaffeinyl analogues (**5a–g**). The inhibitors traverse both cavities of MAO-B with the caffeinyl moiety oriented towards the FAD co-factor in the substrate cavity while the benzyloxy side chain protrudes into the entrance cavity. As shown by example with inhibitor **5a**, the carbonyl oxygen at C-6 of the caffeinyl ring forms hydrogen bonds with the phenolic hydrogen of Tyr-435 (Fig. 9a). The amide functional group of the Gln-206 side chain possibly interacts with the caffeinyl ring via π–π interactions with an interplane distance of approximately 4.0 Å (Son et al., 2008). The benzyloxy ring is stabilized by Van der Waals interactions in the hydrophobic entrance cavity defined by Phe-103, Trp-119, Leu-164, Leu-167, Phe-168 and Ile-316 (Novarolli et al., 2006). Of importance is observation that the benzyloxy ring is partly located in space that would have been occupied by the side chain of Ile-199 if it were in the normal "closed" conformation. In the MAO-A active site the residue corresponding to Ile-199 in MAO-B is Phe-208. Since the increased size of the Phe aromatic ring compared to the side chain of Ile would prevent it form rotation into an alternative conformation, this binding mode of **5a** would not be possible in the MAO-A active site (Hubalek et al., 2005; Son et al., 2008). As shown in figure 9b the benzyloxy ring would partially overlap with Phe-208 in the MAO-A active site.

The best-ranked docking solutions obtained with the structure of MAO-A showed that the inhibitors bind with the caffeinyl moiety oriented towards the FAD co-factor (Fig. 10a). This binding mode is similar to that observed in the MAO-B active site. As illustrated by example with compound **5a**, one hydrogen bond is observed between the carbonyl oxygen at C-2 of the caffeinyl ring and the phenolic hydrogen of Tyr-444 in the active site. Interestingly, the caffeinyl ring is rotated through ~180 ° compared to the orientation in MAO-A. As expected, the benzyloxy side chains of the inhibitors are rotated to avoid unfavourable interactions with the side chain of Phe-208. For **5a**, the benzyloxy side chain is bent at the CH_2–O ether bond by about a 34 ° angle from the plane of the caffeinyl ring (Fig. 11). The relatively large degree of conformational freedom of the benzyloxy side chain may be an important structural feature required for MAO-A inhibition. As mentioned in the Introduction, the benzyloxy side chain is relatively flexible and free to rotate about the carbon-oxygen ether bond which would enable these inhibitors to avoid structural overlap with MAO-A active site amino acid residues (Van der Walt et al., 2009). This bended orientation would not be possible in MAO-B since the benzyloxy ring would partially overlap with Tyr-326 in the MAO-B active site (Fig. 10b). Other interactions between the inhibitors and the enzyme include π–π interactions between the caffeinyl ring and the amide functional group of the Gln-215 side chain with an interplane distance of approximately 3.5 Å (Son et al., 2008). The benzyloxy side chain may be stabilized via Van der Waals interactions with Val-210, Ile-325, Ile-335 and Leu-337 (La Regina et al., 2008).

3. Discussion

As mentioned in the introduction, based on the observation that several (*E*)-8-styrylcaffeinyl analogues are potent reversible inhibitors of MAO-B (Vlok et al., 2006; Van den Berg et al., 2007; Pretorius et al., 2008), a series of 8-benzyloxycaffeinyl analogues (**5a–g**) were synthesized and evaluated as inhibitors of baboon liver MAO-B and recombinant human MAO-B. The 8-benzyloxycaffeinyl analogues were found to reversibly and potently inhibit MAO-B with K_i values ranging from 0.023 to 0.59 μM for the inhibition of human MAO-B. Similar results were obtained using baboon MAO-B as enzyme source. In general, the 8-benzyloxycaffeinyl analogues were found to be approximately equipotent as inhibitors of MAO-B than the corresponding (*E*)-8-styrylcaffeinyl analogues. For example, (*E*)-8-(3-chlorostyryl)caffeine (**1a**) (Fig. 1) has a reported IC_{50} value of 0.146 μM for the inhibition of

mitochondrial baboon liver MAO-B while the corresponding 8-benzyloxycaffeinyl analogue **5b** inhibits baboon MAO-B with an IC_{50} value of 0.120 μM (Pretorius et al., 2008). Similarly, (*E*)-8-(3-bromostyryl)caffeine (**1b**) inhibits baboon MAO-B with an IC_{50} value of 0.107 μM while the corresponding 8-benzyloxycaffeinyl analogue **5c** exhibits an IC_{50} value of 0.113 μM (Pretorius et al., 2008). These results confirm that the styryl and benzyloxy side chains have similar biological properties with respect to binding to MAO-B and probably exhibit similar binding modes within the active site of MAO-B. The molecular docking studies suggest that the 8-benzyloxycaffeinyl analogues binds with the caffeinyl ring located within the substrate cavity of MAO-B while the benzyloxy side chain is located within the entrance cavity. (*E*)-8-Styrylcaffeinyl analogues are also thought to exhibit this dual binding mode, with the styryl side chain extending towards the entrance cavity of the enzyme (Vlok et al., 2006). The notion that the benzyloxy and styryl side chains bind within the entrance cavity of MAO-B is supported by the observation that, in the crystal structures of safinamide (**3**) and 7-(3-chlorobenzyloxy)-4-formylcoumarin (**4**) in complex with human MAO-B, the benzyloxy side chains of these inhibitors also occupy the entrance cavity of the enzyme (Binda et al., 2007).

Interestingly, the 8-benzyloxycaffeinyl analogues were also found to be reversible inhibitors of recombinant human MAO-A with K_i values ranging from 0.14 to 1.30 μM. In general, the 8-benzyloxycaffeinyl analogues, however, displayed a higher binding affinities for MAO-B than for MAO-A. The molecular docking studies indicate that the ability of the 8-benzyloxycaffeinyl analogues to bind to the MAO-A active site may, to a large degree, depend on the relatively large degree of rotation freedom of the benzyloxy side chain at the carbon-oxygen ether bond. This is in accordance to previous studies which suggested that relatively flexible inhibitors may be better accommodated in the MAO-A active site, by avoiding unfavourable interactions with active site amino acid residues (Van der Walt et al., 2009).

In the present study, substitution at C-3 of the benzyloxy ring has been shown to have a considerable effect on MAO-B inhibition potencies of 8-benzyloxycaffeinyl analogues. Since the benzyloxy side chain is predicted to bind within the entrance cavity of MAO-B, different interactions between the different C-3 substituents and the entrance cavity residues may explain this apparent SAR. The entrance cavity of MAO-B is reported to be composed of hydrophobic amino acid residues where hydrophobic inhibitor side chains may be stabilized by Van der Waals interactions (Novaroli et al., 2006). It can therefore be expected that

hydrophobic substituents at C-3 of the benzyloxy ring should enhance binding affinity of the 8-benzyloxycaffeinyl analogues to MAO-B. Accordingly, the QSAR study indicates that the inhibition potencies of the test inhibitors correlate with the lipophilicity constant of the C-3 substituents, with a higher degree of lipophilicity leading to enhanced inhibition potency.

These results further support the findings of the molecular docking studies which suggest that the benzyloxy side chain is bound to the entrance cavity of MAO-B. The observed correlations between MAO-B inhibition potency and the electronic parameters (σ_m and F) are not well understood. A possible explanation of the enhancement of inhibition potency by electron withdrawing C-3 substituents may be that electron withdrawing groups produce a dipole in the benzyloxy side chain which may interact with other dipoles and induced dipoles in the entrance cavity.

4. Experimental

Caution – MMTP is a structural analogue of the nigrostriatal neurotoxin, 1-methyl-4-phenyl-1,2,3,6-tetrahydropyridine (MPTP), and should be handled using disposable gloves and protective eyewear. Procedures for the safe handling of MPTP have been described previously (Pitts et al., 1986).

4.1. Chemicals and instrumentation

All starting materials not described elsewhere were obtained from Sigma-Aldrich and were used without purification. The oxalate salt of MMTP (Bissel et al., 2002) was prepared according to previously reported procedures. Kynuramine.2HBr was obtained from Sigma-Aldrich. Proton (^{1}H) and carbon (^{13}C) NMR spectra were recorded on a Varian Gemini 300 or on a Bruker Avance III 600 spectrometer. All NMR measurements were conducted in $CDCl_3$. Chemical shifts are reported in parts per million (δ) downfield from the signal of tetramethylsilane added to the deuterated solvent. Spin multiplicities are given as s (singlet), d (doublet), t (triplet) or m (multiplet). Direct insertion electron impact ionization (EIMS) and high resolution mass spectra (HRMS) were obtained on an Autospec ETOF (Micromass) mass spectrometer. Melting points (mp) were determined on a Stuart SMP10 melting point apparatus and are uncorrected. UV-Vis spectra were recorded on a Shimadzu Multispec-1501 photodiode array spectrophotometer while fluorescence spectrophotometry was conducted with a Varian Cary Eclipse fluorescence spectrophotometer. Microsomes from

insect cells containing recombinant human MAO-A and –B (5 mg/mL) were obtained from Sigma-Aldrich.

4.2. Synthesis of 8-chlorocaffeine (7)

8-Chlorocaffeine was prepared according to a previously described procedure (Fischer et al., 1883) by reaction of caffeine (**2**) with chlorine in chloroform. The required chlorine gas was prepared from the reaction between concentrated HCl and $KMnO_4$ and was dried by passing through concentrated H_2SO_4. High yields of 8-chlorocaffeine was obtained (94–100%) with a melting point of 188 °C. This corresponds to the melting point reported in literature (188 °C) (Fischer et al., 1882). NMR data also correlated to the corresponding published values (Sono et al., 1996).

4.3. General procedure for the synthesis of the 8-benzyloxycaffeinyl analogues (5a–g)

The 8-benzyloxycaffeinyl analogues (**5a–g**) were prepared according to a previously reported procedure (Huston et al., 1934). Metallic sodium (1.76 mmol) was allowed to react with the appropriately substituted benzylalcohol (**6**, 24.65 mmol). 8-Chlorocaffeine (**7**, 1.75 mmol) was added to the mixture and the reaction was heated at 170 °C for a period of 6 hours. After the reaction was cooled, the 8-benzyloxycaffeine analogues were obtained by crystallization. In most cases the yields obtained were improved by the addition of 10–20 mL ethanol and cooling the mixture to 4 °C during the crystallization process. For previously reported **5a** the melting point was found to be 173 °C while the literature value is 172–173.5 °C (Huston et al. 1934).

4.3.1. 8-Benzyloxycaffeine (5a)

The title compound was prepared from 8-chlorocaffeine (**7**) and benzyl alcohol in a yield of 29%: mp 173 °C, lit mp 172–173.5 °C (Huston et al. 1934); ^{1}H NMR ($CDCl_3$) δ 3.36 (s, 3H), 3.52 (s, 3H), 3.69 (s, 3H), 5.47 (s, 2H), 7.32 – 7.46 (m, 5H); ^{13}C NMR ($CDCl_3$) δ 29.79 (CH_3), 29.71 (CH_3), 27.68 (CH_3), 72.52 (CH_2), 103.53 (C), 135.00 (CH), 128.84 (CH), 128.66 (CH), 128.41 (CH), 155.51 (C), 154.79 (C), 151.66 (C), 146.16 (C); EIMS *m/z* 300 ($M^{+\cdot}$); HRMS calcd. 300.12224, found 300.12351

4.3.2. 8-(3-Chlorobenzyloxy)caffeine (5b)

The title compound was prepared from 8-chlorocaffeine (**7**) and 3-chlorobenzyl alcohol in a yield of 22%: mp 174 °C; ^{1}H NMR ($CDCl_3$) δ 3.40 (s, 3H), 3.54 (s, 3H), 3.74 (s, 3H), 5.42 (s, 2H), 7.45 (s, 1H), 7.35 (m, 3H); ^{13}C NMR ($CDCl_3$) δ 29.85 (CH_3), 29.70 (CH_3), 27.69 (CH_3), 71.49 (CH_2), 103.63, 126.34, 128.44, 128.96, 129.96, 134.58, 136.96, 146.03, 151.62, 154.79, 155.17; EIMS *m/z* 334 (M^{+}); HRMS calcd. 334.08327, found 334.08352.

4.3.3. 8-(3-Bromobenzyloxy)caffeine (5c)

The title compound was prepared from 8-chlorocaffeine (**7**) and 3-bromobenzyl alcohol in a yield of 33%: mp 169 °C; ^{1}H NMR ($CDCl_3$) δ 3.34 (s, 3H), 3.49 (s, 3H), 3.68 (s, 3H), 5.43 (s, 2H), 7.58 (s, 1H), 7.48 (d, 1H), 7.36 (d, 1H), 7.22 –7.29 (t, 1H); ^{13}C NMR ($CDCl_3$) δ 29.86 (CH_3), 29.71 (CH_3), 27.69 (CH_3), 71.43 (CH_2), 103.64, 126.85, 130.23, 131.41, 131.90, 122.66, 137.18, 146.03, 151.62, 154.79, 155.15; EIMS *m/z* 378 (M^{+}); HRMS calcd. 380.03070, found 380.02580.

4.3.4. 8-(3-Fluorobenzyloxy)caffeine (5d)

The title compound was prepared from 8-chlorocaffeine (**7**) and 3-fluorobenzyl alcohol in a yield of 44%: mp 185 °C; ^{1}H NMR ($CDCl_3$) δ 3.35 (s, 3H), 3.5 (s, 3H), 3.69 (s, 3H), 5.43 (s, 2H), 6.98–7.08 (m, 1H), 7.11–7.22 (m, 2H), 7.30–7.38 (m, 1H); ^{13}C NMR ($CDCl_3$) δ 29.83 (CH_3), 29.69 (CH_3), 27.69 (CH_3), 71.51 (CH_2), 103.62, 115.29, 115.86, 123.74, 130.33, 137.45, 155.19, 146.05, 151.62, 161.18, 164.46; EIMS *m/z* 318 (M^{+}); HRMS calcd. 318.11282, found 318.11033.

4.3.5. 8-[(3-Trifluoromethyl)benzyloxy]caffeine (5e)

The title compound was prepared from 8-chlorocaffeine (**7**) and 3-(trifluoromethyl)benzyl alcohol in a yield of 22%: mp 146 °C; ^{1}H NMR ($CDCl_3$) δ 3.34 (s, 3H), 3.56 (s, 3H), 3.69 (s, 3H), 5.50 (s, 2H), 7.27–7.51 (m, 4H); ^{13}C NMR ($CDCl_3$) δ 29.85 (CH_3), 29.66 (CH_3), 27.69 (CH_3), 71.52 (CH_2), 103.67, 129.23, 131.26, 335.96, 125.65, 131.26, 122.93, 125.65, 146.01, 151.62, 154.81, 155.09; EIMS *m/z* 368 (M^{+}); HRMS calcd. 368.10963, found 368.10714.

4.3.6. 8-(3-Methylbenzyloxy)caffeine (5f)

The title compound was prepared from 8-chlorocaffeine (**7**) and 3-methylbenzyl alcohol in a yield of 13%: mp 145 °C; ^{1}H NMR ($CDCl_3$) δ 3.42 (s, 3H), 3.58 (s, 3H), 3.74 (s, 3H), 2.43 (s,

3H), 5.49 (s, 2H), 7.24–7.34 (m, 4H); ^{13}C NMR ($CDCl_3$) δ 21.30 (CH_3), 27.64 (CH_3), 29.66 (CH_3), 29.77 (CH_3), 72.59 (CH_2), 103.47, 125.48, 128.54, 129.13, 129.56, 134.87, 138.37, 146.15, 151.63, 154.75, 155.54; EIMS *m/z* 314 ($M^{\cdot+}$); HRMS calcd. 314.13789, found 314.13983.

4.3.7. 8-(3-Methoxybenzyloxy)caffeine (5g)

The title compound was prepared from 8-chlorocaffeine (**7**) and 3-methoxybenzyl alcohol in a yield of 30%: mp 144 °C; ^{1}H NMR ($CDCl_3$) δ 3.42 (s, 3H), 3.56 (s, 3H), 3.73 (s, 3H), 3.85 (s, 3H), 5.51 (s, 2H), 6.92 –7.35 (m, 4H); ^{13}C NMR ($CDCl_3$) δ 29.85 (CH_3), 29.75 (CH_3), 27.72 (CH_3), 55.27 (CH_3), 72.38 (CH_2), 103.56, 114.14, 114.07, 120.56, 129.79, 136.48, 146.16, 151.68, 154.80, 155.49, 159.80; EIMS *m/z* 330 ($M^{\cdot+}$); HRMS calcd. 330.13281, found 330.13554.

4.4. Mitochondrial baboon liver MAO-B inhibition studies

Baboon liver mitochondrial fractions were isolated as described previously (Salach & Weyler, 1987) and stored at –70 °C. Following addition of an equal volume of sodium phosphate buffer (100 mM, pH 7.4) containing glycerol (50%, w/v) to the mitochondrial isolate, the protein concentration was determined by the method of Bradford using bovine serum albumin as reference standard (Bradford, 1976). MMTP (K_m = 68.3 ± 1.60 µM) (Inoue et al., 1999; Pretorius et al., 2008), served as substrate for the inhibition studies. The enzymatic reactions were prepared in sodium phosphate buffer (100 mM, pH 7.4) and contained MMTP (50 µM), the mitochondrial isolate (0.15 mg protein/mL) and various concentrations of the test inhibitors (0–100 µM). The stock solutions of the inhibitors were prepared in DMSO and were added to the incubation mixtures to yield a final DMSO concentration of 4% (v/v). DMSO concentrations higher than 4% are reported to inhibit MAO-B (Gnerre et al., 2000). The final volume of the incubations was 500 µL. Following incubation at 37 °C for 10 min, the enzyme reactions were terminated by the addition of 10 µL perchloric acid (70%). The MAO-B catalyzed production of $MMDP^+$ is reported to be linear for the first 10 minutes of incubation under these conditions (Pretorius et al., 2008). The samples were centrifuged at 16,000 *g* for 10 minutes, and the concentrations of the MAO-B generated product, $MMDP^+$, were measured spectrophotometrically at 420 nm (ε = 25,000 M^{-1}) in the supernatant fractions (Inoue et al., 1999). The IC_{50} values were determined by plotting the initial rates of oxidation vs. the logarithm of the inhibitor concentrations to obtain a sigmoidal dose-response curve.

This kinetic data were fitted to the one site competition model incorporated into the Prism software package (GraphPad Software Inc.). The IC_{50} values were determined in duplicate and are expressed as mean ± standard error of the mean (SEM).

4.5. Recombinant human MAO-A and –B inhibition studies

Microsomes from insect cells containing recombinant human MAO-A and –B (5 mg/mL) were obtained from Sigma-Aldrich, pre-aliquoted and stored at –70 °C. All enzymatic reactions were carried out in potassium phosphate buffer (100 mM, pH 7.4, made isotonic with KCl) containing MAO-A (0.0075 mg/mL) or MAO-B (0.015 mg/mL), various concentrations of the test inhibitor (0–100 μM) and kynuramine. The final concentrations of kynuramine in the reactions were 45 μM and 30 μM where MAO-A and –B, respectively, served as substrates. The final volume of the reactions was 500 μL. Stock solutions of the test inhibitors were prepared in DMSO and added to the reactions to yield a fiinal concentration of 4% (v/v) DMSO. The reactions were incubated for 20 minutes at 37 °C and terminated with the addition of 200 μL NaOH (2 N). Distilled water (1200 μL) was added to each reaction before it was centrifuged for 10 minutes at 16,000 *g*. The concentrations of the MAO generated 4-hydroxyquinoline in the reactions were determined by measuring the fluorescence of the supernatant at an excitation wavelength of 310 nm and an emission wavelength of 400 nm (Novarolli et al., 2005). Quantitative estimations of 4-hydroxyquinoline were made by means of a linear calibration curve ranging from 0.188–6.25 μM. Each calibration standard was prepared to a final volume of 500 μL in potassium phosphate buffer (100 mM, pH 7.4) and contained 4% DMSO. To each standard was added 200 μL NaOH (2 N) and 1200 μL distilled water. IC_{50} values were determined by plotting the initial rate of oxidation versus the logarithm of the inhibitor concentration to obtain a sigmoidal dose–response curve. This kinetic data were fitted to the one site competition model incorporated into the Prism software package and the IC_{50} values were determined in duplicate and are expressed as mean ± SEM.

4.6. Lineweaver–Burk plots

For selected inhibitors, lineweaver–Burk plots were constructed in order to determine the modes of inhibition. For this purpose the initial rates of oxidation at four different substrate concentrations in the absence and presence of three different concentrations of the inhibitors were used to construct Lineweaver-Burke plots. Where baboon liver mitochondrial MAO-B was used as enzyme source, compound **5e** (0.0325–0.130 μM) was selected as inhibitor and

MMTP (30–120 μM) served as substrate. Where recombinant human MAO-A or –B was used as enzyme source, compound **5e** at concentrations of 0.931–3.722 μM and 0.0325–0.130 μM, respectively, was selected as inhibitor and kynuramine (15–90 μM) served as substrate. All enzymatic reactions and measurements were carried out as described above. Linear regression analysis was performed using the SigmaPlot software package (Systat Software Inc.).

4.7. Time-dependant inhibition studies

Time dependant inhibition studies were carried out in order to determine whether a selected inhibitor, **5b**, acts as a reversible inhibitor or as a time-dependant inactivator of baboon liver MAO-B, human MAO-A and human MAO-B. The respective MAO preparations were preincubated for periods of 0, 15, 30, 60 min at 37 °C with **5b** at concentrations of 0.28 μM, 1.31 μM and 0.23 μM for baboon liver MAO-B, human MAO-A and human MAO-B, respectively (Ogunrombi et al., 2008; Manley-King et al., 2009). For this purpose the concentrations of the enzyme preparations were 0.3 mg/mL baboon liver MAO-B, 0.015 mg/mL human MAO-A and 0.03 mg/mL human MAO-B. The incubations were carried out in sodium phosphate buffer (100 mM, pH 7.4) for the studies with baboon liver MAO-B and in potassium phosphate buffer (100 mM, pH 7.4, made isotonic with KCl) for studies with the recombinant human enzymes. A final concentration of 50 μM MMTP for baboon liver MAO-B, 45 μM kynuramine for human MAO-A and 30 μM kynuramine for human MAO-B were then incubated with the preincubated enzyme preparations at 37 °C for 15 minutes. The final volumes of these incubations were 500 μL and the final concentrations of **5b** were 0.14 μM, 0.65 μM and 0.115 μM for baboon liver MAO-B, human MAO-A and human MAO-B, respectively. These concentrations of the inhibitor are approximately equal to the IC_{50} values for the inhibition of the respective enzyme preparations by **5b**. The final concentrations of the enzyme preparations were 0.15 mg/mL baboon liver MAO-B, 0.0075 mg/mL human MAO-A and 0.015 mg/mL human MAO-B. The reactions with baboon liver MAO-B were terminated with 10 μL perchloric acid (70%) while the reactions with the recombinant human enzymes were terminated with 200 μL NaOH (2 N). A volume of 1200 μL distilled water was added to the incubations containing the recombinant human MAO preparations. The rates of formation of $MMDP^+$ and 4-hydroxyquinoline were measured as described above. All measurements were carried out in triplicate and are expressed as mean ± SEM.

4.8. K_m determination of kynuramine for recombinant human MAO-A and –B

The steady-state oxidation rates of kynuramine by recombinant human MAO-A and –B were measured at 6 different substrate concentrations ranging from 2.5 µM to 80 µM. For MAO-A the final enzyme concentration in the incubations was 0.0075 mg/mL while the final concentration of MAO-B was 0.015 mg/mL. All the incubations were prepared in potassium phosphate buffer (100 mM, pH 7.4, made isotonic with KCl) and were carried out for 20 minutes at 37 °C. The reactions were terminated with 200 µL NaOH (2 N) and 1200 µL distilled water was added. The rates of the MAO catalyzed formation of 4-hydroxyquinoline were measured as described above. The kinetic data (initial rates as a function of substrate concentration) were fitted to a Michaelis–Menten equation using the one site binding model incorporated into the Prism software package. All measurements were carried out in duplicate and the K_m values are expressed as mean ± SEM.

4.9. QSAR studies

The values of the substituent descriptors σ_m, F, π, E_s, V_w were obtained from standard compilations (Hansch & Leo, 1995; Van de Waterbeemb & Testa, 1987). Stepwise multiple linear regression analysis of the inhibition potencies ($\log IC_{50}$ values) as a function of the substituent descriptor values was carried out with the Statistica software package (StatSoft Inc.). In order to estimate the significance of the regression equations, the *F* statistic was employed. An *F* value higher than the critical *F* value (F_{max}) was judged to be significant. The F_{max} value for 95% significance for models constructed from seven $\log IC_{50}$ values (Tables 3 and 4) and which contains one descriptor (out of a possible five: σ_m, F, π, E_s, V_w) was calculated to be 25.32, while the F_{max} value for models containing two descriptors was calculated to be 30.18 (Livingstone et al., 2005)

4.10. Molecular docking studies

The molecular docking studies were carried out in the Windows based Discovery Studio 1.7 molecular modelling software (Accelrys). All the inhibitors (**5a–g**) were constructed and geometry optimized in Discovery Studio and prepared for docking with the Prepare Ligands protocol. The crystallographic structures of MAO-A co-crystallized with harmine (PDB code: 2Z5X) (Son et al., 2008) and MAO-B co-crystallized with safinamide (PDB code: 2V5Z) (Binda et al., 2007) were retrieved from the Brookhaven Protein Data Bank (www.rcsb.org/pdb). Following the addition of hydrogen atoms and the correction of the

valences of the FAD cofactors and co-crystallized ligands, the receptor models were automatically typed with the Momany and Rone CHARMm forcefield and subjected to a three step energy minimization cascade while the protein backbone was constrained. Minimisation of the receptor models were carried out since the X-ray crystal structures may contain residual energetic tensions as a result of the crystallisation process. The first step was a steepest descent minimization with the termination criteria set to a maximum of 2500 steps or a minimum value of 0.1 for the root mean square of the energy gradient. The second step was conjugate gradient minimization with the same termination criteria. The third step was an adopted basis Newton-Rapheson minimization with the termination criteria set to a maximum of 5000 steps or a minimum value for the root mean square of the energy gradient of 0.01. For this minimization cascade the implicit generalized Born solvation model with simple switching was used with the dielectric constant set to 4. The co-crystallized ligands, crystal waters and the backbone constraints were removed and the binding site was identified by a flood-filling algorithm. Automated docking was subsequently carried out with the LigandFit application of Discovery Studio. This docking protocol employed total ligand flexibility whereby the final ligand conformations are determined by the Monte Carlo conformation search method set to a variable number of trial runs. The docked ligands were further refined using in situ ligand minimization with the Smart Minimizer algorithm. Unless otherwise specified (see above), all the application modules within Discovery Studio were set to their default values and 10 docking solutions were allowed for each ligand (Ogunrombi et al., 2008; Van der Walt et al., 2009). The illustrations were generated in PyMOL (DeLano, 2002).

Acknowledgements

The NMR and MS spectra were recorded by André Joubert and Johan Jordaan of the SASOL Centre for Chemistry, North-West University. This work was supported by grants from the National Research Foundation and the Medical Research Council, South Africa.

References

1. Youdim, M. B. H.; Bakhle, Y. S. *Br. J. Pharmacol.* **2006,** *147*, S287.
2. Youdim, M. B. H.; Edmondson, D.; Tipton, K. F. *Nat. Rev. Neurosci.* **2006,** *7*, 295.
3. Fernandez, H. H.; Chen, J. J. *Pharmacotherapy.* **2007,** *27*, 174S.

4. Collins, G. G. S.; Sandler, M.; Williams, E. D.; Youdim, M. B. H. *Nature*. **1970,** *225*, 817.

5. Youdim, M. B. H.; Collins, G. G. S.; Sandler, M.; Bevan-Jones, A. B.; Pare, C. M.; Nicholson, W. J. *Nature*. **1972,** *236*, 225.

6. Di Monte, D. A.; DeLanney, L. E.; Irwin, I.; Royland, J. E.; Chan, P.; Jakowec, M. W.; Langston, J. W. *Brain. Res*. **1996,** *738*, 53.

7. Finberg, J. P.; Wang, J.; Bankiewich, K.; Harvey-White, J; Kopin, I. J.; Goldstein, D. S. *J. Neural Transm. Suppl*. **1998,** *52*, 279.

8. Nicotra, A.; Pierucci, F.; Parvez, H.; Senatori, O. *Neurotoxicology*. **2004,** *25*, 155.

9. Fowler, J. S.; Volkow, N. D.; Wang, G. J.; Logan, J.; Pappas, N.; Shea, C.; MacGregor, R. *Neurobiol. Aging*. **1997,** *18*, 431.

10. Vlok, N.; Malan, S. F.; Castagnoli, N., Jr.; Bergh, J. J.; Petzer, J. P. *Bioorg. Med. Chem.* **2006,** *14*, 3512.

11. Van den Berg, D.; Zoellner, K. R.; Ogunrombi, M. O.; Malan, S. F.; Terre'Blanche, G.; Castagnoli, N., Jr.; Bergh, J. J.; Petzer, J. P. *Bioorg. Med. Chem*. **2007,** *15*, 3692.

12. Pretorius, J.; Malan, S. F.; Castagnoli, N., Jr.; Bergh, J. J.; Petzer, J. P. *Bioorg. Med. Chem*. **2008,** *16*, 8676.

13. Van der Walt, E. M.; Milczek, E. M.; Malan, S. F.; Edmondson, D. E.; Castagnoli, N., Jr.; Bergh, J. J.; Petzer, J. P. *Bioorg. Med. Chem. Lett*. **2009,** *19*, 2509.

14. Binda, C.; Wang, J.; Pisani, L.; Caccia, C.; Carotti, A.; Salvati, P.; Edmondson, D. E.; Mattevi, A. *J. Med. Chem*. **2007**, *50*, 5848.

15. Huston, R. R.; Allen, W. F. *J. Am. Chem. Soc*. **1934,** *56*, 1356.

16. Fischer, E.; Reese, L. *Justus Liebigs Ann. Chem*. **1883,** *221*, 336.

17. Cheng, Y. C.; Prusoff, W. H. *Biochem. Pharmacol*. **1973,** *22*, 3099.

18. Inoue, H.; Castagnoli, K.; Van der Schyff, C. J.; Mabic, S.; Igarashi, K.; Castagnoli, N., Jr. *J. Pharmacol. Exp. Ther*. **1999,** *291*, 856.

19. Novaroli, L.; Reist, M.; Favre, E.; Carotti, A.; Catto, M.; Carrupt, P. A. *Bioorg. Med. Chem*. **2005,** *13*, 6212.

20. Khalil, A. A.; Steyn, S.; Castagnoli, N, Jr. *Chem. Res. Toxicol*. **2000,** *13*, 31.

21. Manley-King, C. I.; Terre'Blanche, G.; Castagnoli, N., Jr.; Bergh, J. J.; Petzer, J. P. *Bioorg. Med. Chem*. **2009,** *17*, 3104.

22. Van de Waterbeemb, H.; Testa, B. In *Advances in drug research*; Testa, B., Ed.; Academic Press: London, 1987; pp 85–225.

23. Hansch, C.; Leo, A. *Exploring QSAR. Fundamentals and applications in chemistry and biology*; American Chemical Society: Washington, DC, 1995; pp 1–124.
24. Livingstone, D. J.; Salt, D. W. *J. Med. Chem.* **2005,** *48*, 661.
25. Son, S. –Y.; Ma, J.; Kondou, Y.; Yoshimura, M.; Yamashita, E.; Tsukihara, T. *Proc. Natl. Acad. Sci. U.S.A.* **2008**, *105*, 5739.
26. Hubálek, F.; Binda, C.; Khalil, A.; Li, M.; Mattevi, A.; Castagnoli, N., Jr.; Edmondson, D. E. *J. Biol. Chem.* **2005,** *280*, 15761.
27. Accelrys Discovery Studio 1.7, Accelrys Software Inc., San Diego, CA, USA. 2006, http://www.accelrys.com.
28. Ogunrombi, M. O.; Malan, S. F.; Terre'Blanche, G.; Castagnoli, N., Jr.; Bergh, J. J.; Petzer, J. P. *Bioorg. Med. Chem.* **2008**, *16*, 2463.
29. Novaroli, L.; Daina, A.; Favre, E.; Bravo, J.; Carotti, A.; Leonetti, F.; Catto, M.; Carrupt, P. A.; Reist, M. *J. Med. Chem.* **2006,** *49*, 6264.
30. La Regina, G.; Silvestri, R.; Gatti, V.; Lavecchia, A.; Novellino, E.; Befani, O.; Turini, P.; Agostinelli, E. *Bioorg. Med. Chem.* **2008,** *16*, 9729.
31. Pitts, S. M.; Markey, S. P.; Murphy, D. L.; Weisz, A. In *MPTP: A neurotoxin producing a Parkinsonian syndrome*; Markey, S. P.; Castagnoli, N., Jr.; Trevor, A. J.; Kopin, I. J., Ed.; Academic Press: New York, 1986; pp 703–716.
32. Bissel, P., Bigley, M. C., Castagnoli, K., and Castagnoli, N., Jr. *Bioorg. Med. Chem.* **2002,** *10*, 3031.
33. Fischer, E. *Justus Liebigs Ann. Chem.* **1882,** *215*, 267.
34. Sono, M.; Toyoda, N.; Shimizu, K.; Noda, E.; Shizuri, Y.; Tori, M. *Chem. Pharm. Bull.* **1996,** *44*, 1141.
35. Salach, J. I.; Weyler, W. *Meth. Enzymol.* **1987,** *142*, 627.
36. Bradford, M. M. *Anal. Biochem.* **1976,** *72*, 248.
37. Gnerre, C.; Catto, M.; Leonetti, F.; Weber, P.; Carrupt, P. -A.; Altomare, C.; Carotti, A.; Testa, B. *J. Med. Chem.* **2000,** *43*, 4747.
38. DeLano, W. L. Palo Alto, CA, USA. 2002.

Table 1. The IC_{50} values for the inhibition of baboon liver MAO-B, human MAO-B and human MAO-A by 8-benzyloxycaffeinyl analogues **5a–g**

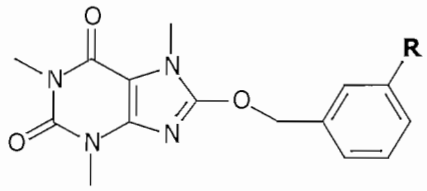

	R	IC_{50} MAO-B (baboon) μM	IC_{50} MAO-B (human) μM	IC_{50} MAO-A (human) μM
5a	H	2.49 ± 0.029	1.77 ± 0.151	1.24 ± 0.035
5b	Cl	0.120 ± 0.031	0.107 ± 0.013	0.666 ± 0.011
5c	Br	0.113 ± 0.005	0.068 ± 0.003	0.941 ± 0.007
5d	F	0.534 ± 0.065	0.542 ± 0.042	1.07 ± 0.092
5e	CF_3	0.112 ± 0.016	0.152 ± 0.003	3.72 ± 0.179
5f	CH_3	0.698 ± 0.007	0.546 ± 0.022	0.397 ± 0.013
5g	OCH_3	1.59 ± 0.431	1.01 ± 0.196	3.15 ± 0.017

All values are expressed as the mean ± SEM of duplicate determinations.

Table 2. The calculated K_i values for the inhibition of baboon liver MAO-B, human MAO-B and human MAO-A by 8-benzyloxycaffeinyl analogues **5a–g**

	R	K_i MAO-B (baboon) μM[a]	K_i MAO-B (human) μM[a]	K_i MAO-A (human) μM[a]	SI[b]
5a	H	1.44	0.59	0.43	1.37
5b	Cl	0.069	0.036	0.23	0.16
5c	Br	0.065	0.023	0.33	0.069
5d	F	0.31	0.18	0.37	0.49
5e	CF_3	0.065	0.051	1.30	0.039
5f	CH_3	0.40	0.18	0.14	1.29
5g	OCH_3	0.92	0.34	1.10	0.31

[a] The K_i values were calculated from the experimental IC_{50} values according to the equation by Cheng and Prusoff: $K_i = IC_{50}/(1 + [S]/K_m)$ with [S] = 50 μM and K_m (MMTP) = 68.3 μM for baboon liver MAO-B. For human MAO-B, [S] = 30 μM and K_m (kynuramine) = 22.7 μM while [S] = 45 μM and K_m (kynuramine) = 16.1 μM for human MAO-A. (Cheng & Prusoff, 1973).

[b] The selectivity index is the selectivity for the A isoform and is given as the ratio of K_i(MAO-B)/K_i(MAO-A).

Table 3. Correlations of the baboon liver MAO-B inhibition potencies ($\log IC_{50}$) of 8-benzyloxycaffeinyl analogues **5a–g** with steric, electronic and hydrophobic descriptors of the substituents at C-3 of the benzyloxy ring[a]

Para-meter	slope	*y*-intercept	R^2	*F*	Significance[b]
σ_m	–2.25 ± 0.68	0.12 ± 0.20	0.62	10.8	0.022
F	–1.96 ± 0.89	0.18 ± 0.30	0.39	4.87	0.079
V_w	–0.49 ± 0.44	0.045 ± 0.46	0.02	1.13	0.337
π	–1.29 ± 0.24	0.19 ± 0.14	0.82	27.8	0.003
E_s	0.53 ± 0.22	0.13 ± 0.27	0.44	5.61	0.065
$\sigma + \pi$	–1.23 ± 0.19	0.31 ± 0.05	0.98	147	0.003
	–0.93 ± 0.10				0.0007
$F + \pi$	–1.12 ± 0.19	0.41 ± 0.064	0.98	120	0.005
	–1.07 ± 0.10				0.0004

[a] The logarithm of the IC_{50} values (expressed in μM) was used in the linear regression analysis.

[b] The significance is the fractional probability that the coefficient of the added variable is zero.

Table 4. Correlations of the recombinant human MAO-B inhibition potencies ($\log IC_{50}$) of 8-benzyloxycaffeinyl analogues **5a–g** with steric, electronic and hydrophobic descriptors of the substituents at C-3 of the benzyloxy ring[a]

Para-meter	slope	*y*-intercept	R^2	*F*	Significance[b]
σ_m	–2.14 ± 0.71	0.01 ± 0.23	0.51	7.31	0.043
F	–1.97 ± 0.92	0.071 ± 0.31	0.37	4.58	0.085
V_w	–0.56 ± 0.43	0.024 ± 0.44	0.11	1.72	0.247
π	–1.27 ± 0.29	0.075 ± 0.17	0.75	18.8	0.008
E_s	0.45 ± 0.27	0.061 ± 0.32	0.23	2.83	0.153
$\sigma + \pi$	–1.10 ± 0.54	0.18 ± 0.14	0.84	17.3	0.112
	–0.95 ± 0.28				0.027
$F + \pi$	–1.15 ± 0.42	0.30 ± 0.14	0.89	25.4	0.052
	–1.04 ± 0.21				0.008

[a] The logarithm of the IC_{50} values (expressed in μM) was used in the linear regression analysis.

[b] The significance is the fractional probability that the coefficient of the added variable is zero.

Figure and Scheme Legends

Figure 1. The structures of (*E*)-8-styrylcaffeinyl analogues (**1a–b**) and caffeine (**2**).

Figure 2. The structures of safinamide (**3**), 7-(3-chlorobenzyloxy)-4-formylcoumarin (**4**) and 8-benzyloxycaffeinyl analogues **5a–g**.

Figure 3. The sigmoidal dose-response curve of the initial rates of oxidation of kynuramine by recombinant human MAO-B vs. the logarithm of concentration of inhibitor **5c** (expressed in nM). The rates are expressed as nmoles 4-hydroxyquinoline formed/min/mg protein. The concentration kynuramine used was 30 μM, the determinations were carried out in duplicate and all values are the mean ± SEM.

Figure 4. Lineweaver-Burk plots of the oxidation of MMTP by baboon liver MAO-B in the absence (open squares) and presence of various concentrations of **5e** (filled squares, 0.0325 μM; open circles, 0.065 μM and filled circles, 0.130 μM). The rate (V) is expressed as nmol product formed/min/mg protein.

Figure 5. Time-dependant inhibition of the baboon liver mitochondrial MAO-B catalyzed oxidation of MMTP (50 μM) by **5b**. The enzyme preparation was preincubated for various periods of time (0–60 min) with **5b** (0.28 μM). The rates are expressed as nmoles $MMDP^+$ formed/min/mg protein.

Figure 6. Lineweaver-Burk plots of the oxidation of kynuramine by recombinant human MAO-A in the absence (open squares) and presence of various concentrations of **5e** (filled squares, 0.931 μM; open circles, 1.861 μM and filled circles, 3.722 μM). The rate (V) is expressed as nmol product formed/min/mg protein.

Figure 7. Time-dependant inhibition of the recombinant human MAO-A catalyzed oxidation of kynuramine (45 μM) by **5b**. The enzyme preparation was preincubated for various periods of time (0–60 min) with **5b** (1.31 μM). The rates are expressed as nmoles 4-hydroxyquinoline formed/min/mg protein.

Figure 8. Correlations of the $\log IC_{50}$ values for the inhibition of baboon liver MAO-B by **5a–g** with the Hansch constant (π) of the substituents at C-3 of the benzyloxy ring. The π values were adjusted by the contribution of the Hammett constant (σ) as indicated on the x-axis title. The linear regression line is a representation of equation 1 with a correlation coefficient of 0.98.

Figure 9. Stereo view representation of compound **5a** (cyan) docked within the active site of MAO-B. In panel A the active site residues (grey) of MAO-B are displayed while in panel B the active site residues of both MAO-B (grey) and MAO-A (yellow) are displayed. The FAD co-factor is shown in yellow and hydrogen bonds are indicated by the dashes. The residues are numbered based on the structure of MAO-B. The numbers given in parenthesis are the corresponding MAO-A residue identifiers.

Figure 10. Stereo view representation of compound **5a** (cyan) docked within the active site of MAO-A. In panel A the active site residues (grey) of MAO-A are displayed while in panel B the active site residues of both MAO-B (grey) and MAO-A (yellow) are displayed. The FAD co-factor is shown in yellow and hydrogen bonds are indicated by the dashes. In panel B, the residues are numbered based on the structure of MAO-B. The numbers given in parenthesis are the corresponding MAO-A residue identifiers.

Figure 11. The docked orientations of **5a** within the active site of MAO-B (cyan) and MAO-A (green) with the caffeine rings of the two respective orientations superimposed.

Scheme 1. Synthetic pathway to the 8-bezyloxycaffeinyl analogues **5a–g**. Reagents and conditions: (i) Na, 170 °C.

Figure 1.

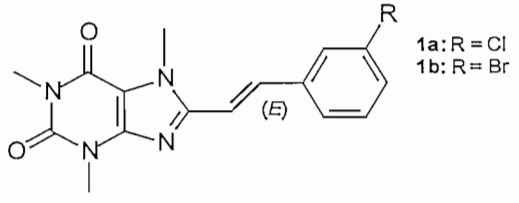

1a: R = Cl
1b: R = Br

(*E*)-8-styrylcaffeinyl analogues (**1a-b**)

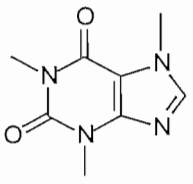

Caffeine (**2**)

Figure 2.

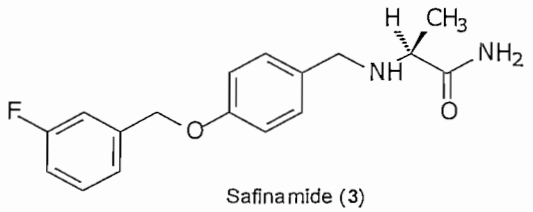

Safinamide (3)

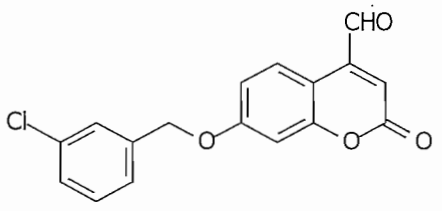

7-(3-Chlorobenzyloxy)-4-formylcoumarin (4)

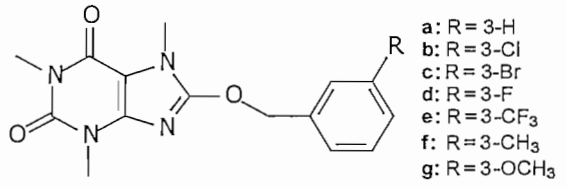

a: R = 3-H
b: R = 3-Cl
c: R = 3-Br
d: R = 3-F
e: R = 3-CF_3
f: R = 3-CH_3
g: R = 3-OCH_3

8-Benzyloxycaffeinyl analogues (5 a-g)

Figure 3.

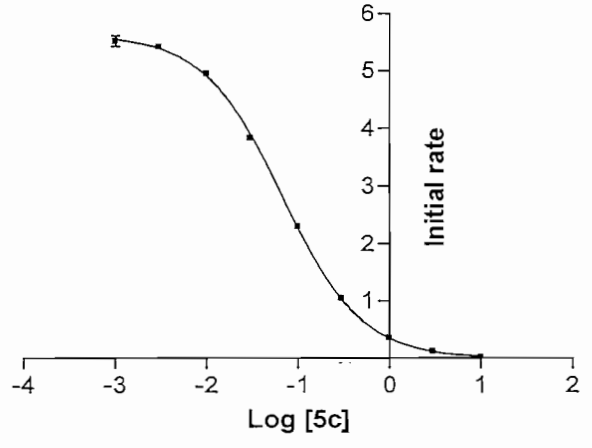

Figure 4.

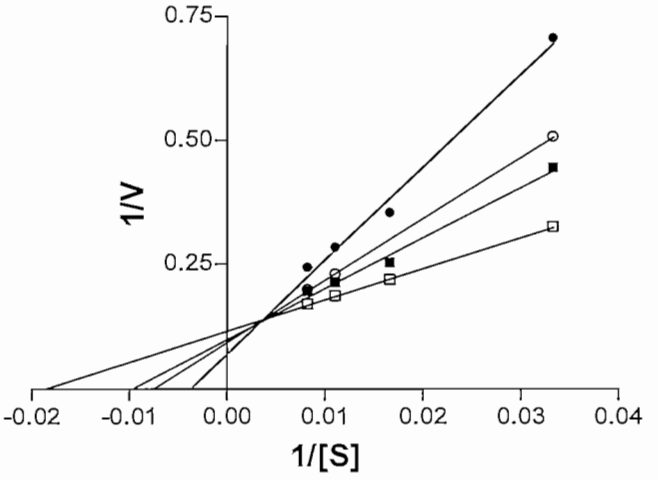

Figure 5.

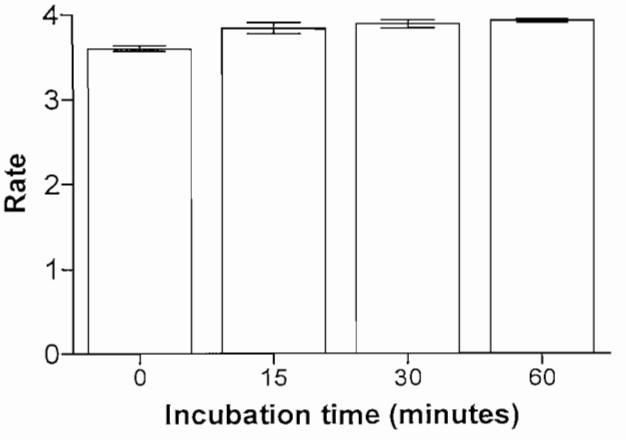

Figure 6.

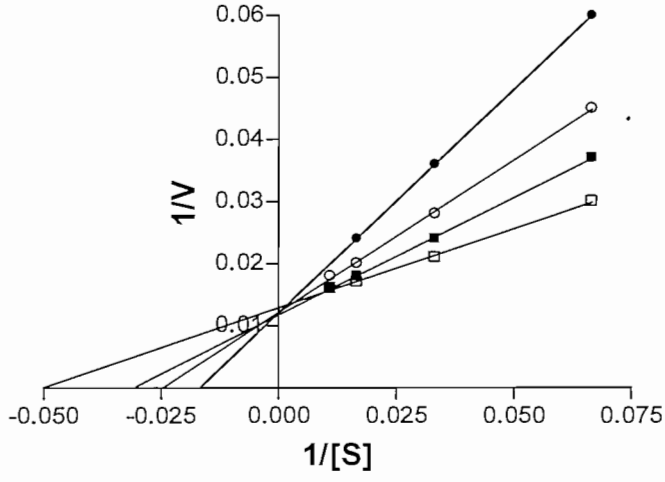

Figure 7.

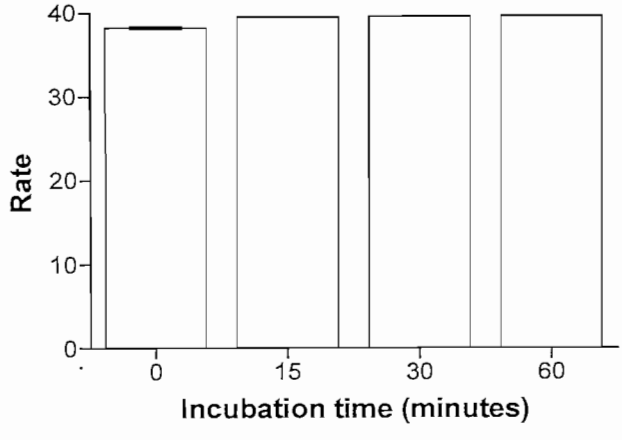

Figure 8.

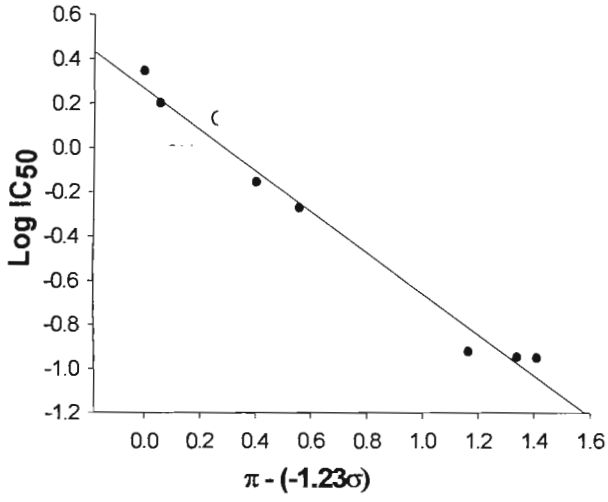

Figure 9a.

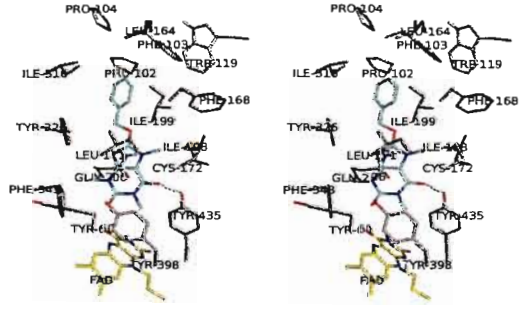

Figure 9b.

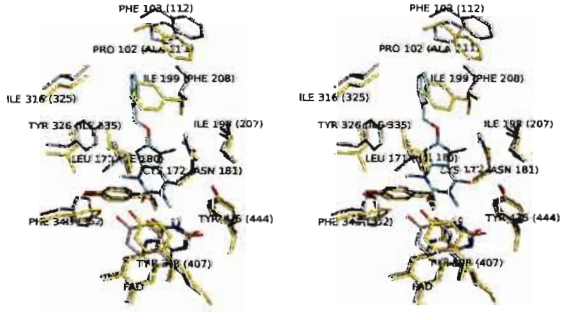

Figure 10a.

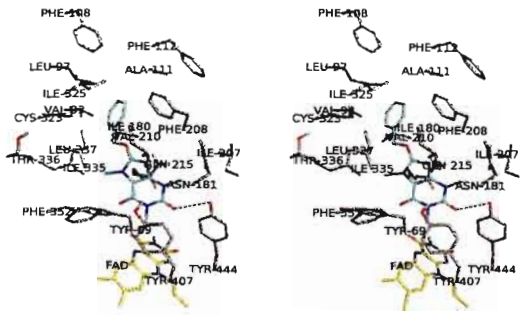

Figure 10b.

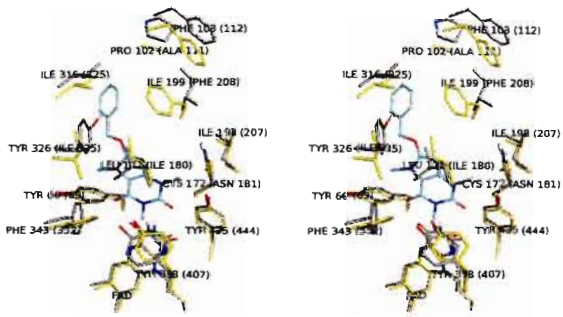

Figure 11.

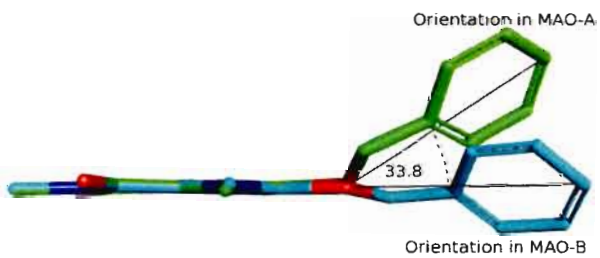

Scheme 1.

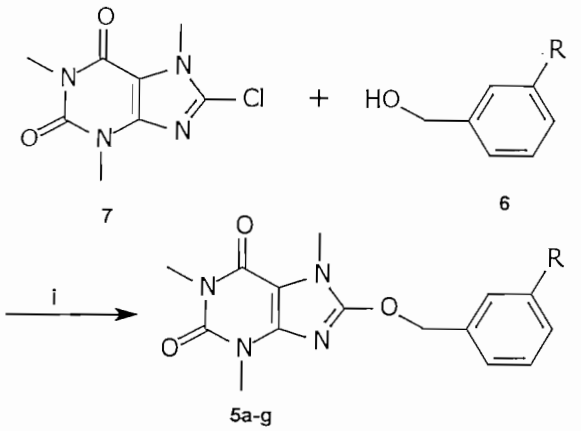

BIBLIOGRAPHY

Binda, C., Hubalek, F., Li, M., Herzig, Y., Sterling, J., Edmondson, D.E. & Mattevi, A. (2004). Crystal structures of monoamine oxidase B in complex with four inhibitors of the N-propargylaminoindan class. *Journal of Medicinal Chemistry, 47*, 1767-1774.

Binda, C., Li, M., Hubalek, F., Restelli, N., Edmondson, D.E. & Mattevi, A. (2003). Insights into the mode of inhibition of human mitochondrial monoamine oxidase B from high-resolution crystal structures. *Proceedings of the National Academy of Sciences of the United States of America, 100*, 9750-9755.

Binda, C., Mattevi, A., & Edmondson, D.E. (2002). Structure-function relationships in flavoenzyme-dependent amine oxidations: a comparison of polyamine oxidase and monoamine oxidase. *Journal of Biological Chemistry, 277*, 23973-23976.

Binda, C., Newton-Vinson, P., Hubalek, F., Edmondson, D.E. & Mattevi, A. (2002). Structure of human monoamine oxidase B, a drug target for the treatment of neurological disorders. *Nature Structural Biology, 9*, 22-26.

Binda, C., Wang, J., Pisani, L., Caccia, C., Carotti, A., Salvati, P., Edmonson, D.E. & Mattevi, A. (2007). Structures of human monoamine oxidase B complexes with selective noncovalent inhibitors: safinamide and coumarin analogues. *Journal of Medicinal Chemistry, 50*, 5848-5852.

Blum, D., Torch, S., Lambeng, N., Nissou, M., Benabid, A., Sadoul, R. & Verna, J. (2001). Molecular pathways involved in the neurotoxicity of 6-OHDA, dopamine and MPTP: contribution to the apoptotic theory in Parkinson's disease. *Progress in Neurobiology, 65*, 135-172.

Bové, J., Prou, D., Perier, C. & Przedborski, S. (2005). Toxin-induced models of Parkinson's disease. *The Journal of the American Society for Experimental Neurotherapeutics, 2*, 484-494.

Chen, J.F., Xu, K., Petzer, J.P., Staal, R., Xu, Y.H., Beilstein, M., Sonsalla, P.K., Castagnoli, K., Castagnoli Jr., N., Schwarzschild, M.A. (2001). Neuroprotection by caffeine and A(2A) adenosine receptor inactivation in a model of Parkinson's disease. *The Journal of Neuroscience : The Official Journal of the Society for Neuroscience,* 21, RC143.

Cheng, Y. & Prusoff, W. (1973). Relationship between the inhibition constant (K_i) and the concentration of inhibitor which causes 50 per cent inhibition (I_{50}) of an enzymatic reaction. *Biochemical Pharmacology, 22*, 3099-3108.

Dauer, W. & Przedborski, S. (2003). Parkinson's disease: mechanisms and models. *Neuron, 39*, 889-909.

De Colibus, L., Li, M., Binda, C., Lustig, A., Edmondson, D.E. & Mattevi, A. (2005). Three-dimensional structure of human monoamine oxidase A (MAO-A): Relation to the structures of rat MAO-A and human MAO-B. *The National Academy of Sciences of the USA, 102*, 12684-12689.

Dixon, M. (1952). The determination of enzyme inhibitor constants. *Biochemical Journal, 55*, 170-171.

Edmondson, D.E., Mattevi, A., Binda, C., Li, M. & Hubalek, F. (2004). Structure and mechanism of monoamine oxidase. *Current Medicinal Chemistry, 11*, 1983-1993.

Elbaz, A. & Tranchant, C. (2007). Epidemiologic studies of environmental exposures in Parkinson's disease. *Journal of the Neurological Sciences, 262*, 37-44.

Fernandez, H. & Chen, J. (2007). Monoamine oxidase-B inhibition in the treatment of Parkinson's disease. *Pharmacotherapy, 27*, 174S-185S.

Fischer, E. & Reese, L. (1883). Ueber Caffein, Xanthin und Guanin. *Liebigs Annalen der Chemie, 221*, 336-344.

Gnerre, C., Catto, M., Leonetti, F., Weber, P., Carrupt, P., Altomare, C., Carotti, A. & Testa, B. (2000). Inhibition of monoamine oxidase by functionalized coumarin derivatives: biological activities, QSAR's, and 3D-QSAR's. *Journal of Medicinal Chemistry, 43*, 4747-4758.

Guttman, M., Kish, S. & Furukawa, Y. (2003). Current concepts in the diagnosis and management of Parkinson's disease. *Canadian Medical Association Journal, 168*, 293-301.

Hansch, C. & Leo, A. (1995). Exploring QSAR. Fundamentals and applications in chemistry and biology. Washington DC: American Chemical Society. 1–124.

Holt, A., Sharman, D., Baker, G. & Palcic, M. (1997). A continuous spectophotometric assay for monoamine oxidase and related enzymes in tissue homogenates. *Analytical Biochemistry, 244*, 384-392.

Hubalek, F., Binda, C., Khalil, A., Li, M., Mattevi, A., Castagnoli, N. & Edmondson, D.E. (2005). Demonstration of isoleucine 199 as a structural determinant for the selective inhibition of human monoamine oxidase B by specific reversable inhibitors. *Journal of Biological Chemistry, 280*, 15761-5766.

Huston, R. & Allen, W. (1934). Caffeine derivatives. I. The 8-Ethers of caffeine. *Journal of the American Chemical Society, 56*, 1356-1358.

Huston, R. & Allen, W. (1934). Caffeine derivatives. II. Molecular rearrangement of the 8-ethers of caffeine. *Journal of the American Chemical Society, 56*, 1358-1359.

Inoue, H., Castagnoli, K., Vand der Schyf, C., Mabic, S., Igarashi, K. & Castagnoli, N. J. (1999). Species-dependant differences in monoamine oxidase A and B-catalyzed oxidation of various C4 substituted 1-methyl-4-phenyl-1,2,3,6-tetrahydropyridinyl derivatives. *Journal of Pharmacology and Experimental Therapeutics, 291*, 856-864.

Jalkanen, S. & Salmi, M. (2001). Cell surface monoamine oxidases: enzymes in search of a function. *The EMBO Journal, 20*, 3893-3901.

Knetgel, R.M.A., Kuntz, I.D. & Oshiro, C.M. (1997). Molecular docking to ensembles of protein structures. *Journal of Molecular Biology, 266*,424-440.

Lee, Y., Ling, K., Lu, X., Silverman, R.B., Shepard, E.M., Dooley, D.M. & Sayre, L.M. (2002). 3-Pyrrolines are mechanism-based inactivators of the quinone-dependant amine oxidases but only substrates of the flavin-dependent amine oxidases. *Journal of the American Chemical Society, 124*, 12135-12143.

Lees, A. (2005). Alternatives to levodopa in the initial treatment of early Parkinson's disease. *Drugs and Aging, 22*, 731-740.

Leroy, E., Boyer, R., Auburger, G., Leube, B., Ulm, G. & Mezey, E. (1998). The ubiquitine pathwayin Parkinson's disease. *Nature, 395*, 451-452.

LeWitt, P. & Taylor, D. (2008). Protection against Parkinson's disease progression: Clinical experience. *Neurotherapeutics: The Journal of the American Society for Experimental NeuroTherapeutics, 5*, 210-225.

Li, M., Binda, C., Mattevi, A. & Edmondson, D.E. (2006). Functional role of the "aromatic cage" in human monoamine oxidase B: Structures and catalytic properties of Tyr435 mutant proteins. *Biochemistry, 45*, 4775-4784.

Livingstone, D.J. & Salt, D.W. (2005). Judging the significance of multiple linear regretion models. *Journal of Medicinal Chemistry, 48*, 661.

Mandel, S., Grunblatt, E., Riederer, P., Amariglio, N., Hirsch, J.J., Rechavi, G., Youdim, M.B.H. (2005). Gene expression profiling of sporadic Parkinson's disease substantia nigra pars compacta reveals impairment of ubiquitin-proteasome subunits, SKP1A, aldehyde dehydrogenase, and chaperone HSC-70. *Annals of the New York Academy of Sciences, 1053*, 356-375.

Matsumoto, T., Suzuki, O., Furuta, T., Asai, M., Kurokawa, Y., Nimura, Y., Katsumata, Y. & Takahashi, I. (1985). A sensitive fluorometric assay for serum monoamine oxidase with kynuramine as substrate. *Clinical Biochemistry, 18*, 126-129.

Meyerson, L., McMurtrey, K. & Davis, V. (1978). A rapid and sensitive potentiometric assay for monoamine oxidase using a ammonia-selective electrode. *Analytical Biochemistry, 86*, 287-297.

Mochizuki, H., Imai, H., Endo, K., Yokomizo, K., Murata, Y., Hattori, N. & Mizuno, Y. (1994). Iron accumulation in the substantia nigra of 1-methyl-4-phenyl-1,2,3,6-tetrahydropyridine (MMTP)-induced hemiparkinsonian monkeys. *Neuroscience Letters,* 168, 251-253.

Murray, R., Granner, D., Mayes, P. & Rodwell, V. (2003). Enzyme kinetics. In R. Murray, D. Granner, P. Mayes, & V. Rodwell, *Harper's Illustrated Biochemistry* (26 ed.). McGraw-Hill.

Nagatsu, T. (2004). Progress in monoamine oxidase (MAO) research in relation to genetic engineering. *NeuroToxicology, 25*, 197-217.

Naoi, M. & Nagatsu, T. (1988). Inhibition of type A monoamine oxidase by Methylquinolines and structurally related compounds. *Journal of Neurochemistry, 50*, 1105-1110.

Newton-Vinson, P., Hubalek, F. & Edmondson, D.E. (2000). High-level expression of human liver monoamine oxidase B in Pichia pastoris. *Protein Expression and Purification, 20*, 334-345.

Nicklas, W.J., Vyas, I., Heikkila, R.E. (1985). Inhibition of NADH-linked oxidation in brain mitochondria by 1-methyl-4-phenyl-pyridine, a metabolite of the neurotoxin, 1-methyl-4-phenyl-1,2,5,6-tetrahydropyridine. *Life Sciences, 36*, 2503-2508.

Nicotra, A. & Parvez, S. (1999). Methods for assaying monoamine oxidase A and B activity: recent developments. *Biogenic amines, 15*, 307-320.

Novaroli, L., Reist, M., Favre, E., Carotti, A., Catto, M. & Carrupt, P. (2005). Human recombinant monoamine oxidase B as reliable and efficient enzyme source for inhibitor screening. *Bioorganic & Medicinal Chemistry, 13*, 6212-6217.

O'Brien, E., Kiely, K. & Tipton, K. (1978). A discontinuous luminometric assay for monoamine oxidase using an ammonia-selective electrode. *Analytical Biochemistry, 86*, 287-297.

Ogunrombi, M., Malan, S., Terre'Blanche, G., Castagnoli, K., Castagnoli, N.J. & Bergh, J.J. (2007). Neurotoxicity studies with the monoamine oxidase B substrate 1-methyl-3-phenyl-3-pyrroline. *Life Sciences, 81*, 458-467.

Ooms, F., Frederick, R., Durant, F., Petzer, J.P., Castagnoli, N., Van der Schyf, C.J. & Wouters, J. (2003). Rational approaches towards reversible inhibition of type B monoamine oxidase. Design and evaluation of a novel 5H-Indenol[1,2-c]pyridazin-5-one derivative. *Bioorganic & Medicinal Chemistry Letters, 13*, 69-73.

Parsons, M.R., Convery, M.A, Wilmot, C.M., Yadav, K.D.S., Blakeley, V., Corner, A.S., Phillips, S.E.V., McPherson, M.J. & Knowles, P.F. (1995). Crystal srtucture of a quinoenzyme: copper amine oxidase of Escherichia coli at 2 A resolution. *Structure, 3*, 1171-1184.

Petzer, J.P., Steyn, S., Castagnoli, K., Chen, J., Schwarzschild, M. & Van der Schyf, C.J. (2003). Inhibition of monoamine oxidase B by selective adenosine A2A receptor antagonists. *Bioorganic & Medicinal Chemistry, 11*, 1299-1310.

Polymeropoulos, M., Lavedan, C., Leroy, E., Ide, S., Dehejia, A.& Dutra, A. (1997). Mutation in the α-synuclein gene indentified in families with Parkinson's disease. *Science, 276*, 2045-2047.

Pretorius, J., Malan, S., Castagnoli Jr., N., Bergh, J. & Petzer, J. (2008). Dual inhibition of monoamine oxidase B and antagonism of the adenosine A_{2A} receptor by (E,E)-8-(4-phenylbutadien-1-yl)caffeine analogues. *Bioorganic and Medicinal Chemistry, 16*, 8676-8684.

Przedborski, S. (2005). Pathogenesis of nigral cell death in Parkinson's disease. *Parkinsonism and Related Disorders, 11*, S3-S7.

Ramsay, R.R., Krueger, M.J., Youngster, S.K., Gluck, M.R., Casida, J.E., Singer, T.P. (1991). Interaction of 1-methyl-4-phenylpyridinium ion (MPP^+) and its analogs with the rotenone/piericidin binding site of NADH dehydrogenase. *Journal of Neurochemistry, 56*, 1184-1190.

Rascol, O., Goetz, C., Koller, W., Poewe, W. & Sampaio, C. (2002). Treatment interventions for Parkinson's disease. *Lancet, 359*, 1589-1598.

Riederer, P., Danielczyk, W. & Grunblatt, E. (2004). Monoamine oxidase-B inhibition in Alzheimer's disease. *Neurotoxicology, 25*, 271-277.

Riederer, P., Lachenmayer, L. & Laux, G. (2004). Clinical applications of MAO-inhibitors. *Current Medicinal Chemistry, 11*, 2033-2043.

Salach, J. & Weyler, W. (1987). Preperation of the flavin-containing aromatic amine oxidases of human placenta and beef liver. *Methods in Enzymology, 142*, 627-637.

Shih, J., Chen, K. & Ridd, M. (1999). Monoamine oxidase: from genes to behaviour. *Annual Review of Neuroscience, 22*, 197-217.

Silverman, R. (1995). Radical ideas about monoamine oxidase B. *Accounts of Chemical Research, 28*, 335-342.

Singer, T., Ramsay, R., McKeown, K., Trevor, A. & Castagnoli, N. J. (1988). Mechanism of the neurotoxicity of 1-methyl-4-phenylpyridinium (MPP+), the toxic bioactivation product of 1-methyl-4-phenyl-1,2,3,6-tetrahydropyridine by monoamine oxidase inhibitors. *Nature, 49*, 17-23.

Smeyne, R. & Jackson-Lewis, V. (2004). The MPTP model of Parkinson's disease. *Molecular Brain Research, 134*, 57-66.

Son, Y., Ma, J., Kondou, Y., Yoshimura, M., Yamashita, E. & Tsukihara, T. (2008). Structure of human monoamine oxidase A at 2.2-Å resolution: The control of opening the entry for substrates/inhibitors. *The National Academy of Sciences of the USA, 105*, 5739-5744.

Van den Berg, D., Zoellner, K., Ogunrombi, M., Malan, S., Terre'Blanche, G., Castagnoli, N. J., Bergh, J.J. & Petzer, J.P. (2007). Inhibition of monoamine oxidase B by selected benzimidazole and caffeine analogue. *Bioorganic & Medicinal Chemistry, 15*, 3692-3702.

Van de Waterbeemb, H. & Testa, B. (1987). The parametrization of lipophilicity and other structural properties in drug design. In Testa, B., *Advances in Drug Research.* London: Academic press. 85 – 225.

Vlok, N., Malan, S., Castagnoli, N. J., Bergh, J. & Petzer, J. (2006). Inhibition of monoamine oxidase B by analogues of the adenosine A2A receptor antagonist (E)-8-(3-chlorostyryl)caffeine(CSC). *Bioorganic & Medicinal Chemistry, 14*, 3512-3521.

Vogel, A., Tatchell, A., Furnis, B., Hannaford, A. & Smith, P. Chlorine. In A. Vogel, A. Tatchell, B. Furnis, A. Hannaford, & P. Smith, *Vogel's Textbook of Practical Organic Chemistry.* 5 ed., 424.

Youdim, M. & Bakhle, Y. (2006). Monoamine oxidase: isoforms and inhibitors in Parkinson's disease and depressive illness. *British Journal of Pharmacology, 147* (Suppl 1), S287-S296.

Youdim, M., Edmondson, D.E. & Tipton, K. (2006). The therapeutic potential of monoamine oxidase inhibitors. *Nature Reviews. Neuroscience, 7*, 295-309.

Zhou, J., Zhong, B. & Silverman, R. (1996). Direct continuous fluorometric assay for monoamine oxidase. *Analytical Biochemistry, 234*, 9-12.

ACKNOWLEDGEMENTS

- Prof. J.P. Petzer, thank you for your patience and knowledge. Your commitment and enthusiasm inspires us all.
- Prof. J.J. Bergh and Prof. S.F. Malan, thanks for your valuable advice and guidance.
- My parents, for their unwavering support and love. I know you have sacrificed a lot for me.
- Jan, who always listens and is endlessly patient. I never take you for granted.

"When I consider Your heavens, the work of Your fingers,
The moon and the stars, which You have ordained..." (Ps. 8:3)